UNIVERSITY OF CALIFORNIA, SAN DIEGO

Temperature Equilibration and Three-body Recombination in Strongly Magnetized Pure Electron Plasmas

A dissertation submitted in partial satisfaction of the

requirements for the degree Doctor of Philosophy

in Physics

by

Michael Edwin Glinsky

Committee in charge:

Professor Thomas M. O'Neil, Chairman
Professor Marshall N. Rosenbluth
Professor Daniel H. E. Dubin
Professor David R. Miller
Professor John H. Weare

1991

The dissertation of Michael Edwin Glinsky is approved, and it is acceptable in quality and form for publication on microfilm:

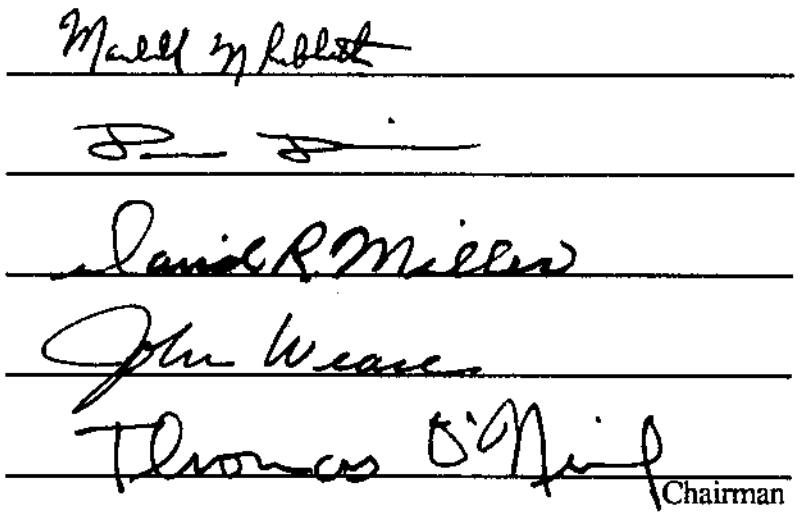

University of California, San Diego

1991

This thesis is dedicated to my grandpa McKenzie, on whose broad shoulders I have stood to see this far.

TABLE OF CONTENTS

LIST OF FIGURES AND TABLES

ACKNOWLEDGEMENTS

I would like to thank my research supervisor, Prof. Tom O'Neil, from whom I learned how to rigorously solve scientific problems starting from fundamentals but at the same time paying attention to the "basic physics" of the problem. I would also like to thank Prof. Marshall Rosenbluth, whose analytic insight aided me greatly in finding the asymptotic expression for the temperature equipartition rate, and Dr. Ralph Smith who gave invaluable assistance with the numerical aspects of my work. The time that the other members of my committee (Prof. Dan Dubin, Prof. David Miller, and Prof. John Weare) spent reviewing my work has been greatly appreciated.

In addition, I would like to thank my fellow students, most especially Dr. Poul Hjorth, Kenji Tsuruta, Dr. Bret Beck, and Dr. Harris Flaum for their help and encouragement over the course of my studies.

Finally, I would like to thank my family for their encouragement and support. The road though graduate school would have been much rougher without them.

This work was supported by a National Science Foundation Graduate Fellowship, the San Diego Supercomputer Center and National Science Foundation Grant PHY87-06358. The work on three-body recombination (Ch. 3) has been published as an article in Physics of Fluids B [1.1] by my research supervisor and me.

VITAE

18 October 1960	Born, Akron, Ohio
1983	B.S. in Physics, Case Western Reserve University, Cleveland, Ohio
1983-1985	Geophysicist, Shell Oil Co., Houston, Texas
1985	Physicist, Lawrence Livermore National Laboratory Livermore, California
1985-1991	Research Assistant, University of California, San Diego
1986	M.S. in Physics, University of California, San Diego
1991	Ph.D. in Physics, University of California, San Diego

PUBLICATIONS

1. M. E. Glinsky and T. M. O'Neil, "Guiding Center Atoms: Three-body Recombination in a Strongly Magnetized Plasma", Phys. Fluids B **3**, 1279 (1991).

2. M. E. Glinsky, T.M. O'Neil, M.N. Rosenbluth, K. Tsuruta and S. Ichimaru, "Collisional Equipartition Rate for a Magnetized Pure Electron Plasma", in preparation for Phys. Fluids B.

3. M. E. Glinsky, T.M. O'Neil, M.N. Rosenbluth, K. Tsuruta and S. Ichimaru, "Collisional Equipartition Rate for a Magnetized Pure Electron Plasma", Bul. Am. Phys. Soc. **35**, 2134 (1990).

4. M. E. Glinsky and T. M. O'Neil, "Three-body Recombination in a Strong Magnetic Field", Bul. Am. Phys. Soc. **34**, 1934 (1989).

5. M. E. Glinsky and T. M. O'Neil, "Guiding Center Atoms", Bul. Am. Phys. Soc. **33**, 1899 (1988).

6. M. E. Glinsky, "Neon K-edge as a Tool to Measure Crystal resolving Power at 870 eV", *Lawrence Livermore National Laboratory Technical Report*, RP-85-106, September 20, (1985).

7. M. E. Glinsky, "ROCKIT: A Program to Calculate Spectrometer Rocking Curves", *Lawrence Livermore National Laboratory Technical Report*, RP-85-105, September 19, (1985).

8. M. E. Glinsky, "Optical Resolving Power of a Curved Mica Crystal", *Lawrence Livermore National Laboratory Technical Report*, RP-85-104, September 19, (1985).

9. M. E. Glinsky, P. A. Waide, "Resolving Power of Muscovite Mica (002)", *Lawrence Livermore National Laboratory Technical Report*, RP-85-91, August 2, (1985).

10. M. E. Glinsky, "DOWCON Jr.: A Method for Determining Near Surface Velocities from First Arrivals", *Proceedings of Shell Geophysical Conference*, paper 31, (1985).

FIELDS OF STUDY

Major Field: Physics

Studies in Plasma Physics
Professors Thomas M. O'Neil, Marshall N. Rosenbluth, and Patrick H. Diamond

Studies in Classical Mechanics
Professor Thomas M. O'Neil

Studies in Quantum Mechanics
Professor Julius Kuti

Studies in Statistical Mechanics
Professors F. Duncan Haldane, and Donald R. Fredkin

Studies in Mathematical Physics
Professor Frank B. Thiess

Studies in Differential Geometry and Exterior Calculus
Professors Theodore T. Frankel, and Michael H. Freedman

Studies in Electromagnetism
Professor Donald R. Fredkin

ABSTRACT OF THE DISSERTATION

Temperature Equilibration and Three-body Recombination
in Strongly Magnetized Pure Electron Plasmas

by

Michael Edwin Glinsky
Doctor of Philosophy in Physics
University of California, San Diego, 1991
Professor Thomas M. O'Neil, Chairman

Two properties of a weakly correlated pure electron plasma that is immersed in a uniform magnetic field are calculated. The strength of the magnetic field is determined by the dimensionless parameter r_{ce}/b, where $r_{ce} = \sqrt{k_B T_e / m_e} / \Omega_{ce}$ is the cyclotron radius and $b = e^2 / k_B T_e$ is the classical distance of closest approach.

The first property examined is the collisional equipartition rate between the parallel and perpendicular velocity components. Here, parallel and perpendicular refer to the direction of the magnetic field. For a strongly magnetized plasma (i.e., $r_{ce}/b << 1$), the equipartition rate is exponentially small ($\sim \exp\left[-2.34\left(b/r_{ce}\right)^{2/5}\right]$). For a weakly magnetized plasma (i.e., $r_{ce}/b >> 1$), the rate is the same as for an unmagnetized plasma except that r_{ce}/b replaces λ_D/b in the Coulomb logarithm. (It is assumed here that $r_{ce} < \lambda_D$; for $r_{ce} > \lambda_D$, the plasma is effectively unmagnetized.) Presented is a numerical

treatment that spans the intermediate regime $r_{ce} / b \sim 1$, connects on to asymptotic results in the two limits $r_{ce} / b << 1$ and $r_{ce} / b >> 1$ and is in good agreement with experiments. Also, an improved asymptotic expression for the rate in the high field limit is derived.

Secondly, the three-body recombination rate for an ion introduced into a cryogenic electron plasma in the high field limit is calculated. An ensemble of plasmas characterized by classical guiding center electrons and stationary ions is described with the BBGKY hierarchy. Under the assumption of weak electron correlation, the hierarchy is reduced to a master equation. Insight to the physics of the recombination process is obtained from the variational theory of reaction rates and from an approximate Fokker-Planck analysis. The master equation is solved numerically using a Monte Carlo simulation, and the recombination rate is determined to be $0.070(10) n_e^2 v_e b^5$ per ion, where n_e is the electron density and $v_e = \sqrt{k_B T_e / m_e}$ is the thermal velocity. Also determined by the numerical simulation is the transient evolution of the distribution function from a depleted potential well about the ion to its steady state.

Chapter 1

General Introduction

1.1. Overview

This thesis contains the solution to two problems in the kinetic theory of pure electron plasmas. Chapter 2 contains a calculation of the collisional equipartition rate for a plasma characterized by an anisotropic velocity distribution ($T_\perp \neq T_\parallel$). The plasma is assumed to be in a uniform magnetic field, and parallel (||) and perpendicular ($\perp$) refer to the direction of the magnetic field. Chapter 3 contains a calculation of the collisional recombination rate (three-body recombination) for an ion that is introduced into a cold and magnetized pure electron plasma. These two chapters are presented as free-standing papers, one of which has been published [1.1] and the other of which will be submitted shortly. The purpose of this introduction is to place the work in a more general context than is apparent from the papers alone.

In both calculations, the plasma is assumed to be weakly correlated, the condition for which is $n_e \lambda_D^3 >> 1$, where n_e is the electron density and $\lambda_D = \sqrt{k_B T_e / 4\pi n_e e^2}$ is the Debye length. Here, T_e is the electron temperature, k_B is the Boltzmann constant, and e and m_e are the electron charge and mass respectively. One can easily show that this inequality implies the length scale ordering $b << \lambda_D$, where $b = e^2 / k_B T_e$ is the classical distance of closest approach. When the plasma is magnetized, the cyclotron radius

$r_{ce} = \sqrt{k_B T_e / m_e} / \Omega_{ce}$ introduces another length scale that can be ordered arbitrarily relative to the other length scales. Here, $\Omega_{ce} = eB / m_e c$ is the electron cyclotron frequency. When $r_{ce} > \lambda_D$, the plasma is effectively unmagnetized for collisional dynamics, since an unperturbed particle orbit is nearly a straight line over the range of the Debye shielded interaction. We exclude this case here, since we are particularly interested in the influence of the magnetic field on the collisional dynamics. We say that a plasma is weakly magnetized when $b << r_{ce} << \lambda_D$, and that it is strongly magnetized when $r_{ce} << b$.

The theory of collisional relaxation for a plasma with an anisotropic velocity distribution has a long history. For an unmagnetized plasma, the Fokker-Planck collision operator, which describes the collisional evolution of the electron velocity distribution, was written down by Landau in 1936 [1.2], and was put on a rigorous footing by several others [1.3-1.5] in the late 1950's. Using this operator, one can show that the characteristic time for an electron moving at the thermal velocity $v_e = \sqrt{k_B T_e / m_e}$ to undergo collisional deflection through 90° is [1.6]

$$\tau_{ee} \approx \frac{1}{(5.59)\, n_e v_e b^2 \ln(\lambda_D / b)} \tag{1.1}$$

The inverse of this time is the electron-electron collision frequency $\nu_{ee} = 1/\tau_{ee}$, and as one would expect, this frequency sets the basic rate for the collisional relaxation of an anisotropic velocity distribution in an unmagnetized plasma.

For an electron velocity distribution of the form

$$f(v_\parallel, v_\perp) = \left(\frac{m_e}{2\pi k_B T_\parallel}\right)^{1/2} \left(\frac{m_e}{2\pi k_B T_\perp}\right) \exp\left[-\frac{m_e v_\parallel^2}{2k_B T_\parallel} - \frac{m_e v_\perp^2}{2k_B T_\perp}\right], \tag{1.2}$$

the equipartition rate is defined though the equation

$$\frac{dT_\perp}{dt} = \nu\left(T_\parallel - T_\perp\right), \tag{1.3}$$

where $(T_\parallel - T_\perp)$ is assumed to be small, and $dT_\perp / dt$ is interpreted as the rate of increase of the mean perpendicular kinetic energy. The assumption of small temperature anisotropy $(T_\parallel - T_\perp) << T_\parallel, T_\perp$ is necessary to insure that $dT_\perp / dt$ is linear in $(T_\parallel - T_\perp)$. For the case where the magnetic field is sufficiently weak that the collisional dynamics is effectively unmagnetized ($r_{ce} >> \lambda_D$), Ichimaru and Rosenbluth [1.7] calculated the equipartition rate

$$\nu = \frac{8\sqrt{\pi}}{15} n_e \upsilon_e b^2 \ln(\lambda_D / b) \tag{1.4}$$

In 1960, Rostoker [1.8] generalized the collision operator to include the effect of a magnetic field. The Rostoker operator is valid in the unmagnetized regime ($r_{ce} >> \lambda_D$) and in the weakly magnetized regime ($b << r_{ce} << \lambda_D$). By carrying out extensive numerical solutions of model collision operators based on the Rostoker operator; Montgomery, Joyce, and Turner [1.9] concluded that the main effect of the magnetic field is to introduce a kind of dynamical shielding on a length scale r_{ce}. For weakly magnetized plasmas ($b << r_{ce} << \lambda_D$) this dynamical shielding supersedes the Debye shielding, and the cutoff in the Coulomb logarithm is replaced by an r_{ce} cutoff [i.e., $\ln(\lambda_D / b) \rightarrow \ln(r_{ce} / b)$]. Making this replacement in the Ichimaru-Rosenbluth formula, yields an asymptotic expression for the rate in the regime of weak magnetization

$$\nu = \frac{8\sqrt{\pi}}{15} n_e \upsilon_e b^2 \ln(r_{ce} / b) \tag{1.5}$$

The parameter regime of strong magnetization is quite unusual, as can be seen by rewriting the inequality $r_{ce} << b$ in the form $(k_B T_e)^{3/2} << 10^{-4} B$, where $k_B T_e$ is in eV and B is in kG. Even for B as large as 100 kG (the largest field that one can conveniently use for plasma confinement in laboratory experiments), the inequality requires that $k_B T_e << 0.1$ eV, and this means that a neutral plasma would recombine. However, recent experiments [1.10] have involved the magnetic confinement of pure electron plasmas and these plasmas cannot recombine, since there are negligibly few ions in the confinement

region. Moreover, these plasmas have been cooled to the cryogenic temperature regime where they are deep within the regime of strong magnetization. In fact, it is experimental access to the regime of strong magnetization ($r_{ce} << b$) and intermediate magnetization ($r_{ce} \sim b$) that motivates the theory presented here. This is the reason that we take up problems in plasma kinetic theory at this late date in the history of the subject.

O'Neil and Hjorth [1.11] recently calculated an asymptotic formula for the equipartition rate in the strongly magnetized limit ($r_{ce} << b$). In this limit, the rate is constrained by a novel adiabatic invariant, the total cyclotron action ($J = \sum_j m_e v_{j\perp}^2 / 2\Omega_{ce}$), and the rate is exponentially small ($\nu \sim \exp\left[-2.34\left(b / r_{ce}\right)^{2/5}\right]$).

To understand the adiabatic invariant consider a binary collision between two electrons in a strongly magnetized plasma. The electrons spiral towards and then away from each other in tight helical orbits with the radii of the helixes being much smaller than the minimum separation between the electrons. The picture of such a collision is much different than what one imagines for Rutherford scattering. The condition for strong magnetization ($r_{ce} << b$) can be rewritten as ($\Omega_{ce} >> v_e / b$); so the cyclotron frequency is the highest dynamical frequency in the problem. One can think of the two cyclotron angles as high frequency oscillators that resonantly exchange quanta (or action) and the remaining variables as slowly varying parameters that modulate the oscillators. Under these conditions it is not surprising that the total cyclotron action is conserved, or, more precisely, is an adiabatic invariant. For the case of a uniform magnetic field, which we consider here, one can equivalently say that the total perpendicular kinetic energy is an adiabatic invariant.

On the time scale of a few collisions, the adiabatic invariant is well conserved, and there is negligible exchange of energy between the degrees of freedom parallel and perpendicular to the magnetic field. The distribution of velocities relaxes to Maxwellians separately for the perpendicular and parallel velocities, with the parallel temperature $T_\parallel$ not

necessarily equal to the perpendicular temperature $T_\perp$. However, an adiabatic invariant is not an exact constant of the motion, so the evolution does not stop at this stage. During each collision, the adiabatic invariant is broken by an exponentially small amount, and these small energy exchanges act cumulatively to allow $T_\parallel$ and $T_\perp$ to relax to a common value. The rate for this process (i.e., the equipartition rate) is exponentially small. Subsequent experiments by Beck, Fajans, and Malmberg [1.12] verified the dramatic drop in the equipartition rate as the plasma becomes strongly magnetized.

These experiments also provided good data for the regime of intermediate magnetization ($r_{ce} \sim b$), where there was no theory. Motivated by this, my collaborators (T.M. O'Neil, M.N. Rosenbluth, K. Tsuruta, and S. Ichimaru) and I developed a comprehensive theory that spans the intermediate regime ($r_{ce} \sim b$) and connects on to asymptotic formulas valid in the limits of weak and strong magnetization. Also, we derived an improved asymptotic formula for the rate in the strong field limit.

The comprehensive theory is based on the same Boltzmann-like collision operator used by O'Neil and Hjorth [1.13]. One may be surprised at the use of such an operator for a problem in plasma kinetic theory, since the operator does not include the effect of Debye shielding. Recall that Landau introduced shielding in an *ad hoc* fashion when deriving the Fokker-Planck operator from the Boltzmann operator. However, the magnetic field produces a kind of dynamical shielding on a length scale that is shorter than the Debye length, so it is not a problem that the Boltzmann operator omits Debye shielding.

The dynamical screening is a consequence of the adiabatic invariant discussed previously. For a collision in which $\Omega_{ce}\tau >> 1$, where τ is the duration of the collision, the perpendicular kinetic energy changes by an exponentially small amount [i.e., $\Delta E_\perp \sim \exp(-\Omega_{ce}\tau)$]. The time τ is of order $\tau \sim r_m / v_e$, where $r_m = \min|\mathbf{r}_1 - \mathbf{r}_2|$ is the minimum separation between the two electrons during the collision. Thus, the quantity $\Omega_{ce}\tau \sim \Omega_{ce} r_m / v_e$ is large and the dynamical shielding is active when $r_m > r_{ce}$. On energetic

grounds two electrons cannot get much closer than b; so the dynamical shielding is active for all collisions in a plasma with $r_{ce} << b$. This is the reason that the equipartition rate is exponentially small for a strongly magnetized plasma. For weak magnetization (i.e., $r_{ce} >> b$), there are some Rutherford-like collisions where the dynamical shielding is not active (and $\Delta E_\perp$ is large), but for all collisions with $r_m > r_{ce}$ the shielding is active. Consequently, these latter collisions have negligible effect. Both b and r_{ce} are assumed here to be small compared to λ_D ($b << \lambda_D$ for a weakly correlated plasma and $r_{ce} << \lambda_D$ by hypothesis); so Debye shielding plays no role. Note that Montgomery, Joyce, and Turner had observed the effect of the screening in their numerical solutions of the model Rostoker equation, and thus proposed the rule that r_{ce} replace λ_D as an upper cutoff for the Coulomb logarithm.

By using the Boltzmann-like collision operator, one can obtain an integral expression for the equipartition rate -- a four dimensional integral of $(\Delta E_\perp)^2$ over all possible collisions. This reduces the problem of calculating the equipartition rate to the problem of calculating $\Delta E_\perp$, the change in the perpendicular kinetic energy that occurs during an isolated binary collision. For the case of a strongly magnetized plasma, O'Neil and Hjorth obtained an asymptotic expression for $\Delta E_\perp$ based on the smallness of r_{ce} / b. One can obtain an analytic expression for $\Delta E_\perp$ in the limit of large r_{ce} / b by treating the dynamics perturbatively. This is justified by the weakness of the interaction for the large impact parameter collisions ($>> b$) that make the dominant contribution to the equipartition rate. In general for arbitrary r_{ce} / b, an analytic expression for $\Delta E_\perp$ cannot be obtained for all important collisions.

Even though the equations of motion for the two colliding electrons are not integrable, one can still numerically integrate them given the initial conditions. We therefore evaluate the integral expression for the equipartition rate by the Monte Carlo method, where points in the domain of integration (initial conditions for the binary electron

collision) are chosen at random. A numerical solution for $\Delta E_{\perp}$ is obtained for each set of initial conditions. The value of the integral is estimated as the average value of the integrand over the points chosen. Using this technique, we determine the equipartition rate for values of r_{ce} / b which span the range 10^{4} to 10^{-4}.

These results connect onto the analytic expression in the limit of a weak magnetic field. They also give a numerical estimate of what the free parameter A in the expression

$$\nu = \frac{8\sqrt{\pi}}{15} n_e \upsilon_e b^2 \ln\left(A\, r_{ce} / b\right) \tag{1.7}$$

should be. The free parameter was introduced by Montgomery, Joyce and Turner as an arbitrary lower impact parameter cutoff of order b; but is usually neglected by making the dominate approximation that $\ln\left(r_{ce} / b\right) >> \ln(A)$. The cutoff was needed to prevent a divergence in the integral for the equipartition rate, which arises since unperturbed orbits are used in the derivation of the Rostoker collision operator. Using unperturbed orbits is no longer a valid procedure for binary collisions with impact parameters of order b or smaller where the interaction between the electrons becomes strong. Such an arbitrary cutoff is not necessary for our numerical treatment, since the dynamics naturally provides cutoffs at both small impact parameter and large impact parameter. The small impact parameter cutoff arises as a result of Coulomb repulsion and the large impact parameter cutoff arises as a result of dynamical shielding.

The statistical uncertainty in the Monte Carlo determination of ν was less than 5%. This low uncertainty allowed us to discern a discrepancy between the asymptotic expression of O'Neil and Hjorth and the Monte Carlo values for $r_{ce} << b$. A more exact and complicated calculation of the asymptotic formula by us reveals that, although the exponential factor of the old expression was correct, the algebraic factor needs to be modified [see Eq. (2.2)]. Higher order terms in the new asymptotic series for the

equipartition rate enter with surprisingly large coefficients; it is necessary to retain these higher order terms in order to obtain good agreement with the Monte Carlo results.

We now have theoretical values of the equipartition rate which span the region of intermediate magnetization and connect on to asymptotic expressions (with no free parameters) in the limits of strong and weak magnetization. The theory agrees, to within experimental error, with the measurements of Beck, Fajans, and Malmberg (see Fig. 2.3). These measurements span a range of r_{ce} / b from 10^{2} to 10^{-2}, where the value of $\nu / n_e v_e b^2$ drops from 10^{0} to 10^{-4} as the magnetic field is increased. The experimental data set can be further enlarged by experiments conducted by Hyatt, Driscoll and Malmberg [1.14] on a magnetically confined pure electron plasma at room temperature. These experiments measured the equipartition rate for values of r_{ce} / b from 10^{4} to 10^{6}. The agreement of this data with our calculation extends the realm of correspondence between theory and experiment to over eight decades in the relevant physical parameter r_{ce} / b (see Fig. 2.3).

We now turn our attention to the problem discussed in Ch. 3 – collisional (three-body) recombination of an ion introduced into a cryogenic and strongly magnetized pure electron plasma. There are two ways in which an electron can recombine with the ion. The first is radiative recombination

$$A^{+} + e^{-} \rightarrow A + \hbar\nu, \tag{1.8}$$

where a photon carries off the excess energy. This can be either a single step process, where the ion goes directly from an unbound state to the ground state with the release of a single photon; or a multiple step process, where the electron first becomes bound to the ion in an excited state and at least one subsequent spontaneous transition occurs to allow the atom to reach the ground state. The second is collisional (three-body) recombination

$$A^{+} + e^{-} + e^{-} \rightarrow A + e^{-}, \tag{1.9}$$

where a second electron carries off the excess energy. This can also be either a single step process with only one three-body collision; or a multiple step process, where the electron becomes bound to the atom in an excited state and suffers subsequent electron collisions until the atom either reaches the ground state or is re-ionized. Whether collisional or radiative processes dominate (or whether one must consider a combination of both processes in a multiple step cascade) depends on the temperature and density of the plasma.

Early research on radiative recombination in a tenuous plasma was done in the 1930's [1.15], and extensive calculations of the recombination rate were done in the 1950's [1.16] and are summarized by Bates and Dalgarno [1.17]. At temperatures much below a Rydberg, the expression for the radiative recombination rate per ion is

$$R_\gamma \sim n_e \frac{e^4}{m_e^2 c^3}\left(\frac{Ry}{k_B T_e}\right)^{1/2} \propto n_e T_e^{-1/2} \qquad (1.10)$$

where c is the speed of light, and Ry is the Rydberg energy (~13 eV). The density scaling of R_γ is obviously due to the fact that only one electron is involved in the fundamental recombination reaction. The temperature scaling is determined by the fact that the quantum-mechanical cross section for radiative electron capture scales inversely as the electron velocity squared at small electron velocity. The flux of electrons is proportional to the electron velocity so that the radiative recombination rate (electron capture rate) scales inversely as the electron thermal velocity.

Giovanelli [1.18] in 1948 first proposed that three-body collisions increase the recombination rate in plasmas of moderate to high density (and we will see, in plasmas of low temperature). Although laboratory experiments [1.19] existed at that time which confirmed Giovanelli's prediction, the connection between the theory and experiment was not made. It was not until new experimental results from Stellerator-B at Princeton [1.20] were generated in the early 1960's that the connection was made. Several people [1.21],

using Giovanelli's ideas, developed the theory of collisional-radiative recombination and used them to explain the experimental results.

By going to the limit of high densities and low temperatures, several others [1.22] were able to simplify the theory to involve only three-body recombination. They found at low temperatures (i.e., $k_B T_e << Ry$) that a kinetic bottleneck determines the three-body recombination rate. This bottleneck is located a few $k_B T_e$ below the ionization threshold and can be understood in terms of a minimum in the one-way thermal equilibrium flux. This flux is the product of a Boltzmann factor $\exp(E / k_B T_e)$, where E is the binding energy taken to be positive toward deeper binding; and the phase space factor E^{-3}. The product has a strong minimum at $E \approx 3k_B T_e$ which is the location of the bottleneck. From the existence of the bottleneck, one may deduce the following picture. As atoms are formed and cascade to deeper binding, only a small fraction get though the bottleneck; the rest are re-ionized. If an atom makes it through the bottleneck, it continues to ever deeper binding with only a small probability of being re-ionized. The recombination rate is the rate at which atoms make it though the bottleneck.

The dynamics of the three-body collisions with atoms bound in the rate determining states near the kinetic bottleneck may be treated classically since it is assumed that the plasma is of low temperature. One can estimate the recombination rate by determining the rate at which classical Rydberg atoms [1.23] bound with $k_B T_e$ are formed via three-body collisions. Note that the scale length of electron-ion separations in Rydberg atoms near the bottleneck is b the distance of closest approach. The frequency of electron-ion collisions characterized by an impact parameter in this range is $n_e v_e b^2$, and the probability that another electron is close enough to carry off the binding energy of the atom is of order $n_e b^3$. The three-body recombination rate is estimated as the product

$$R_3 \sim \left(n_e v_e b^2\right)\left(n_e b^3\right) \propto n_e^2 T_e^{-9/2} \tag{1.11}$$

This rate scales as n_e^2 because two electrons are involved in the fundamental recombination reaction. The dramatic temperature scaling is caused by the bottleneck which sets the rate determining scale length as b which is proportional to T_e^{-1}.

Comparing the three-body recombination rate, Eq. (1.11), to the radiative recombination rate, Eq. (1.10), one finds that

$$\frac{R_3}{R_\gamma} \sim 10^2 \, n_e\left(\text{in cm}^{-3}\right)\left[T_e\left(\text{in }^\circ\text{K}\right)\right]^{-4} \tag{1.12}$$

We have in mind a cryogenic pure electron plasma with a temperature of 4 °K and a density of 10^8 cm^{-3}, and for such a plasma one finds that the three-body recombination is a factor of 10^7 greater than radiative recombination. For the density considered, three-body collisions dominate the recombination whenever the temperature is much less than 300 °K, room temperature.

The work up to 1969 on collisional recombination used collision cross sections derived by using either a diffusive approximation (small energy exchange) or an impulse approximation (large energy exchange). A general analytic expression for the collisional cross sections cannot be obtained because the equations of motion for two electrons and an ion are not integrable. Mansbach and Keck [1.24] realized that neither one of these approximations is strictly valid for the collisions which contribute the most to the three-body recombination rate. To extricate themselves from this dilemma, they numerically integrated the equations of motion to determine the needed cross sections by a Monte Carlo technique. Using these results they were able to solve for both the three-body recombination rate $R_3 \approx 0.76\, n_e^2 v_e b^5$ and the steady state distribution function $f_{ss}(E)$. Above the bottleneck (i.e., $E < 3k_B T_e$) they found that $f_{ss}(E)$ is near its thermal equilibrium value, but below the bottleneck (i.e., $E > 3k_B T_e$) it falls well below the value expected in thermal equilibrium. Both the recombination rate and the steady state distribution function agreed well with the results of experiment [1.20,1.19,1.25].

Recent experimental access to the regime of strong magnetization in cryogenic pure electron plasmas leads one to think about how an ion recombines with an electron when it is introduced into one of these plasmas. Surprisingly, it is the antimatter analog of the electron-ion three-body recombination process that is of the most interest. Positron plasmas have already been produced [1.26], and antiprotons have been trapped and cooled to less than 0.1 eV [1.27]. A logical next step is to introduce antiprotons into a positron plasma (of the same character as the cryogenic strongly magnetized electron plasma) so that the antiprotons and positrons recombine [1.28]. The recombination rate is a design parameter for such experiments. The antihydrogen produced by the recombination would then be used in gravitational and spectroscopic studies [1.29].

Motivated by this, my collaborator (T.M. O'Neil) and I have studied how the three-body recombination process is changed in a strongly magnetized pure electron plasma [1.1]. We have found that the three-body recombination rate is reduced by an order of magnitude ($R_3 \approx 0.07\, n_e^2 b^5 v_e$) when a strong magnetic field is present, since a constraint is imposed on the electron dynamics (the electrons cannot move freely across the field). A further reduction in the rate may also occur if there is a large ion velocity perpendicular to the field. We have also determined the transient evolution of the distribution function from a depleted potential well about the ion to its steady state.

The kinetics of three-body recombination in a strong magnetic field are still controlled by a bottleneck a few $k_B T_e$ below the ionization energy. Since $k_B T_e$ is much less than a Rydberg the dynamics are classical. Also, the dynamics can be treated by guiding center drift theory [1.30], because the cyclotron radius is much smaller than the scale length on which the interaction potential varies (i.e., $r_{ce} << b$). Equivalently, the cyclotron frequency is much larger than the next largest dynamical frequency (i.e., $\Omega_{ce} >> v_e / b$). This implies that the high-frequency cyclotron motion may be averaged out and the number

of degrees of freedom correspondingly reduced; the center of the cyclotron orbit (guiding center) moves according to guiding center drift theory.

In the energy range of the bottleneck, a bound electron-ion pair form a novel atom, which we call a guiding center atom. The electron guiding center oscillates back and forth along a field line in the Coulomb well of the ion and more slowly $\mathbf{E}\times\mathbf{B}$ drifts around the ion (see Fig. 3.1). The frequency of oscillation back and forth along a field line is of order $\omega_z \sim \sqrt{e^2/m_e b^3} \sim v_e/b$, and the frequency of the $\mathbf{E}\times\mathbf{B}$ drift motion is of order $\omega_{\mathbf{E}\times\mathbf{B}} \sim ec/Bb^3$. One can see that a consequence of the ordering $r_{ce} << b$ is the ordering $\Omega_{ce} >> \omega_z >> \omega_{\mathbf{E}\times\mathbf{B}}$.

In this discussion and in our calculations the ion is treated as stationary. This approximation makes sense when the electron motion is rapid compared to the ion motion. For example, we require that $v_e >> v_{i\parallel}$, where $v_{i\parallel}$ is the characteristic ion velocity parallel to the magnetic field. The requirements on the transverse motion are most easily stated as the frequency orderings: $\omega_{\mathbf{E}\times\mathbf{B}} >> \Omega_{ci}$ and $\omega_{\mathbf{E}\times\mathbf{B}} >> v_{i\perp}/b$, where $v_{i\perp}$ is the characteristic ion velocity transverse to the field and $\Omega_{ci} = eB/m_i c$ is the ion cyclotron frequency. When the first of these two inequalities is reversed the electron and ion drift together across the magnetic field maintaining a constant separation. The results of our calculations should still apply since it does not matter to the cascade process whether the electron is $\mathbf{E}\times\mathbf{B}$ drifting around a fixed ion at constant separation or the electron and ion are drifting together at constant separation.

When the second of the two inequalities is reversed, the ion can run away from the electron before the electron completes an $\mathbf{E}\times\mathbf{B}$ drift circuit around the ion. In this case, one expects a substantial reduction in the recombination rate. A simple dimensional argument suggests a rate of order $R_3 \sim n_e^2 v_e r_0^5$, which is a reduction by the factor $(r_0/b)^5$, where r_0 is the electron-ion separation for which the $\mathbf{E}\times\mathbf{B}$ drift velocity equals the perpendicular ion velocity (i.e., $v_{i\perp} = ec/Br_0^2$).

We use the BBGKY hierarchy as the basis for our analysis of the collisional recombination kinetics [1.31]. The equations of the hierarchy contain two small parameters, $r_{ce}/b << 1$ and $n_e b^3 << 1$, and we analyze the equations to lowest nontrivial order in these parameters. The smallness of r_{ce}/b implies that the $\mathbf{E}\times\mathbf{B}$ drift motion that occurs during a collision is negligible; recall that $r_{ce}/b << 1$ implies that $v_e/b >> \omega_{\mathbf{E}\times\mathbf{B}}$. Because the most important collisions are close collisions (particle separation $\sim b$) and because the plasma is low density (i.e., $n_e b^3 << 1$), the hierarchy can be truncated by neglecting three-electron collisions. The first and second equations of the hierarchy then form a closed set. These two equations are formally reduced to a master equation; but the transition rates in the master equation (for steps in the recombination cascade) are not known analytically. In general, these rates depend on the complicated collision dynamics of two electrons in the force field of an ion. Consequently, a rigorous analytic solution of the master equation is not possible.

This situation is essentially the same as that encountered for an unmagnetized plasma. We present a unified and systematic treatment of three different approaches similar to those used to analyze collisional recombination in an unmagnetized plasma. The first two are approximate treatments that yield important physical insights into the recombination process. These are a Fokker-Planck analysis which treats the kinetics as a diffusive process with a small energy exchange ($\Delta E << k_B T_e$) during a three-body collision, and a variational analysis which assumes that the energy exchange is large.

Because neither approximate treatment is entirely satisfactory, we followed the cascade dynamics numerically by using a Monte Carlo simulation. In this simulation, guiding center atoms are formed and then followed through a sequence of collisions, with the incident electron picked at random from a Maxwellian distribution. This procedure can be justified formally as a Monte Carlo solution of the master equation [1.32]. The solution verifies the existence of the bottleneck and determines the recombination rate. In addition,

the time dependent behavior of the distribution function is obtained. The result is a quantitative understanding of how the initially depleted potential well is filled to the steady state condition.

1.2. References

[1.1] M.E. Glinsky and T.M. O'Neil, Phys. Fluids B **3**, 1279 (1991).

[1.2] L.D. Landau, Physic. Z. Sowjet. **10**, 154 (1936).

[1.3] A. Lenard, Ann. Phys. (N.Y.) **10**, 390 (1960); R. Belescu, Phys. Fluids **3**, 52 (1960).

[1.4] M.N. Rosenbluth, W.M. McDonald and D.L. Judd, Phys. Rev. **107**, 1 (1957).

[1.5] W.B. Thompson and J. Hubbard, Rev. Mod. Phys. **32**, 714 (1960); J. Hubbard, Proc. Roy. Soc. **A260**, 114 (1961).

[1.6] D.C. Montgomery and D.A. Tidman, *Plasma Kinetic Theory* (McGraw-Hill, 1964).

[1.7] S. Ichimaru and M.N. Rosenbluth, Phys. Fluids **13**, 2778 (1970).

[1.8] N. Rostoker, Phys. Fluids **3**, 922 (1960).

[1.9] D. Montgomery, L. Turner and G. Joyce, Phys. Fluids **17**, 954 (1974); D. Montgomery, G. Joyce and L. Turner, Phys. Fluids **17**, 2201 (1974).

[1.10] J.H. Malmberg, T.M. O'Neil, A.W. Hyatt and C.F. Driscoll, "The Cryogenic Pure Electron Plasma," in *Proceedings of 1984 Sendai Symposium on Plasma Nonlinear Phenomena* (Tohoku U. P., Sendai, Japan, 1984), pp. 31-37.

[1.11] T.M. O'Neil and P.J. Hjorth, Phys. Fluids **28**, 3241 (1985).

[1.12] B. Beck, J. Fajans and J. H. Malmberg, Bul. Am. Phys. Soc. **33**, 2004 (1988).

[1.13] T.M. O'Neil, Phys. Fluids **26**, 2128 (1983).

[1.14] A.W. Hyatt, C.F. Driscoll and J.H. Malmberg, Phys. Rev. Lett. **59**, 2975 (1987).

[1.15] J.R. Oppenheimer, Z. Phys. **55**, 725 (1929); E.C.G. Stueckelberg and P.M. Morse, Phys. Rev. **36**, 16 (1930); W. Wessel, Ann. Phys. (Leipzig) **5**, 611

(1930); D.R. Bates, R.A. Buckingham, H.S.W. Massey and J.J. Unwin, Proc. R. Soc. London **A170**, 322 (1939).

[1.16] A. Burgess, Mon. Not. R. Astron. Soc. **118**, 477 (1958); M.J. Seaton, Mon. Not. R. Astron. Soc. **119**, 81 (1959).

[1.17] D.R. Bates and A. Dalgarno, *Atomic and Molecular Processes* (Academic, New York, 1962), p. 245.

[1.18] R.G. Giovanelli, Aust. J. Sci. Res. **A1**, 275, 289 (1948).

[1.19] C. Kenty, Phys. Rev. **32**, 624 (1928); F.L. Mohler, J. Res. Natl. Bur. Stand. **19**, 447, 559 (1937); J.D. Craggs and W. Hopwood, Proc. Phys. Soc. London **59**, 771 (1947).

[1.20] E. Hinnov and J.G. Hirschberg, Phys. Rev. **125**, 795 (1962).

[1.21] N. D'Angelo, Phys. Rev. **121**, 505 (1961); D.R. Bates, A.E. Kingston and R.W.P. McWhirter, Proc. R. Soc. London **A267**, 297 (1962).

[1.22] S. Byron, R.C. Stabler and P.I. Bortz, Phys. Rev. Lett. **9**, 376 (1962); B. Makin and J.C. Keck, Phys. Rev. Lett. **11**, 281 (1963); A.V. Gurevich and L.P. Pitaevskii, Sov. Phys. JETP **19**, 870 (1964).

[1.23] D. Kleppner, M.G. Littman and M. I. Zimmerman, Sci. Am. **244**, 130 (1981).

[1.24] P. Mansbach and J. Keck, Phys. Rev. **181**, 275 (1969).

[1.25] Y.M. Aleskovskii, Sov. Phys. JETP **17**, 570 (1963); N. D'Angelo and N. Rynn, Phys. Fluids **4**, 1303 (1961); J.Y. Wada and R. C. Knechtli, Proc. IRE **49**, 1926 (1961).

[1.26] C.M. Surko, M. Leventhal and A. Passner, Phys. Rev. Lett. **62**, 901 (1989).

[1.27] G. Gabrielse, X. Fei, K. Helmerson, S.L. Rolston, R.T. Tjoelker, T.A. Trainor, H. Kalinowsky, J. Hass and W. Kells, Phys. Rev. Lett. **57**, 2504 (1986); G. Gabrielse, X. Fei, L.A. Orozco, R.L. Tjoelker, J. Haas, H. Kalinowsky, T.A. Trainor and W. Kells, Phys. Rev. Lett. **63**, 1360 (1989).

[1.28] G. Gabrielse, S.L. Rolston, L. Haarsma and W. Kells, Phys. Lett. A **129**, 38 (1988).

[1.29] G. Gabrielse, Hyperfine Interactions **44**, 349 (1988).

[1.30] R.G. Littlejohn, Phys. Fluids **24**, 1730 (1981); T.G. Northrop, *The Adiabatic Motion of Charged Particles* (Interscience, New York, 1963).

[1.31] G.E. Uhlenbeck and G.W. Ford, *Lectures in Statistical Mechanics* (American Mathematical Society, Providence, R.I., 1963).

[1.32] N.G. Van Kampen, *Stochastic Processes in Physics and Chemistry* (North-Holland, New York, 1981).

Chapter 2

Collisional Equipartition Rate for a Magnetized Plasma

2.1. Abstract

The collisional equipartition rate between the parallel and perpendicular velocity components is calculated for a weakly correlated electron plasma that is immersed in a uniform magnetic field. Here, parallel and perpendicular refer to the direction of the magnetic field. The rate depends on the parameter $\overline{\kappa} = \left(\overline{b} / r_{ce}\right) / \sqrt{2}$, where $r_{ce} = \sqrt{k_B T_e / m_e} / \Omega_{ce}$ is the cyclotron radius and $\overline{b} = 2e^2 / k_B T_e$ is twice the distance of closest approach. For a strongly magnetized plasma (i.e., $\overline{\kappa} >> 1$), the equipartition rate is exponentially small ($\nu \sim \exp\left[-5(3\pi\overline{\kappa})^{2/5} / 6\right]$). For a weakly magnetized plasma (i.e., $\overline{\kappa} << 1$), the rate is the same as for an unmagnetized plasma except that $r_{ce} / \overline{b}$ replaces $\lambda_D / \overline{b}$ in the Coulomb logarithm. (It is assumed here that $r_{ce} < \lambda_D$; for $r_{ce} > \lambda_D$, the plasma is effectively unmagnetized.) This paper contains a numerical treatment that spans the intermediate regime $\overline{\kappa} \sim 1$, and connects on to asymptotic results in the two limits $\overline{\kappa} << 1$ and $\overline{\kappa} >> 1$. Also, an improved asymptotic expression for the rate in the high field limit is derived. Our theoretical results are in good agreement with recent measurements of the equipartition rate over eight decades in $\overline{\kappa}$ and four decades in the scaled rate $\nu / n_e \overline{v} \overline{b}^2$, where n_e is the electron density and $\overline{v} = \sqrt{2k_B T_e / m_e}$.

2.2. Introduction

We consider a weakly correlated pure electron plasma that is immersed in a uniform magnetic field **B**, and is characterized by an anisotropic velocity distribution ($T_{\parallel} \neq T_{\perp}$). Here, parallel ($\parallel$) and perpendicular ($\perp$) are referred to the direction of the magnetic field. We calculate the collisional equipartition rate between the parallel and perpendicular velocity components, paying particular attention to the dependence on magnetic field strength. Formally, the rate, ν, is defined through the relation $dT_{\perp} / dt = \nu\left(T_{\parallel} - T_{\perp}\right)$, where $dT_{\perp} / dt$ is interpreted as the rate of change of the mean perpendicular kinetic energy and $\left(T_{\parallel} - T_{\perp}\right)$ is assumed to be small. In general this latter assumption is necessary for $dT_{\perp} / dt$ to be linear in $\left(T_{\parallel} - T_{\perp}\right)$.

The equipartition rate does not depend on the magnetic field strength when the characteristic cyclotron radius $r_{ce} = \sqrt{k_B T_e / m_e} / \Omega_{ce}$ is large compared to the Debye length $\lambda_D = \left(k_B T_e / 4\pi n_e e^2\right)^{1/2}$; for this case a particle orbit is nearly a straight line over the range of the shielded interaction. Here, $\Omega_{ce} = eB / m_e c$ is the cyclotron frequency, n_e is the electron density, and we have set $T_e = T_{\parallel} \approx T_{\perp}$. Since our purpose is to investigate the influence of the magnetic field on the rate, we consider only the opposite case ($r_{ce} < \lambda_D$). For this case, the rate can be written as

$$\nu = n_e \overline{\upsilon} \overline{b}^2 \, I(\overline{\kappa}), \tag{2.1}$$

where $\overline{\upsilon} = \sqrt{k_B T_e / \mu}$ is the thermal spread for the distribution of relative velocities, $\overline{b} = 2e^2 / k_B T_e$ is twice the classical distance of closest approach, and $\overline{\kappa} = \Omega_{ce} \overline{b} / \overline{\upsilon} = \left(\overline{b} / r_{ce}\right) / \sqrt{2}$ is a measure of magnetic field strength. In these definitions, $\mu = m_e / 2$ is the reduced mass, and the odd factors of 2 are introduced to match notation used previously [2.1]. The combination of factors $n_e \overline{\upsilon} \overline{b}^2$ is very nearly the equipartition

rate for an unmagnetized plasma [2.2] [i.e., $\nu = \left(\sqrt{2\pi}/15\right) n_e \bar{v} \bar{b}^2 \ln\left(\lambda_D / \bar{b}\right)$], and the function $I(\bar{\kappa})$ accounts for all dependence on magnetic field strength.

Previous theory [2.1-2.3] has provided asymptotic expressions for $I(\bar{\kappa})$ in the two limits $\bar{\kappa} >> 1$ and $\bar{\kappa} << 1$. We say that the plasma is strongly magnetized when $\bar{\kappa} >> 1$; in this limit, the collisional dynamics is constrained by a many electron adiabatic invariant (the total cyclotron action, $J = \sum_j m_e v_{j\perp}^2 / 2\Omega_{ce}$, and the equipartition rate is exponentially small {i.e., $I(\bar{\kappa}) \sim \exp\left[-5(3\pi\bar{\kappa})^{2/5}/6\right]$} [2.1]. We say that the plasma is weakly magnetized when $\bar{\kappa} << 1$; in this limit, the equipartition rate is the same as for an unmagnetized plasma [2.2], except that r_{ce} replaces λ_D in the Coulomb logarithm [2.3] [i.e., $\ln\left(\lambda_D / \bar{b}\right) \to \ln\left(r_{ce} / \bar{b}\right)$]. In our notation, this implies that $I(\bar{\kappa}) \sim \ln(\bar{\kappa})$.

This paper contains a numerical calculation that spans the intermediate regime $\bar{\kappa} \sim 1$ and matches onto asymptotic formulas in the two limits $\bar{\kappa} >> 1$ and $\bar{\kappa} << 1$. In Sec. 2.3, a Boltzmann-like collision operator is used to obtain an integral expression for the rate. This reduces the problem of calculating the rate to the problem of calculating $\Delta E_\perp$, the change in the perpendicular kinetic energy that occurs during an isolated binary collision. In general, an analytic expression for $\Delta E_\perp$ cannot be obtained. In Sec. 2.4, numerical solutions for $\Delta E_\perp$ are obtained for many initial conditions chosen at random, and the integral expression is evaluated by Monte Carlo techniques.

The paper also contains a new analytic result. In Sec. 2.5, we derive an improved asymptotic formula for the rate in the large field limit $\bar{\kappa} >> 1$. A solution for $\Delta E_\perp$ is obtained as an asymptotic expansion and is then substituted into the integral expression for the rate. After substantial algebera and some numerical integrations one obtains the large $\bar{\kappa}$ asymptotic result .

$$I(\bar{\kappa}) \cong \exp\left[-5(3\pi\bar{\kappa})^{2/5}/6\right] \left\{ \begin{array}{l} (1.83)\bar{\kappa}^{-7/15} + (20.9)\bar{\kappa}^{-11/15} + (0.347)\bar{\kappa}^{-13/15} \\ + (87.8)\bar{\kappa}^{-15/15} + (6.68)\bar{\kappa}^{-17/15} + O\left(\bar{\kappa}^{-19/15}\right) \end{array} \right\}. \qquad (2.2)$$

The exponential is the same as was obtained previously [2.1], but the algebraic factor in curly brackets is different and is more accurate. Note that the second and fourth terms enter with surprisingly large numerical coefficients; it is necessary to retain these higher order terms to obtain good agreement with the numerical results.

In recent experiments [2.4] with magnetically confined plasmas, the equipartition rate was measured over a wide range in magnetic field strength and temperature, corresponding to a range of $\overline{\kappa}$ values from $\overline{\kappa} \cong 10^{-2}$ to $\overline{\kappa} \cong 10^{2}$. Our theoretical results agree with the experimental results to within the estimated experimental error over this whole range of $\overline{\kappa}$. In fact, it was the existence of the experimental results for intermediate field strength $\overline{\kappa} \sim 1$ that motivated the theory. In addition, a previous experiment [2.5] measured the equipartition rate over a range of $\overline{\kappa}$ values from $\overline{\kappa} \cong 10^{-6}$ to $\overline{\kappa} \cong 3 \times 10^{-5}$. An extrapolation of the numerical results based on the theory of Ref. 2.3 agrees well with these additional experimental results.

2.3. Integral Expression for the Equipartition Rate

In this section, a Boltzmann-like collision operator [2.1,2.6] is used to obtain an integral expression for the equipartition rate. The reader may be surprised at the use of such an operator for a problem in plasma kinetic theory, since the operator does not include the effect of Debye shielding. Recall that Landau introduced shielding in an *ad hoc* fashion when deriving the Fokker-Planck operator from the Boltzmann operator [2.7]. However, the magnetic field produces a kind of dynamical shielding on a length scale that is shorter than the Debye length, so it is not a problem that the Boltzmann operator omits Debye shielding.

The dynamical screening is a consequence of the adiabatic invariant discussed in Ref. 2.1. For a collision in which $\Omega_{ce}\tau >> 1$, where τ is the duration of the collision, the

perpendicular kinetic energy changes by an exponentially small amount [i.e., $\Delta E_\perp \sim \exp(-\Omega_{ce}\tau)$]. The time τ is of order $\tau \sim r_m / \upsilon$, where $r_m = \min|\mathbf{r}_1 - \mathbf{r}_2|$ is the minimum separation between the two electrons during the collision and υ is a characteristic relative velocity. Thus, the quantity $\Omega_{ce}\tau \sim \Omega_{ce} r_m / \upsilon$ is large and the dynamical shielding is active when $r_m > r_{ce}$. On energetic grounds two electrons cannot get much closer than $\bar{b}$; so the dynamical shielding is active for all collisions in a plasma with $\bar{\kappa} >> 1$ (i.e., $\bar{b} >> r_{ce}$). This is the reason that the equipartition rate is exponentially small for such a plasma. Also, one can see that the most effective collisions in producing equipartition for such a plasma are close collisions (i.e., $r_m \sim \bar{b}$). Now let us turn our attention to the regime where $\bar{\kappa} < 1$ (i.e., $r_{ce} > \bar{b}$). Here, there are some collisions where the dynamical shielding is not active (and $\Delta E_\perp$ is large), but for all collisions with $r_m > r_{ce}$ the shielding is active. Consequently, these latter collisions have negligible effect. Both $\bar{b}$ and r_{ce} are assumed here to be small compared to λ_D ($\bar{b} << \lambda_D$ for a weakly correlated plasma and $r_{ce} < \lambda_D$ by hypothesis); so Debye shielding plays a negligible role.

Another way to look at this is to realize that the Rostoker collision operator [2.8] (the analog of the Lenard-Belescu operator [2.9] for a magnetized plasma) provides a correct description for the large impact parameter collisions where Debye shielding is most important. Debye shielding enters this equation through the plasma dielectric function. By using the fact that $r_{ce} << \lambda_D$, one can argue that the dielectric function is unity with a correction of order $(r_{ce} / \lambda_D)^2$. We replace the dielectric function with unity in our analysis and thereby neglect the small effect of Debye shielding.

The Boltzmann-like operator can be written as

$$\frac{\partial f}{\partial t}(\mathbf{v}_1, t) = \int_0^\infty 2\pi\rho \, d\rho \int d\mathbf{v}_2 \left|\hat{z} \bullet (\mathbf{v}_2 - \mathbf{v}_1)\right| \left[f(\mathbf{v}_1')f(\mathbf{v}_2') - f(\mathbf{v}_1)f(\mathbf{v}_2)\right], \tag{2.3}$$

where $f(\mathbf{v},t)$ is the electron velocity distribution and $\hat{z}$ is the direction of the magnetic field [2.1]. To understand the notation used, it is useful to imagine that a coordinate system is

established on electron 1 and that planes are defined at $z = \pm l$, where l is much larger than the maximum of $\bar{b}$ and r_{ce}. A collision is considered to begin when electron 2 passes into the region between the planes and to end when it passes out of the region. In the usual manner, the velocities $(\mathbf{v}_1', \mathbf{v}_2')$ evolve into $(\mathbf{v}_1, \mathbf{v}_2)$ during a collision. The quantity $\rho = |\hat{z} \times (\mathbf{r}_2 - \mathbf{r}_1)|$ is the transverse separation between the electrons at the beginning of a collision; one can think of ρ as a kind of impact parameter and of $\int 2\pi\rho \, d\rho$ as an integral over the impact parameter (or scattering cross section). The factor $|\hat{z} \bullet (\mathbf{v}_1 - \mathbf{v}_2)|$ is necessary to give the flux of electrons 2 incident on either one of the planes. Because of the magnetic field, electron 2 can interact with electron 1 only by first passing through one of the planes. Also, the dynamical shielding will provide a natural cutoff on the integral over ρ.

The rate of change of the mean perpendicular kinetic energy is given by

$$\frac{dT_\perp}{dt} = \int d\mathbf{v}_1 \, \frac{m_e v_{1\perp}^2}{2} \frac{\partial f}{\partial t}(\mathbf{v}_1, t) \tag{2.4}$$

Using Eq. (2.3) to evaluate $\partial f / \partial t$ yields the expression

$$\frac{dT_\perp}{dt} = n_e \int_0^\infty 2\pi\rho \, d\rho \int d\mathbf{v}_1 \int d\mathbf{v}_2 \, \frac{m_e v_{1\perp}^2}{2} |\hat{z} \bullet (\mathbf{v}_2 - \mathbf{v}_1)| \left[f(\mathbf{v}_1') f(\mathbf{v}_2') - f(\mathbf{v}_1) f(\mathbf{v}_2) \right], \tag{2.5}$$

where the distributions in the bracket are assumed to be of the form

$$f(\mathbf{v}) = \left(\frac{m_e}{2\pi k_B T_\parallel} \right)^{1/2} \left(\frac{m_e}{2\pi k_B T_\perp} \right) \exp\left[-\frac{m_e v_\parallel^2}{2 k_B T_\parallel} - \frac{m_e v_\perp^2}{2 k_B T_\perp} \right]. \tag{2.6}$$

By using detailed balance, Eq. (2.5) can be rewritten as

$$\frac{dT_\perp}{dt} = \frac{n_e}{4} \int_0^\infty 2\pi\rho \, d\rho \int d\mathbf{v}_1 \int d\mathbf{v}_2 \, \Delta E_\perp |\hat{z} \bullet (\mathbf{v}_2 - \mathbf{v}_1)| \left[f(\mathbf{v}_1') f(\mathbf{v}_2') - f(\mathbf{v}_1) f(\mathbf{v}_2) \right], \tag{2.7}$$

where

$$\Delta E_\perp = \frac{m_e v_{1\perp}^2}{2} + \frac{m_e v_{2\perp}^2}{2} - \frac{m_e v_{1\perp}'^2}{2} - \frac{m_e v_{2\perp}'^2}{2}, \tag{2.8}$$

is the change in the perpendicular kinetic energy that occurs during a collision.

It is useful to change variables from $(\mathbf{v}_1, \mathbf{v}_2)$ to $(\mathbf{V}, \mathbf{v})$, where $\mathbf{V} = (\mathbf{v}_1 + \mathbf{v}_2)/2$ is the center of mass velocity and $\mathbf{v} = (\mathbf{v}_2 - \mathbf{v}_1)$ is the relative velocity. First let us note that the binary dynamics separates under this change of variables. The equations of motion for the two interacting electrons are

$$\frac{d\mathbf{v}_1}{dt} + \Omega_{ce}\, \mathbf{v}_1 \times \hat{z} = \frac{e^2}{m_e} \frac{(\mathbf{r}_1 - \mathbf{r}_2)}{|\mathbf{r}_1 - \mathbf{r}_2|^3}, \tag{2.9}$$

$$\frac{d\mathbf{v}_2}{dt} + \Omega_{ce}\, \mathbf{v}_2 \times \hat{z} = \frac{e^2}{m_e} \frac{(\mathbf{r}_2 - \mathbf{r}_1)}{|\mathbf{r}_1 - \mathbf{r}_2|^3}. \tag{2.10}$$

By adding and subtracting these two equations, we obtain separate equations for the center of mass motion and for the relative motion

$$\frac{d\mathbf{V}}{dt} + \Omega_{ce}\, \mathbf{V} \times \hat{z} = 0, \tag{2.11}$$

$$\frac{d\mathbf{v}}{dt} + \Omega_{ce}\, \mathbf{v} \times \hat{z} = \frac{e^2}{\mu} \frac{\mathbf{r}}{|\mathbf{r}|^3}. \tag{2.12}$$

Here, $\mathbf{r} = \mathbf{r}_2 - \mathbf{r}_1$ is the relative position vector and $\mu = m_e/2$ is the reduced mass. The center of mass motion is simply motion in a uniform **B** field, so it follows trivially that $|\mathbf{V}_\perp'| = |\mathbf{V}_\perp|$ and $|\mathbf{V}_\parallel'| = |\mathbf{V}_\parallel|$. The solution for the relative motion is not trivial, but conservation of energy guarantees that $\mu v'^2/2 = \mu v^2/2$. From these relations and the relations

$$E_\perp \equiv \frac{m_e v_{1\perp}^2}{2} + \frac{m_e v_{2\perp}^2}{2} = \frac{\mu v_\perp^2}{2} + \frac{2\mu V_\perp^2}{2}, \tag{2.13a}$$

$$E_\parallel \equiv \frac{m_e v_{1\parallel}^2}{2} + \frac{m_e v_{2\parallel}^2}{2} = \frac{\mu v_\parallel^2}{2} + \frac{2\mu V_\parallel^2}{2}, \tag{2.13b}$$

it follows that

$$\Delta E_\perp = -\Delta E_\parallel = \Delta\left(\mu v_\perp^2 / 2\right) \tag{2.14}$$

By carrying out the change of variables and by using the relation $d\mathbf{v}_1\, d\mathbf{v}_2 = d\mathbf{V}\, d\mathbf{v}$ as well as Eqs. (2.13) and (2.14), Eq. (2.7) can be rewritten in the form

$$\frac{dT_\perp}{dt} = \frac{n_e}{4}\int_0^\infty 2\pi\rho\, d\rho \int dv\, |v_\parallel|\, \Delta\left(\frac{\mu v_\perp^2}{2}\right) f_r(v_\parallel, v_\perp) \times\left\{\exp\left[\left(\frac{1}{k_B T_\perp} - \frac{1}{k_B T_\parallel}\right)\Delta\left(\frac{\mu v_\perp^2}{2}\right)\right] - 1\right\}, \tag{2.15}$$

where the integral over $\mathbf{V}$ has been carried out and

$$f_r(v_\parallel, v_\perp) = \left(\frac{\mu}{2\pi k_B T_\parallel}\right)^{1/2}\left(\frac{\mu}{2\pi k_B T_\perp}\right)\exp\left[-\frac{\mu v_\parallel^2}{2k_B T_\parallel} - \frac{\mu v_\perp^2}{2k_B T_\perp}\right] \tag{2.16}$$

is the distribution of relative velocities. Finally, to first order in the small quantity $(T_\parallel - T_\perp)$ we obtain the rate equation $dT_\perp / dt = \nu\,(T_\parallel - T_\perp)$, where the rate ν is given by the integral expression

$$\nu = \frac{n_e}{4k_B^2 T_\parallel T_\perp}\int_0^\infty 2\pi\rho\, d\rho \int dv\, |v_\parallel|\left[\Delta\left(\frac{\mu v_\perp^2}{2}\right)\right]^2 f_r(v_\parallel, v_\perp). \tag{2.17}$$

In this expression, one may set $T_\parallel \approx T_\perp = T_e$.

2.4. Numerical Calculation of the Equipartition Rate

Eq. (2.17) reduces the problem of calculating the equipartition rate to the problem of solving Eq. (2.12) for $\Delta\left(\mu v_\perp^2 / 2\right)$. In general this equation has only two constants of the motion, the energy and the canonical angular momentum, so an analytic solution is not possible. In this section, Eq. (2.12) is solved numerically for many initial conditions chosen at random, and the integral in Eq. (2.17) is evaluated by Monte Carlo techniques.

In terms of the scaled variables

$$\mathbf{u} = \mathbf{v}/\bar{v} \quad , \quad \boldsymbol{\eta} = \mathbf{r}/\bar{b} \quad , \quad s = t\left(\bar{v}/\bar{b}\right) \tag{2.18}$$

Equation (2.12) takes the form

$$\frac{d\mathbf{u}}{ds} + \bar{\kappa}\,\mathbf{u} \times \hat{z} = \frac{1}{2}\frac{\boldsymbol{\eta}}{|\boldsymbol{\eta}|^3}, \tag{2.19}$$

where $\mathbf{u} = d\boldsymbol{\eta}/ds$, and Eq. (2.17) takes the form $\nu = n_e \bar{v}\bar{b}^2\, I(\bar{\kappa})$, where

$$I(\bar{\kappa}) = \frac{\pi}{2}\int_0^\infty \eta_\perp\, d\eta_\perp \int_0^\infty u_\perp\, du_\perp \int_{-\infty}^{\infty} du_\parallel \int_0^{2\pi} d\psi\, \frac{e^{-u^2/2}}{(2\pi)^{3/2}}\,|u_\parallel|\left[\Delta\left(u_\perp^2/2\right)\right]^2 \tag{2.20}$$

We evaluate this integral with two completely separate Monte Carlo calculations.

The first of these starts with the transformation [2.10,2.11]

$$(u_\parallel, u_\perp, \psi, \eta_\perp) \rightarrow (x_1, x_2, x_3, x_4),$$

where

$$x_1(u_\parallel) = \frac{1}{A_1}\int_0^{u_\parallel} du_\parallel \int_0^\infty d\eta_\perp \int_0^\infty du_\perp \int_0^{2\pi} d\psi\, W(u_\parallel, u_\perp, \psi, \eta_\perp), \tag{2.21a}$$

$$x_2(u_\parallel, \eta_\perp) = \frac{1}{A_2}\int_0^{\eta_\perp} d\eta_\perp \int_0^\infty du_\perp \int_0^{2\pi} d\psi\, W(u_\parallel, u_\perp, \psi, \eta_\perp), \tag{2.21b}$$

$$x_3(u_\parallel, \eta_\perp, u_\perp) = \frac{1}{A_3}\int_0^{u_\perp} du_\perp \int_0^{2\pi} d\psi\, W(u_\parallel, u_\perp, \psi, \eta_\perp), \tag{2.21c}$$

$$x_4(u_\parallel, \eta_\perp, u_\perp, \psi) = \frac{1}{A_4}\int_0^{\psi} d\psi\, W(u_\parallel, u_\perp, \psi, \eta_\perp), \tag{2.21d}$$

and

$$A_1 = \int_0^\infty du_\parallel \int_0^\infty d\eta_\perp \int_0^\infty du_\perp \int_0^{2\pi} d\psi\, W(u_\parallel, u_\perp, \psi, \eta_\perp), \tag{2.22a}$$

$$A_2(u_\parallel) = \int_0^\infty d\eta_\perp \int_0^\infty du_\perp \int_0^{2\pi} d\psi\, W(u_\parallel, u_\perp, \psi, \eta_\perp) \quad , \tag{2.22b}$$

$$A_3(u_\parallel, \eta_\perp) = \int_0^\infty du_\perp \int_0^{2\pi} d\psi\, W(u_\parallel, u_\perp, \psi, \eta_\perp) \quad , \tag{2.22c}$$

$$A_3(u_\parallel, \eta_\perp, u_\perp) = \int_0^{2\pi} d\psi\, W(u_\parallel, u_\perp, \psi, \eta_\perp) \quad . \tag{2.22d}$$

One can easily show that the Jacobian for this transformation is given by

$$\frac{\partial(x_1, x_2, x_3, x_4)}{\partial(u_\parallel, u_\perp, \psi, \eta_\perp)} = \frac{W(u_\parallel, u_\perp, \psi, \eta_\perp)}{A_1} \quad , \tag{2.23}$$

so Eq. (2.20) takes the form

$$I(\bar{\kappa}) = \frac{A_1}{2^{3/2}\sqrt{\pi}} \int_0^1 dx_1 \int_0^1 dx_2 \int_0^1 dx_3 \int_0^1 dx_4\, \frac{u_\parallel u_\perp \eta_\perp e^{-u^2/2}}{W(u_\parallel, u_\perp, \psi, \eta_\perp)} \left[\Delta\left(u_\perp^2/2\right)\right]^2 \quad . \tag{2.24}$$

If we choose

$$W(u_\parallel, u_\perp, \psi, \eta_\perp) \sim u_\parallel u_\perp \eta_\perp e^{-u^2/2} \left[\Delta\left(u_\perp^2/2\right)\right]^2 \quad , \tag{2.25}$$

the integrand in Eq. (2.24) is reasonably uniform over the whole domain of integration, and an efficient Monte Carlo evaluation of the integral can then be obtained by choosing N sample points $p_i = (x_1, x_2, x_3, x_4)_i$ at random in the domain of integration. The value of the integral is given by

$$I(\bar{\kappa}) \approx \frac{A_1}{2^{3/2}\sqrt{\pi}} \frac{1}{N} \sum_{i=1}^{N} \left[\frac{u_\parallel u_\perp \eta_\perp e^{-u^2/2} \left[\Delta\left(u_\perp^2/2\right)\right]^2}{W(u_\parallel, u_\perp, \psi, \eta_\perp)} \right]_i \quad , \tag{2.26}$$

where N is large enough that the average has converged, that is, that fluctuations in the average as N is increased are negligible.

The choice for W requires some knowledge of $\Delta\left(u_\perp^2/2\right)$, but this knowledge need not be detailed. A good choice for W is one that captures the main features of expression (2.25), but is still simple enough that the integrals in transformation (2.21) can be carried

out analytically. This provides for a reasonably rapid convergence and an efficient algorithm for choosing sample points. For the parameter regime $\bar{\kappa} > 1$, we use an expression for $\Delta\left(u_\perp^2/2\right)$ that is based on the large $\bar{\kappa}$ asymptotic analysis of Sec. 2.5, and for the parameter regime $\bar{\kappa} < 1$ we use an expression for $\Delta\left(u_\perp^2/2\right)$ that is based on integration along unperturbed orbits.

For a given set of random numbers $\left(x_1, x_2, x_3, x_4\right)_i$ the corresponding variables $\left(u_\parallel, u_\perp, \eta_\perp, \psi\right)_i$ specify the state of an incident electron when it first crosses one of the two planes at $\eta_\parallel = \pm l/\bar{b}$. Starting from this initial condition, orbit equation (2.19) is integrated forward using a Bulisch-Stoer algorithm [2.11] until the electron again crosses one of the two planes, and $\Delta\left(u_\perp^2/2\right)$ is calculated. The distance l must be chosen to be large enough that further increase in l does not significantly change the numerical result for the rate. Over most of the range in $\bar{\kappa}$, this simply means that l must be many times larger than the maximum of $\bar{b}$ and r_{ce}. However, the orbit integration is particularly time consuming in the limit of large $\bar{\kappa}$; the cyclotron frequency is much larger than the frequency characterizing the duration of a collision, and the quantity to be calculated, $\Delta\left(u_\perp^2/2\right)$, is exponentially small. Consequently, special care must be taken in this limit. The adiabatic invariant is given by an asymptotic series, the first term of which is $u_\perp^2$ [2.12]. The higher order terms are all zero at $\eta_\parallel = \pm\infty$, so $\Delta u_\perp^2$ is the change in the invariant when $\eta_\parallel$ varies from $+\infty$ to $-\infty$. However, at $\eta_\parallel = \pm l/\bar{b}$, the higher order terms are not zero. We assume that the adiabatic invariant (full asymptotic series) does not change significantly when $\eta_\parallel$ varies from $+\infty$ to $l/\bar{b}$ and then again when $\eta_\parallel$ varies from $-l/\bar{b}$ to $-\infty$. The change in $u_\perp^2$ as $\eta_\parallel$ varies from $+\infty$ to $-\infty$ (i.e., $\Delta u_\perp^2$) is then given by the change in the adiabatic invariant (full asymptotic series) as $\eta_\parallel$ varies from $l/\bar{b}$ to $-l/\bar{b}$. This latter quantity must be calculated numerically. In practice, only one higher order term is necessary to give the required accuracy.

Also, the value of $u_{\parallel}$ at $\eta_{\parallel} = l/\bar{b}$ must be related to the value of $u_{\parallel}$ at $\eta_{\parallel} = \infty$. Here, one can approximate $u_{\perp}^2$ as constant and use conservation of energy to write

$$u_{\parallel}^2(\infty) - u_{\parallel}^2(l/\bar{b}) \approx \frac{2}{\sqrt{\eta_{\perp}^2 + (l/\bar{b})^2}} \tag{2.27}$$

This correction becomes important at large values of $\bar{\kappa}$ because $\Delta(u_{\perp}^2/2)$ depends exponentially on $u_{\parallel}(\infty)$. The Monte Carlo calculated values of $I(\bar{\kappa})$ were found to be independent of reasonable changes in both the functional form of W and the parameters used in the integration of Eq. (2.19) (e.g., accuracy of the integration and the location of the plane at $l/\bar{b}$).

The integral expression for the rate was evaluated independently with a second Monte Carlo method. In this method a sample point is chosen by the rejection method [2.11], which allows the treatment of more realistic and complicated weighting functions, but is somewhat slower (particularly when the weighting function is peaked). Also, the orbit equation is solved with a fourth order Runge-Kutta algorithm [2.11]. The results for the two methods are the same to within expected statistical error for the $\bar{\kappa}$ values where both methods were applied.

Table 2.1 lists values for $I(\bar{\kappa})$ obtained with the integral transform method for $\bar{\kappa}$ values ranging from 10^{-4} to 10^{4}. The values of $I(\bar{\kappa})$ obtained by use of the rejection method are shown in Table 2.2. This data covers $\bar{\kappa}$ values from 10^{0} to 10^{3}. In Fig. 2.1 both sets of data are plotted versus $\bar{\kappa}$ and are compared to asymptotic formulas for $\bar{\kappa} >> 1$ and $\bar{\kappa} << 1$. The solid curve is the large $\bar{\kappa}$ asymptotic formula given in Eq. (2.2), and the dashed curve is the small $\bar{\kappa}$ formula $-(\sqrt{2\pi}/15)\ln(C\bar{\kappa})$ originally proposed by Montgomery, Joyce, and Turner [2.3]. Here, C is a constant which we determine numerically to be $C = 0.333(65)$.

Some words of explanation concerning the logarithmic dependence for small $\bar{\kappa}$ may be useful. For collisions characterized by $\bar{b} < r_m < r_{ce}$, where $r_m = \min|\mathbf{r}_1 - \mathbf{r}_2|$ is the

minimum separation between the particles, the change in perpendicular energy $\Delta(u_\perp^2/2)$ can be calculated by integration along unperturbed orbits, and the unperturbed orbits are nearly straight lines. Under this circumstance the distance r_m is very nearly the impact parameter as defined for a collision in an unmagnetized plasma. The contribution of these collisions to the integral expression for $I(\bar{\kappa})$ is $\left(\sqrt{2\pi}/15\right)\int dr_m/r_m$, which is logarithmically divergent. In our numerical treatment the divergence is cut off at the upper end (i.e., $r_m \sim r_{ce}$) by dynamical shielding and at the lower end (i.e., $r_m \sim \bar{b}$) by the repulsion of like charges. At the lower end, integration along unperturbed orbits breaks down. The previous work [2.3] is based on integration along unperturbed orbits taking into account the magnetic field, so the upper cutoff arises naturally but the lower cutoff must be imposed in an *ad hoc* manner. The imposition of either cutoff in an *ad hoc* manner introduces an uncertainty in the argument of the logarithm, that is, the factor C is not determined. In our numerical treatment, the dynamics automatically provides both cutoffs, so the constant C is determined. The value $C = 0.333(65)$ is obtained by matching $-\left(\sqrt{2\pi}/15\right)\ln(C\bar{\kappa})$ to the numerical results for $\bar{\kappa} \le 10^{-2}$. This fit curve is then found to agree with the Monte Carlo results to within statistical error over an even larger range, $\bar{\kappa} \le 1$.

The numerical results match onto both asymptotic results quite well. From Fig. 2.1, one can see that the numerical results track the logarithmic dependence for $\bar{\kappa} << 1$ and fall off exponentially in accord with the asymptotic formula for $\bar{\kappa} >> 1$. To make a more detailed comparison of the numerical results and the large $\bar{\kappa}$ asymptotic formula, we factor out the exponential dependence and plot $I(\bar{\kappa})\exp\left[5(3\pi\bar{\kappa})^{3/5}/6\right]$ versus $\bar{\kappa}$. In Fig. 2.2, the points are numerical results, the solid curve is the new asymptotic formula given in Eq. (2.2), and the dashed curve is the previous asymptotic formula [2.1]. One can see that the new formula is in much better agreement with the numerical results.

Figure 2.3 shows a comparison of our numerical results to measured values of the equipartition rate. The solid curve is an interpolation of the Monte Carlo values for $I(\overline{\kappa})$, and the dashed curve is an extrapolation using the asymptotic formula $I(\overline{\kappa}) = -\left(\sqrt{2\pi}/15\right)\ln\left[(0.333)\overline{\kappa}\right]$. The points are experimental values for $\nu / n_e \overline{v} \overline{b}^2$, which according to theory should equal $I(\overline{\kappa})$. The squares, crosses, and diamonds are results obtained by Beck, Fajans, and Malmberg [2.4] on a magnetically confined pure electron plasma that is cooled to the cryogenic temperature range by cyclotron radiation. The rate was measured for three magnetic field strengths (30 kG, 40 kG, and 60 kG corresponding to the squares, crosses, and diamonds respectively) and for a series of temperatures ranging from 30 K to 10^4 K; this corresponds to a range of $\overline{\kappa}$ values from 10^{-2} to 10^2. The electron density was near $n_e = 8 \times 10^8 / \mathrm{cm}^3$. There is quite good overall agreement between the theory and the experiment; the discrepancy between the measured values and the theory at large $\overline{\kappa}$ may be due to a 30% systematic error in the temperature measurement. Such an error is large enough to account for the discrepancy and would not be unreasonable for the diagnostic procedure used. Finally, the circles are results obtained by Hyatt, Driscoll, and Malmberg [2.5] from a closely related set of experiments also done with a magnetically confined pure electron plasma, but in an apparatus that is at room temperature with a magnetic field of 280 G. The full data set, enlarged by the room temperature experimental data, allows us to compare theory and experiment over a range of eight decades in $\overline{\kappa}$.

2.5. Asymptotic Expression for the Equipartition Rate in the Limit $\overline{\kappa} >> 1$

In this section, we obtain the improved asymptotic formula for $I(\overline{\kappa})$ in the large $\overline{\kappa}$ limit that was written down in Eq. (2.2). As was mentioned earlier, the exponential

dependence is the same as was obtained previously [2.1], but the algebraic factor is different and more accurate; it is correct to higher order as an asymptotic expansion based on the smallness of $1/\bar{\kappa}$. The second and fourth terms in the expansion enter with surprisingly large numerical coefficients, and the first term does not dominate until $\bar{\kappa} > 10^5$, which is beyond the largest value of $\bar{\kappa}$ considered in the numerical calculations. It is necessary to retain the higher order terms to get good agreement with the numerical results. We believe that the numerical coefficients in the expansion are reasonably accurate, but further refinement of the calculation would lead to some modification of these coefficients.

The first step is to obtain a more accurate asymptotic result for the energy exchange $\Delta E_\perp$. To this end we rewrite Eq. (2.12) for the relative motion in Hamiltonian form by using

$$H(r,p_r;z,p_z;\theta,p_\theta)=\frac{\left(p_\theta-\frac{\mu\Omega_{ce}}{2}r^2\right)^2}{2\mu r^2}+\frac{p_r^2}{2\mu}+\frac{p_z^2}{2\mu}+\frac{e^2}{\sqrt{r^2+z^2}}, \tag{2.28}$$

where (r,θ,z) are cylindrical coordinates and (p_r,p_θ,p_z) are the conjugate momenta. Since θ is cyclic, p_θ is a constant of the motion. We can reduce the degrees of freedom to two and write the Hamiltonian as

$$H(r,p_r;z,p_z)=\frac{p_r^2}{2\mu}+\frac{p_z^2}{2\mu}+V(r,z), \tag{2.29}$$

where

$$V(r,z)\equiv\frac{\mu\Omega_{ce}^2}{8}\left(r^2-2r_0^2+\frac{r_0^4}{r^2}\right)+\frac{e^2}{\sqrt{r^2+z^2}} \tag{2.30}$$

and $r_0\equiv\sqrt{2p_\theta/(\mu\Omega_{ce})}$. It is useful to approximate $V(r,z)$ as a harmonic potential in r at constant z by Taylor expanding; this gives

$$V(r,z) \approx V_g(z) + \frac{\mu\,\Omega^2(z)}{2}\left[r - r_g(z)\right]^2 , \tag{2.31}$$

where

$$\left.\frac{\partial V}{\partial r}\right|_{r=r_g} = 0 \quad , \quad V_g(z) = V\left[r_g(z), z\right]$$

and

$$\Omega^2(z) = \frac{1}{\mu}\left.\frac{\partial^2 V}{\partial r^2}\right|_{r=r_g} .$$

As z goes to infinity $\Omega(z)$ approaches Ω_{cc} and $r_g(z)$ approaches r_0. One can identify $r_g(z)$ as the guiding center, $V_g(z)$ as the potential at the guiding center and $\Omega(z)$ as the effective cyclotron frequency.

We have neglected terms in the Taylor expansion of $V(r,z)$ that are of higher than quadratic order in $\left(r - r_g\right)$. It is found in the appendix that the cubic term in the Taylor expansion contributes to terms of order $\bar{\kappa}^{-17/15}$. These terms are not significant when the asymptotic expression is compared to the numerical results.

It is useful to change independent variables from t to z. This is effected by using Hamilton's principle [2.13]

$$0 = \delta\int_{t_1}^{t_2}\left[p_r\frac{dr}{dt} + p_z\frac{dz}{dt} - H\right]dt = \delta\int_{z_1}^{z_2}\left[p_r\frac{dr}{dz} + p_z\frac{dz}{dz} - H\right]dz \tag{2.32}$$

One can identify the new Hamiltonian as

$$H'(r,p_r;z) = -p_z = \mp\sqrt{2\mu\left\{H - V_g(z) - \frac{\mu\,\Omega^2(z)}{2}\left[r - r_g(z)\right]^2 - \frac{p_r^2}{2\mu}\right\}} , \tag{2.33}$$

where $\left(r, p_r\right)$ and $\left(t, -H\right)$ are canonically conjugate coordinates and momenta. Since there is no explicit t-dependence in H', the momentum H is a constant of the motion.

By using the generating function

$$S(P,r;z)=\int_{r'=r_g}^{r}\mu\Omega\sqrt{\frac{2}{\mu\Omega}P-\left(r'-r_g\right)^2}\,dr' \tag{2.34}$$

we introduce the action angle variables

$$P=\frac{1}{2\pi}\oint p_r\,dr=\frac{H-V_g-\dfrac{p_z^2}{2\mu}}{\Omega} \tag{2.35a}$$

and

$$\psi=\sin^{-1}\left[\sqrt{\frac{\mu\Omega}{2P}}\left(r-r_g\right)\right], \tag{2.35b}$$

and obtain the new Hamiltonian $H''=-p_z+\partial S/\partial z\big|_{r,P}$. The generating function can be rewritten as

$$S(\psi,P)=P\sin\psi\cos\psi+P\psi \tag{2.36}$$

so the needed partial derivative is given by

$$\left.\frac{\partial S}{\partial z}\right|_{r,P}=2P\cos^2\psi\left.\frac{\partial\psi}{\partial z}\right|_{r,P}, \tag{2.37}$$

where $\partial\psi/\partial z\big|_{r,P}\cos\psi$ is easily evaluated from $\sin\psi=\sqrt{\mu\Omega/2P}\left(r-r_g\right)$. The new Hamiltonian is then

$$H''(P,\psi;z)=\mp\sqrt{2\mu\left(H-V_g-\Omega P\right)}-\sqrt{2\mu\Omega P}\frac{dr_g}{dz}\cos\psi+\frac{P}{2}\sin 2\psi\frac{d(\ln\Omega)}{dz}. \tag{2.38}$$

We need to solve Hamilton's equations

$$\frac{dP}{dz}=-\sqrt{2\mu\Omega P}\frac{dr_g}{dz}\sin\psi-P\cos 2\psi\frac{d(\ln\Omega)}{dz}, \tag{2.39a}$$

$$\frac{d\psi}{dz}=\mp\frac{\mu\Omega}{\sqrt{2\mu\left(H-V_g-\Omega P\right)}}-\sqrt{\frac{\mu\Omega}{2P}}\frac{dr_g}{dz}\cos\psi+(1/2)\sin 2\psi\frac{d(\ln\Omega)}{dz} \tag{2.39b}$$

in order to obtain the energy exchange $\Delta E_\perp=\Omega_{ce}\Delta P$, and to this end we introduce a perturbative expansion

$$P = P^{(0)} + P^{(1)} + \cdots$$

and

$$\psi = \psi^{(0)} + \psi^{(1)} + \cdots$$

The expansion parameter is r_* / z, where $r_*^3 = mc^2 / B^2 = r_{ce}^2 \bar{b}$. During the collision, the expansion parameter gets no larger than $r_* / \bar{b} \sim \left(v_{\|0} / \Omega_{ce} \bar{b}\right)^{2/3} << 1$. However, we will deform the z-contour used to evaluate $\Delta E_\perp$ from the true trajectory to one which encircles the branch point of the integrand. On the deformed contour, r_* / z will be of order unity. Although the contribution of higher order $\Delta P^{(j)}$ will not be algebraically smaller, they will be numerically smaller. We refer one to the appendix where we show that $\Delta P^{(j)} \sim 1/\left[(2/3)(j-1)\right]!$.

Turning our attention to finding the equations for $P^{(j)}$ and $\psi^{(j)}$, we first note that dr_g / dz and $d\Omega / dz$ are both of fourth order in the expansion parameter. This implies, in conjunction with Eqs. (2.39), that $dP^{(j)} / dz = 0$ and $d\psi^{(j)} / dz = 0$ if $j \neq 0,4,8,\cdots$. In addition one can see that $dP^{(0)} / dz = 0$,

$$\frac{dP^{(4)}}{dz} = -\sqrt{2\mu\Omega P^{(0)}}\,\frac{dr_g}{dz}\sin\psi^{(0)} - P^{(0)}\cos 2\psi^{(0)}\,\frac{d(\ln\Omega)}{dz}, \tag{2.40a}$$

and

$$\frac{d\psi^{(0)}}{dz} = \mp\frac{\mu\Omega}{\sqrt{2\mu\left(H - V_g - \Omega P^{(0)}\right)}}. \tag{2.40b}$$

Since $dP^{(0)} / dz = 0$, we can set $P^{(0)} = P_0$, the precollision value. We will want to integrate Eq. (2.40a) to find $\Delta P^{(4)}$. The first term on the right-hand side of Eq. (2.40a) gives a contribution to $\Delta P^{(4)}$ of the form of an integral of $e^{i\psi^{(0)}}$ times a slowly varying function of $\psi^{(0)}$. The second term gives an integral of $e^{2i\psi^{(0)}}$ times a slowly varying function of $\psi^{(0)}$. This is an exponentially smaller contribution to $\Delta P^{(4)}$ compared to the first term. Hence we drop the second term on the right-hand side and write

$$\frac{dP^{(4)}}{dz} = -\sqrt{2\mu\Omega P_0}\,\frac{dr_g}{dz}\sin\psi^{(0)}, \tag{2.41a}$$

and

$$\frac{d\psi^{(0)}}{dz} = \mp\frac{\mu\Omega}{\sqrt{2\mu\left(H - V_g - \Omega P_0\right)}}. \tag{2.41b}$$

Since $\Delta P^{(0)} = 0$ over the course of a collision, we let $\Delta P \approx \Delta P^{(4)}$ with an estimated error of order $\Delta P^{(8)} / \Delta P^{(4)} \sim 2! / (14/3)! \approx 10^{-2}$. Integration of Eq. (2.41b) gives

$$\psi^{(0)} = \psi_0 + \alpha \mp \beta(z) \tag{2.42}$$

where ψ_0 is the initial gyro angle, α is the constant

$$\alpha \equiv \pm\int_{z_T}^{z_0} \frac{\mu\Omega\, dz}{\sqrt{2\mu\left(H - V_g - \Omega P_0\right)}}, \tag{2.43}$$

z_T is the turning point where $H = V_g(z_T) + P_0\,\Omega(z_T)$, and

$$\beta(z) \equiv \int_{z_T}^{z} \frac{\mu\Omega(z')\, dz'}{\sqrt{2\mu\left(H - V_g(z') - \Omega(z')P_0\right)}}. \tag{2.44}$$

Substitution of the expression for $\psi^{(0)}$ given in Eq. (2.42) into Eq. (2.41a) and integration along the contour shown in Fig. 2.4 gives

$$\Delta^2 E_\perp \approx \Omega_{ce}^2\,\Delta^2 P^{(4)} = 4P_0\Omega_{ce}^2 D\cos^2\left(\psi_0 + \alpha\right), \tag{2.45}$$

where

$$D \equiv \left|\int_C e^{i\beta(z)}\sqrt{\frac{\mu\Omega(z)}{2}}\,\frac{dr_g(z)}{dz}\,dz\right|^2. \tag{2.46}$$

The character of contour integral (2.46) is what one normally encounters when dealing with the breaking of adiabatic invariants. [2.14] When evaluated along the curve in Fig. 2.4 (i.e., along the true z-trajectory), the integrand consists of a slowly varying factor $\sqrt{\Omega}\, dr_g / dz$ times a rapid oscillating factor $e^{i\beta}$. To evaluate such an integral, one deforms

the contour into the complex plane so that the rapid oscillating factor becomes exponentially small. This continuation is extended until a singularity of the integrand is encountered, as shown in Fig. 2.5. For our case, the scale length for this singularity is the larger of r_* and r_0. One can identify these as the germaine length scales by determining on what length scale the two terms on the right hand side of Eq. (2.30), the expression for $V(r,z)$, are of the same order of magnitude.

In the appendix we find $\beta(z)$ as a power series expansion in $\left(\upsilon_{\|0}/\Omega_{ce}\bar{b}\right)^{2/3}$ and $\left(\upsilon_{\perp 0}/\upsilon_{\|0}\right)^2$ whose coefficients are functions of r_0/r_*. Since both $\upsilon_{\|0}/\Omega_{ce}\bar{b} << 1$ and $\upsilon_{\perp 0}/\upsilon_{\|0} << 1$ when the integrand in Eq. (2.20) gives a significant contribution to $I(\bar{\kappa} >> 1)$; we can expand $e^{i\beta}$ in a power series. This series is substituted into Eq. (2.46), the contour integral done and the result squared to obtain $\Delta^2 E_\perp$. We then substitute the power series for $\Delta^2 E_\perp$ into Eq. (2.20) and do the integrals to obtain the asymptotic expression shown in Eq. (2.2).

2.6. APPENDIX: Evaluation of the Integrals in the Asymptotic Expression for $I(\bar{\kappa})$

To evaluate the expression for $\Delta E_\perp$ found in Eq. (2.45), it is convenient to introduce the variables $\zeta \equiv \left(\upsilon_{\perp 0}/\upsilon_{\|0}\right)^2$, $\varepsilon \equiv \left(\Omega_{ce} b_\| / \upsilon_{\|0}\right)^{-2/3}$, $\gamma \equiv \left(r_0/r_*\right)^{3/2}$, and $t \equiv \left(z/r_*\right)$; where $b_\| \equiv 2e^2/\mu\upsilon_{\|0}^2$ and $r_*^3 \equiv 2\mu c^2/B^2$. We also define the functions

$$f(\gamma;\tilde{t}) \equiv \frac{r_s}{r_0}, \tag{2.A1}$$

$$h(\gamma;\tilde{t}) \equiv \left(\frac{\Omega}{\Omega_{ce}}\right)^2, \tag{2.A2}$$

$$g(\gamma;\tilde{t}) \equiv \varepsilon t \left(\frac{V_g}{\mu v_{t0}^2 / 2} \right), \tag{2.A3}$$

and

$$\bar{g}(\gamma,\zeta;\tilde{t}) \equiv \frac{g(\gamma;\tilde{t})}{1+\zeta\left[1-h^{1/2}(\gamma;\tilde{t})\right]}. \tag{2.A4}$$

The functions can all be expressed as convergent power series in $\tilde{t} \equiv 1/t$ for $t >> \max\left(1, \gamma^{2/3}\right)$. Equation (2.46) can now be rewritten as

$$D = \frac{\mu \Omega_{ce} r_0^2}{2} \left| \int_C \exp\left[i\beta(\gamma,\zeta;\tilde{t}) \right] h^{1/4}(\gamma;\tilde{t}) \frac{df(\gamma;\tilde{t})}{dt} dt \right|^2, \tag{2.A5}$$

where

$$i\beta(\gamma,\zeta;\tilde{t}) = \int_{t'=t_T}^{t} \frac{h^{1/2}(\gamma;\tilde{t}')\, g^{-1/2}(\gamma;\tilde{t}')\, (t')^{1/2}\, dt'}{\sqrt{1-\varepsilon t' \bar{g}^{-1}(\gamma,\zeta;\tilde{t}')}}, \tag{2.A6}$$

$\bar{g}\left(\gamma,\zeta;\tilde{t}_T\right) = \varepsilon t_T$, and the contour C is shown in Fig. 2.A1.

Let us first work on the evaluation of integral in the definition of $i\beta$. Make the change of variable from t to s defined by

$$s \equiv \varepsilon t\, \bar{g}^{-1}(\gamma,\zeta;\tilde{t}), \tag{2.A7}$$

The function $\bar{g}^*$ is defined to be the inverse of $\bar{g}$, that is,

$$\tilde{s} = \tilde{t}\ \bar{g}(\gamma,\zeta;\tilde{t}) \tag{2.A8}$$

is equivalent to

$$\tilde{t} = \tilde{s}\ \bar{g}^*(\gamma,\zeta;\tilde{s}), \tag{2.A9}$$

where $\tilde{s} \equiv \varepsilon / s$. Since we can expand $\bar{g}$ in a convergent power series in $\tilde{t}$, we can do a series inversion to find the power series for $\bar{g}^*$. This allows us to write Eq. (2.A6) in the form

$$i\beta = -\varepsilon^{-3/2}\int_{s=\delta}^{1}\left[\frac{h\left[\gamma;\tilde{s}\,\overline{g}^{*}(\gamma,\zeta;\tilde{s})\right]}{1+\zeta\left\{1-h^{1/2}\left[\gamma;\tilde{s}\,\overline{g}^{*}(\gamma,\zeta;\tilde{s})\right]\right\}}\right]^{1/2} \times\left[\overline{g}^{*}(\gamma,\zeta;\tilde{s})\right]^{-2}\left\{\overline{g}^{*}(\gamma,\zeta;\tilde{s})+\tilde{s}\frac{d\overline{g}^{*}(\gamma,\zeta;\tilde{s})}{d\tilde{s}}\right\}\frac{s^{1/2}ds}{\sqrt{1-s}}, \quad (2.A10)$$

where $\delta \equiv \varepsilon t\,\overline{g}^{-1}(\gamma,\zeta;\tilde{t})$. The part of the integrand written as a function of $\tilde{s}$ can be expanded into a power series in $\tilde{s}$ with the expansion coefficients $a_n(\gamma,\zeta)$. Substituting this power series into Eq. (2.A10) and exchanging the summation and integration gives us

$$i\beta = -\varepsilon^{-3/2}\sum_{n=0}^{\infty}a_n(\gamma,\zeta)\,\varepsilon^n\int_{s=\delta}^{1}\frac{s^{1/2-n}ds}{\sqrt{1-s}}. \quad (2.A11)$$

The integral can be done by changing the variable of integration to $u \equiv (1-s)/(1-\delta)$ and applying the integral representation of the hypergeometric function [2.15]

$${}_2F_1(a,b;c;z) = \frac{\Gamma(c)}{\Gamma(b)\,\Gamma(c-b)}\int_0^1 s^{b-1}\,(1-s)^{c-b-1}\,(1-zs)^{-a}\,ds, \quad (2.A12)$$

leaving us with

$$i\beta = -\varepsilon^{-3/2}\sum_{n=0}^{\infty}a_n(\gamma,\zeta)\,\varepsilon^n\,2\,(1-\delta)^{1/2}\;{}_2F_1\left(-\frac{1}{2}+n,\frac{1}{2};\frac{3}{2};1-\delta\right). \quad (2.A13)$$

Application of the linear transformation formula [2.15]

$${}_2F_1(a,b;c;z) = \frac{\Gamma(c)\,\Gamma(c-a-b)}{\Gamma(c-a)\,\Gamma(c-b)}\;{}_2F_1(a,b;a+b-c+1;1-z) + (1-z)^{c-a-b}\frac{\Gamma(c)\,\Gamma(a+b-c)}{\Gamma(a)\,\Gamma(b)}\;{}_2F_1(c-a,c-b;c-a-b+1;1-z), \quad (2.A14)$$

and use of the fact that $a_0 = 1$ and $a_1 = 0$ yields

$$i\beta = -\frac{\pi\kappa}{2} - \sum_{n=0}^{\infty}a_n(\gamma,\zeta)\,\varepsilon^{n-3/2}\,\delta^{3/2-n}\,(1-\delta)^{1/2}\,\frac{2}{2n-3}\;{}_2F_1\left(2-n,1;\frac{5}{2}-n;\delta\right), \quad (2.A15)$$

where $\kappa \equiv \varepsilon^{-3/2}$. Expanding $(1-\delta)^{1/2}\,{}_2F_1\left(2-n,1;\frac{5}{2}-n;\delta\right)$ in a power series in δ and substituting $\delta = \varepsilon t\overline{g}^{-1}$ gives

$$i\beta = -\frac{\pi K}{2} - \sum_{k=0}^{\infty} \varepsilon^k t^{k+3/2} \sum_{n=0}^{\infty} a_n(\gamma,\zeta)\, b_{nk}\, \tilde{t}^n \left[\bar{g}(\gamma,\zeta;\tilde{t})\right]^{n-k-3/2} , \tag{2.A16}$$

where

$$b_{nk} \equiv \frac{2}{2n-3} \sum_{m=0}^{k} \frac{(2-n)_{k-m}(-1/2)_m}{(5/2-n)_{k-m}\, m!} . \tag{2.A17}$$

As a last step, expand $(\bar{g})^{n-k-3/2}$ in a power series such that

$$\left[\bar{g}(\gamma,\zeta;\tilde{t})\right]^{j-3/2} = \sum_{i=0}^{\infty} c_{ji}(\gamma,\zeta)\, \tilde{t}^i \tag{2.A18}$$

and define

$$F_k(\gamma,\zeta;\tilde{t}) \equiv -\sum_{i=0}^{\infty} d_{ki}(\gamma,\zeta)\, \tilde{t}^i , \tag{2.A19}$$

where

$$d_{ki}(\gamma,\zeta) \equiv \sum_{n=0}^{i} a_n(\gamma,\zeta)\, b_{nk}\, c_{n-k,i-n}(\gamma,\zeta) \tag{2.A20}$$

One can further reduce F_k to the form

$$F_k(\gamma,\zeta;\tilde{t}) = \sum_{l=0}^{k} F_{kl}(\gamma;\tilde{t}) \left(\frac{\zeta}{t^3}\right)^l , \tag{2.A21}$$

because of the structure of $d_{ki}(\gamma,\zeta)$. The structure was found by use of the symbolic algebra package Mathematica for $k = 0,1,\cdots,4$. Since we only use $k = 0,1,2$ terms, such a reduction in F_k is justified for our purposes. This gives us the final form for $i\beta$, namely

$$i\beta = -\frac{\pi K}{2} - \sum_{k=0}^{\infty} \sum_{l=0}^{k} \varepsilon^k\, \zeta^l\, t^{k-3l+3/2}\, F_{kl}(\gamma;\tilde{t}) \tag{2.A22}$$

Now substitute $i\beta$ into Eq. (2.A5) to get

$$D = \frac{\mu \Omega_{ce} r_0^2}{2} e^{-\pi\kappa} \left|J(\varepsilon,\zeta;\gamma)\right|^2 , \tag{2.A23}$$

where we have defined

$$J(\varepsilon,\zeta;\gamma)\equiv\int_C \exp\left[\sum_{k=0}^{\infty}\sum_{l=0}^{k}\varepsilon^k\zeta^l t^{k-3l+3/2}\,F_{kl}(\gamma;\tilde{t})\right] h^{1/4}(\gamma;\tilde{t})\frac{df(\gamma;\tilde{t})}{dt}dt \quad . \tag{2.A24}$$

For large values of the magnetic field, we will only need to know J where $\varepsilon,\zeta<<1$. Therefore, we can expand the exponential to give

$$J(\varepsilon,\zeta;\gamma)=\sum_{k=0}^{\infty}\sum_{l=0}^{k}\varepsilon^k\zeta^l\,B_{kl}(\gamma) \quad , \tag{2.A25}$$

where

$$B_{kl}(\gamma)\equiv\int_C G_{kl}(\gamma;\tilde{t})\exp\left[t^{3/2}F_{00}(\gamma;\tilde{t})\right] h^{1/4}(\gamma;\tilde{t})\frac{df(\gamma;\tilde{t})}{dt}dt \quad , \tag{2.A26}$$

and

$$G_{00}(\gamma;\tilde{t})\equiv 1 \quad , \tag{2.A27a}$$

$$G_{10}(\gamma;\tilde{t})\equiv t^{5/2}\,F_{10}(\gamma;\tilde{t}) \quad , \tag{2.A27b}$$

$$G_{20}(\gamma;\tilde{t})\equiv t^{7/2}\,F_{20}(\gamma;\tilde{t})+\frac{1}{2}t^5\,F_{10}^2(\gamma;\tilde{t}) \quad , \tag{2.A27c}$$

$$G_{11}(\gamma;\tilde{t})\equiv t^{-1/2}\,F_{11}(\gamma;\tilde{t}) \quad , \tag{2.A27d}$$

etc. This will allow us to write

$$\gamma^2\left|J(\varepsilon,\zeta;\gamma)\right|^2=\sum_{k=0}^{\infty}\sum_{l=0}^{k}\varepsilon^k\zeta^l\,A_{kl}(\gamma) \quad , \tag{2.A28}$$

where

$$A_{00}(\gamma)\equiv B_{00}^2(\gamma)\,\gamma^2 \quad , \tag{2.A29a}$$

$$A_{10}(\gamma)\equiv 2\,B_{10}(\gamma)\,B_{00}(\gamma)\,\gamma^2 \quad , \tag{2.A29b}$$

$$A_{20}(\gamma)\equiv\left[2\,B_{20}(\gamma)\,B_{00}(\gamma)+B_{10}^2(\gamma)\right]\gamma^2 \quad , \tag{2.A29c}$$

$$A_{11}(\gamma)\equiv 2\,B_{11}(\gamma)\,B_{00}(\gamma)\,\gamma^2 \quad , \tag{2.A29d}$$

etc. Finally we can write the change in the perpendicular energy as

$$\Delta^2 E_\perp = \left(\mu v_{\perp 0}^2\right)\left(\frac{2e^2}{r_0}\right)\cos^2(\psi_0+\alpha)\, e^{-\pi\kappa}\sum_{k=0}^{\infty}\sum_{l=0}^{k}\epsilon^k \zeta^l\, A_{kl}(\gamma) \tag{2.A30}$$

We substitute this expression into Eq. (2.20) to obtain

$$I(\overline{\kappa}) = \frac{1}{9\sqrt{2\pi}}\sum_{k=0}^{\infty}\sum_{l=0}^{k}\left[\int_0^\infty \frac{d\gamma}{\gamma^{1/3}} A_{kl}(\gamma)\right]\left[\int_0^\infty u_\perp^{2l+3} e^{-u_\perp^2/2} du_\perp\right]\left[\int_0^{2\pi} d\psi \cos^2(\psi+\alpha)\right]$$
$$\left[\overline{\kappa}^{-2l/3}\int_0^\infty d\kappa\, \kappa^{-5/3+(2/3)(l-k)} \exp\left\{-\pi\kappa - \frac{1}{2}\left(\frac{\overline{\kappa}}{\kappa}\right)^{2/3}\right\}\right]. \tag{2.A31}$$

Defining $A_{kl} \equiv \int_0^\infty \frac{d\gamma}{\gamma^{1/3}} A_{kl}(\gamma)$ and doing the γ, $u_\perp$ and ψ integrals gives

$$I(\overline{\kappa}) = \frac{\sqrt{2\pi}}{9}\sum_{k=0}^{\infty}\sum_{l=0}^{k} A_{kl}\, 2^l\, \Gamma(l+2)\, \overline{\kappa}^{-2l/3}\left[\int_0^\infty d\kappa\, \kappa^{-5/3+(2/3)(l-k)} \exp\left\{-\pi\kappa - \frac{1}{2}\left(\frac{\overline{\kappa}}{\kappa}\right)^{2/3}\right\}\right]. \tag{2.A32}$$

Evaluation of the κ integral via the method of steepest descent as $\overline{\kappa} \to \infty$ leads us to the asymptotic series

$$I(\overline{\kappa}) \underset{\overline{\kappa}\to\infty}{\to} e^{-(5/6)(3\pi\overline{\kappa})^{2/5}}\frac{\sqrt{2\pi}}{9}\sum_{k=0}^{\infty}\sum_{l=0}^{k}\sum_{n=0}^{\infty}$$
$$A_{kl}\, 2^l\, \Gamma(l+2)\, \Gamma(n+1/2)\, e_{2n}[5/3+(2/3)(k-l)]\, \overline{\kappa}^{-7/15-(2/15)(2k+3l+3n)}, \tag{2.A33}$$

where

$$\omega^2 \equiv \frac{\pi}{x} + \frac{1}{2}x^{2/3} - \frac{5}{6}(3\pi)^{2/5} \tag{2.A34}$$

and

$$\frac{dx}{d\omega}x^{\beta-2} = \sum_{k=0}^{\infty} e_k(\beta)\,\omega^k \tag{2.A35}$$

Keeping terms to order $\overline{\kappa}^{-19/15}$, one finds that

$$I(\bar{\kappa})\, e^{(5/6)(3\pi\bar{\kappa})^{2/3}} \underset{\bar{\kappa}\to\infty}{\to} \left\{ \begin{array}{l} \dfrac{2\pi(3\pi)^{1/5}}{3\sqrt{5}} A_{00}\, \bar{\kappa}^{-7/15} + \dfrac{2\pi(3\pi)^{3/5}}{3\sqrt{5}} A_{10}\, \bar{\kappa}^{-11/15} \\ + \dfrac{14(3\pi)^{1/5}}{135\sqrt{5}} A_{00}\, \bar{\kappa}^{-13/15} + \dfrac{2\pi^2}{\sqrt{5}} A_{20}\, \bar{\kappa}^{-15/15} \\ + \dfrac{8(3\pi)^{6/5}}{135\sqrt{5}} \left(7A_{10} + 15A_{11}\right) \bar{\kappa}^{-17/15} + O\left(\bar{\kappa}^{-19/15}\right) \end{array} \right\}. \tag{2.A36}$$

We have now reduced the problem to that of finding a numerical value for the A_{kl}. We do this by first finding the power series expansions for the functions f, h, and g to $30th$ order in $\tilde{t}$ with the help of the symbolic algebra package Mathematica. The large number of terms were needed to obtain accuracy in the A_{kl} of at least one part in 10^4. It is then a straightforward process to find power series expansions for the $F_{kl}(\gamma;\tilde{t})$, to substitute them into the integral expressions for $B_{kl}(\gamma)$ given in Eq. (2.A26), then to numerically evaluate the integrals along the contour shown in Fig. 2.A2. We choose this particular deformation of the contour to reduce the oscillations of the factor $\exp\left[t^{3/2}F_{00}(\gamma;\tilde{t})\right]$ in the integrand. We cannot take the contour any closer to the origin than $\max\left(1,\gamma^{2/3}\right)$ because of singularities in the integrand which are manifested by the series expansions no longer converging. Once the γ dependence of $B_{kl}(\gamma)$ is found by doing many numerical integrations of Eq. (2.A26), each for a different value of γ; we obtain a graph of $A_{kl}(\gamma)$ by the simple algebraic combination of the $B_{kl}(\gamma)$ given in Eqs. (2.A29). The results are shown in Fig. 2.A3 which displays all the $A_{kl}(\gamma)$ needed to evaluate $I(\bar{\kappa})$ to $\bar{\kappa}^{-19/15}$ order. All four displayed functions have the same basic functional form: they peak at $\gamma \sim 1$, scale as γ^2 at small values of γ, and go to zero exponentially in γ at large values of γ. It is now a simple matter to numerically integrate these functions to find A_{kl}. When the results are substituted into Eq. (2.A36) we are left with the asymptotic formula for $I(\bar{\kappa})$ shown in Eq. (2.2).

We now turn our attention to an estimation of the error we are making by only calculating $\Delta P^{(4)}$. This is most easily seen by examining the expression for $B_{kl}(\gamma)$ given in Eq. (2.A26). Since the A_{kl} are just integrated algebraic combinations of the $B_{kl}(\gamma)$, this is

sufficient to estimate the error of the A_{kl}. We start by noting that the integral for $B_{kl}(\gamma)$ is of the form

$$B_{kl}(\gamma) \sim \int_C e^{i\tilde{t}^{3/2}} \tilde{t}^{-4+n_{kl}} dt \tag{2.A37}$$

where $G_{kl}(\gamma;\tilde{t}) \sim \tilde{t}^{n_{kl}}$ as $\tilde{t} \to 0$. The n_{kl} can easily be found by examination of the expressions for $G_{kl}(\gamma;\tilde{t})$ given in Eqs. (2.A27). One should remember that $F_{kl}(\gamma;\tilde{t}) \sim 1$, $h(\gamma;\tilde{t}) \sim 1$, and $df(\gamma;\tilde{t})/d\tilde{t} \sim \tilde{t}^4$ as $\tilde{t} \to 0$. This will aid one in finding the values of n_{kl} and the form of Eq. (2.A37). The fact that $df/d\tilde{t} \sim \tilde{t}^4$ is why the ΔP we are calculating is of fourth order; remember that $\tilde{t} = r_s / z$. The difference in the calculation of $B_{kl}^{(m)}(\gamma)$ which contributes to $\Delta P^{(m)}$ is the replacement of the 4 in Eq. (2.A37) with m. We can easily evaluate the integral on the right-hand side of Eq. (2.A37). Doing this we find that

$$B_{kl}^{(m)}(\gamma) \sim \frac{1}{\Gamma(2m/3 - 2n_{kl}/3 + 1/3)} \tag{2.A38}$$

By using Eq. (2.A38), we can estimate that the coefficient of $\overline{\kappa}^{-7/15}$ in the asymptotic expression for $I(\overline{\kappa})$, Eq. (2.2), would be changed by about 1% by including the higher order corrections to ΔP. The expected changes in all the coefficients are shown in the following expression of Eq. (2.2)

$$\begin{aligned} I(\overline{\kappa})\, e^{(5/6)(3\pi\overline{\kappa})^{2/5}} \approx\ & (1.83 \pm 1\%)\overline{\kappa}^{-7/15} + (20.9 \pm 10\%)\overline{\kappa}^{-11/15} + (0.347 \pm 1\%)\overline{\kappa}^{-13/15} \\ & + (87.8 \pm 40\%)\overline{\kappa}^{-15/15} + (6.68 \pm 10\%)\overline{\kappa}^{-17/15} \end{aligned} \tag{2.A39}$$

The other approximation we need to examine is neglecting the terms of order $(r - r_s)^3$ and higher in the Taylor expansion of $V(r,z)$, Eq. (2.30). One can see how these terms will effect the final result for $I(\overline{\kappa})$ by including the cubic term and repeating the calculation. When this is done one finds that the Hamiltonian shown as Eq. (2.35) is modified to be

$$H''(P,\psi;z) = \mp\sqrt{2\mu\left(H - V_g - \Omega P\right)} - \sqrt{2\mu\Omega P}\,\frac{dr_g}{dz}\cos\psi + \frac{P}{2}\frac{d(\ln\Omega)}{dz}\sin 2\psi$$
$$+\frac{2}{3}\frac{d^2\Omega}{dz^2}\frac{P^{3/2}}{\Omega\sqrt{2\mu\Omega}}\left(\frac{5}{6} - \frac{1}{6}\cos 2\psi\right)\cos\psi + O\left[\left(r_* / z\right)^3\right] \qquad (2.A40)$$

The second term on the right-hand side gives the contribution to $\Delta P^{(4)}$ due to the quadratic term in the Taylor expansion of $V(r,z)$. The fourth term is due to the retention of the cubic term. The ratio of the fourth term to the second is of order $\left(P_0 / m\Omega_{ce} r_*^2\right)\left(r_* / z\right)$. It is evident that the retention of cubic term will give $\Delta P^{(5)} \neq 0$. Although $\Delta P^{(5)}$ will not be numerically smaller than $\Delta P^{(4)}$ (the r_* / z scaling just is not different enough), it will be smaller by the ratio $\left(P_0 / m\Omega_{ce} r_*^2\right) \sim \left[\left(v_{\perp 0} / \Omega_{ce}\right) / r_*\right]^2 \sim \varepsilon\zeta$. Including $\Delta P^{(5)}$ will modify A_{kl} with $k,l \geq 1$. Hence, keeping higher order terms in the Taylor expansion will modify terms in the asymptotic expression for $I(\overline{\kappa})$ of order $\overline{\kappa}^{-17/15}$ or greater; terms which are small at the large values of $\overline{\kappa}$ of interest to us.

2.7. References

[2.1] T. M. O'Neil and P. G. Hjorth, Phys. Fluids **28**, 3241 (1985).

[2.2] S. Ichimaru and M. N. Rosenbluth, Phys. Fluids **13**, 2778 (1970).

[2.3] D. Montgomery, L. Turner, and G. Joyce, Phys. Fluids **17**, 954 (1974); D. Montgomery, G. Joyce, and L. Turner, Phys. Fluids **17**, 2201 (1974); see also G. Hubner and H. Schamel, Z. Naturforsch. **45a**, 1 (1990).

[2.4] B. Beck, J. Fajans, and J. H. Malmberg, Bull. Am. Phys. Soc. **33**, 2975 (1987).

[2.5] A. W. Hyatt, C. F. Driscoll, and J. H. Malmberg, Phys. Rev. Lett. **59**, 2975 (1987).

[2.6] T. M. O'Neil, Phys. Fluids **26**, 2128 (1983).

[2.7] E. M. Lifshitz and L. P. Pitaevskii, *Physical Kinetics* (Pergamon, Oxford, 1981), p. 168.

[2.8] N. Rostoker, Phys. Fluids **3**, 922 (1960).

[2.9] A. Lenard, Ann. Phys. (N.Y.) **10**, 390 (1960); R. Belescu, Phys. Fluids **3**, 52 (1960).

[2.10] I. M. Sobol, *The Monte Carlo Method* (MIR Publishers, Moscow, 1975).

[2.11] W. H. Press, B. P. Flannery, S. A. Tenkolsky, and W. T. Vetterling, *Numerical Recipes* (Cambridge University Press, Cambridge, 1986).

[2.12] P. G. Hjorth, Ph.D. thesis, University of California at San Diego, 1988; A. J. Lichtenberg and M. A. Lieberman, *Regular and Stochastic Motion* (Springer-Verlag, New York, 1983), p. 130.

[2.13] H. Goldstein, *Classical Mechanics* (Addison-Wesley, Reading, MA, 1980), p. 35.

[2.14] L. D. Landau and E. M. Lifshitz, *Mechanics* (Pergamon, Oxford, 1976), p. 157.

[2.15] M. Abramowitz and I. A. Stegun, *Handbook of Mathematical Functions* (Dover, New York, 1970).

Table 2.1: Results of Monte Carlo calculation using the integral transform method. Statistical error in the last two significant figures is shown in parentheses.

$\overline{K}$	$I(\overline{K})$
1.00×10^{-4}	$1.753(63) \times 10^{0}$
1.00×10^{-3}	$1.335(44) \times 10^{0}$
1.00×10^{-2}	$9.26(45) \times 10^{-1}$
1.00×10^{-1}	$5.90(36) \times 10^{-1}$
3.33×10^{-1}	$3.81(18) \times 10^{-1}$
9.99×10^{-1}	$1.927(46) \times 10^{-1}$
1.25×10^{0}	$1.572(38) \times 10^{-1}$
2.50×10^{0}	$8.17(16) \times 10^{-2}$
5.00×10^{0}	$3.34(20) \times 10^{-2}$
1.25×10^{1}	$5.91(37) \times 10^{-3}$
2.50×10^{1}	$9.19(38) \times 10^{-4}$
5.00×10^{1}	$7.42(27) \times 10^{-5}$
1.00×10^{2}	$2.74(13) \times 10^{-6}$
2.00×10^{2}	$2.94(11) \times 10^{-8}$
5.00×10^{2}	$9.48(44) \times 10^{-12}$
1.00×10^{3}	$2.527(61) \times 10^{-15}$
2.00×10^{3}	$5.16(24) \times 10^{-20}$
5.00×10^{3}	$1.531(57) \times 10^{-28}$
1.00×10^{4}	$2.90(50) \times 10^{-37}$

Table 2.2: Results of Monte Carlo calculation using the rejection method. Statistical error in the last two significant figures is shown in parentheses.

$\overline{K}$	$I(\overline{K})$
1.00×10^{0}	$1.74(13) \times 10^{-1}$
1.78×10^{0}	$1.070(65) \times 10^{-1}$
3.16×10^{0}	$6.34(47) \times 10^{-2}$
5.62×10^{0}	$2.90(22) \times 10^{-2}$
1.00×10^{1}	$9.54(75) \times 10^{-3}$
1.78×10^{1}	$2.70(19) \times 10^{-3}$
3.16×10^{1}	$4.58(36) \times 10^{-4}$
5.62×10^{1}	$4.73(36) \times 10^{-5}$
1.00×10^{2}	$2.75(16) \times 10^{-6}$
3.16×10^{2}	$7.98(38) \times 10^{-10}$
1.00×10^{3}	$2.56(19) \times 10^{-15}$

Figure 2.1: Monte Carlo evaluation of the integral $I(\overline{\kappa})$ defined in Eq. (2.20). The evaluation via the integral transform method is shown as diamonds ($\Diamond$) and via the rejection method is shown as crosses (+). The statistical uncertainty in the evaluation of the integral is approximately 5%. These results match on to the asymptotic formula of Ref. 2.3 (solid line) at small $\overline{\kappa}$ and onto Eq. (2.2) (dashed line) at large $\overline{\kappa}$.

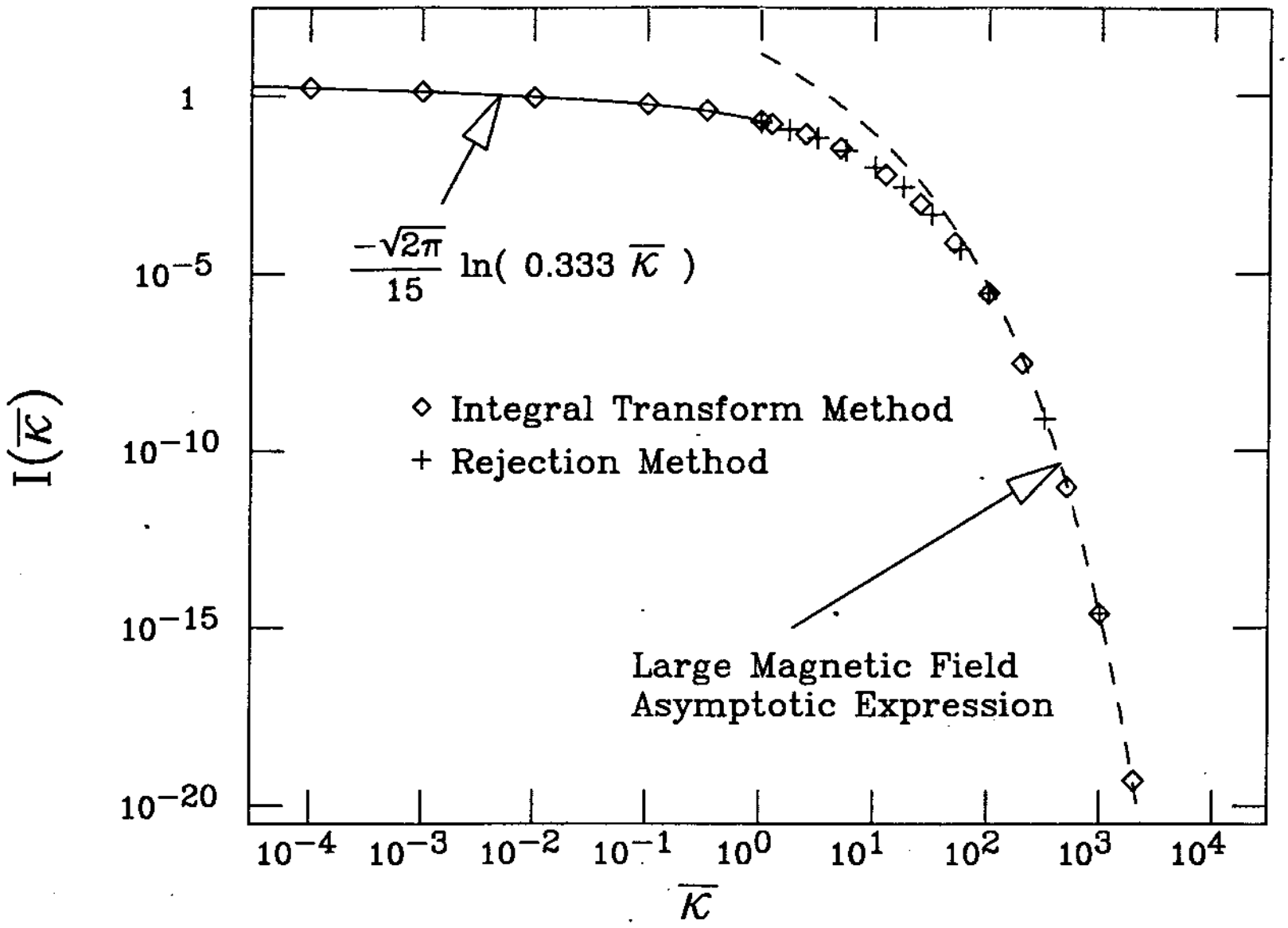
1
10^{-5}
10^{-10}
10^{-15}
10^{-20}
$I(\overline{\kappa})$
$\frac{-\sqrt{2\pi}}{15}\ln(\ 0.333\ \overline{\kappa}\ )$
◇ Integral Transform Method
+ Rejection Method
Large Magnetic Field
Asymptotic Expression
10^{-4} 10^{-3} 10^{-2} 10^{-1} 10^{0} 10^{1} 10^{2} 10^{3} 10^{4}
$\overline{\kappa}$

Figure 2.2: Monte Carlo evaluation of $I(\overline{\kappa})$ for large $\overline{\kappa}$. The constant in the exponential factor multiplying the ordinate is $E = (5/6)(3\pi)^{2/5}$. The integral transform method results are shown as diamonds ($\Diamond$) and the rejection method results are shown as crosses (+). The statistical uncertainty is approximately 5% (the size of the symbols) unless otherwise indicated. The solid line is a plot of the new asymptotic formula Eq. (2.2) and the dashed line a plot of the previous asymptotic prediction of Ref. 2.1.

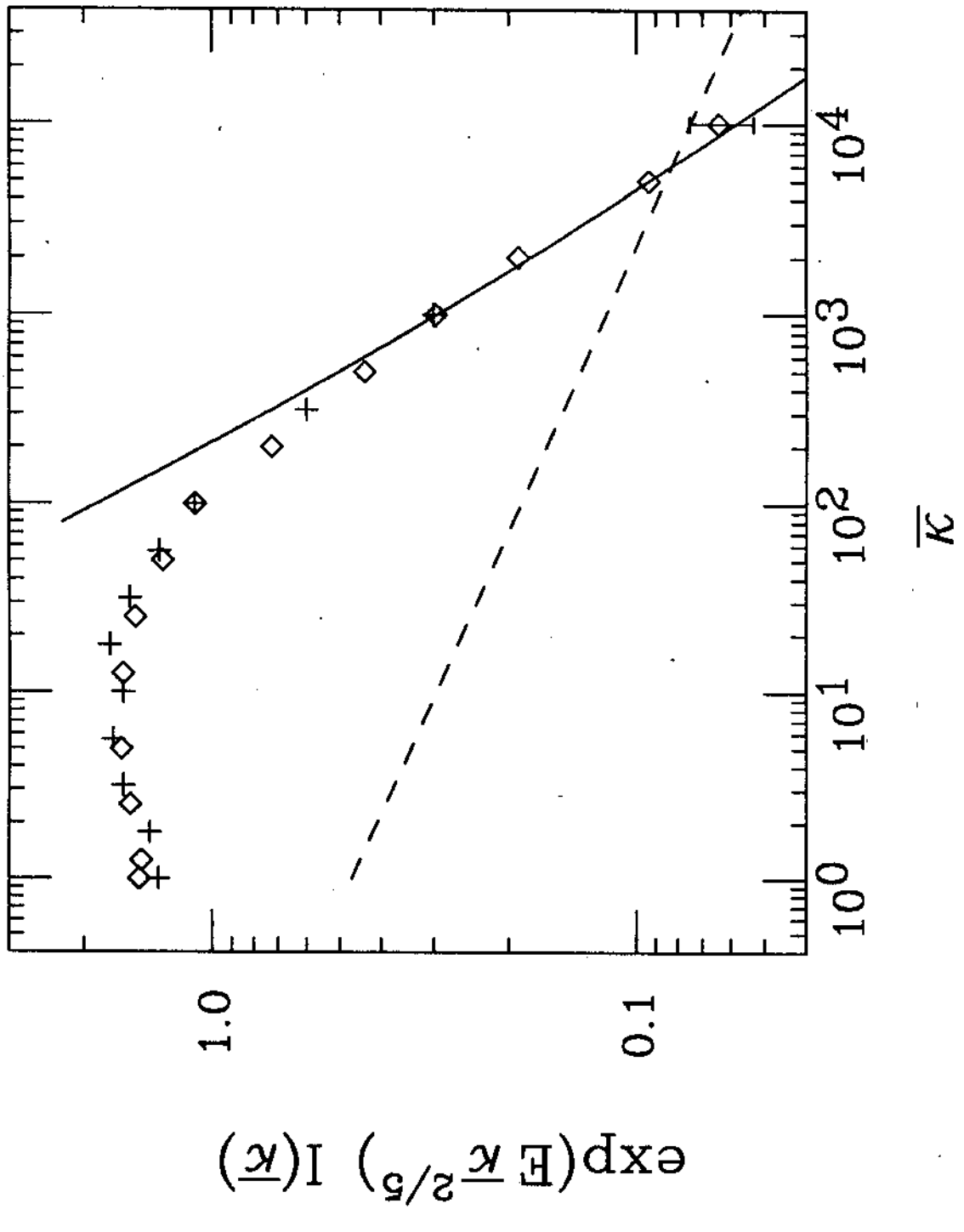
1.0
0.1
10^0
10^1
10^2
10^3
10^4
$\overline{\kappa}$
$\exp(E\,\overline{\kappa}^{2/5})\ I(\overline{\kappa})$

Figure 2.3: Experimental results compared to the Monte Carlo evaluation of $I(\overline{\kappa})$. Shown are two sets of experiments. The first is the cryogenic experiment of Ref. 2.4. The experiment was conducted at three values of the magnetic field (+ = 30 kG, □ = 40 kG, and ◊ = 60 kG). The second is the room temperature experiment of Ref. 2.5, displayed as circles (O). The solid curve is an interpolation of the results of Table 2.1. The dashed curve is an extrapolation using the formula $-\left(\sqrt{2\pi}\,/\,15\right)\ln\left[(0.333)\overline{\kappa}\right]$.

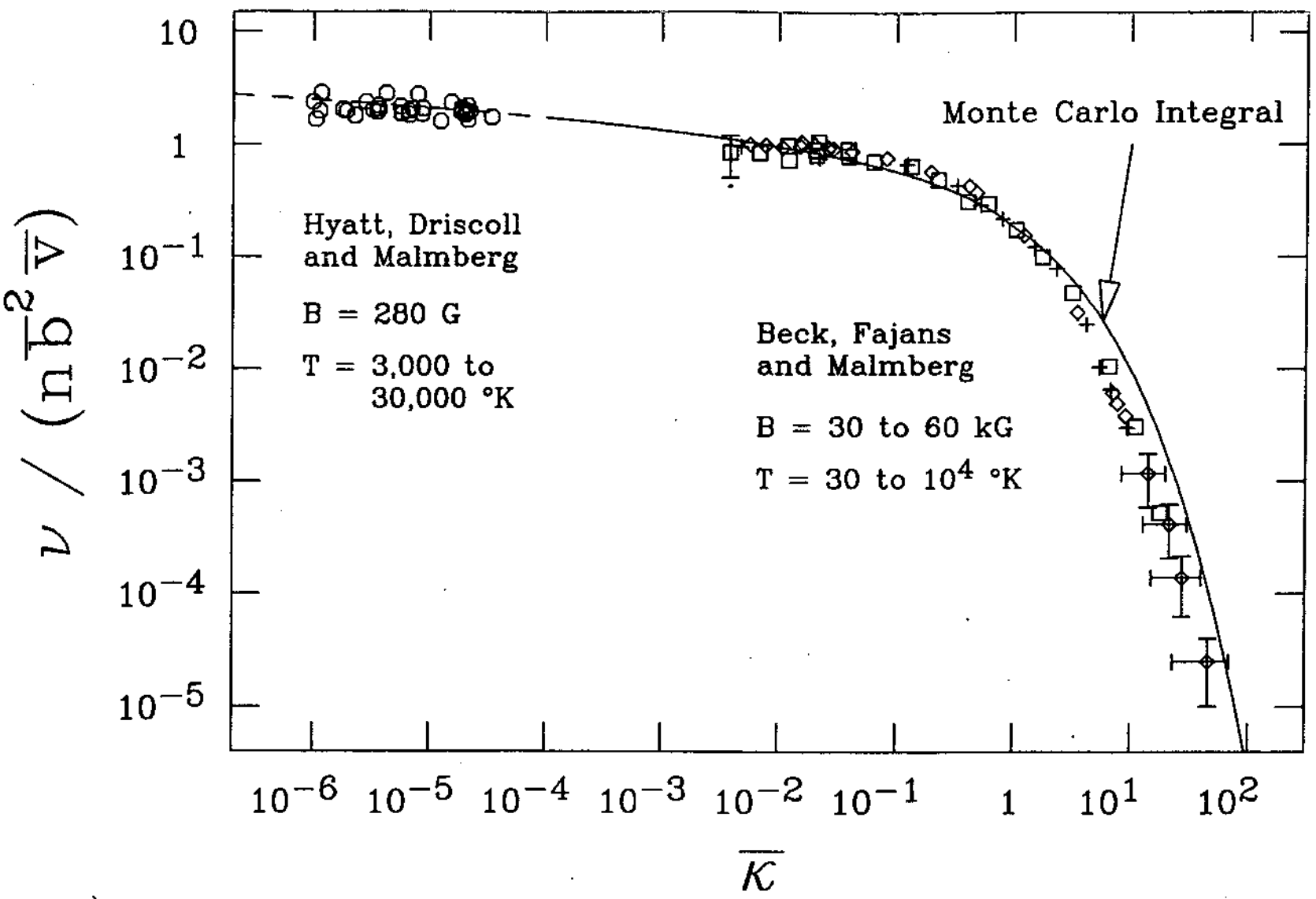
Monte Carlo Integral
Hyatt, Driscoll
and Malmberg
B = 280 G
T = 3,000 to
30,000 °K
Beck, Fajans
and Malmberg
B = 30 to 60 kG
T = 30 to 10^4 °K
$\nu / (n\bar{b}^2\bar{v})$
$\bar{\kappa}$
10
1
10^{-1}
10^{-2}
10^{-3}
10^{-4}
10^{-5}
10^{-6} 10^{-5} 10^{-4} 10^{-3} 10^{-2} 10^{-1} 1 10^{1} 10^{2}

Figure 2.4: Contour in the z-plane used to find $\Delta E_{\perp}$. Here, z_T is the turning point where $p_z = 0$.

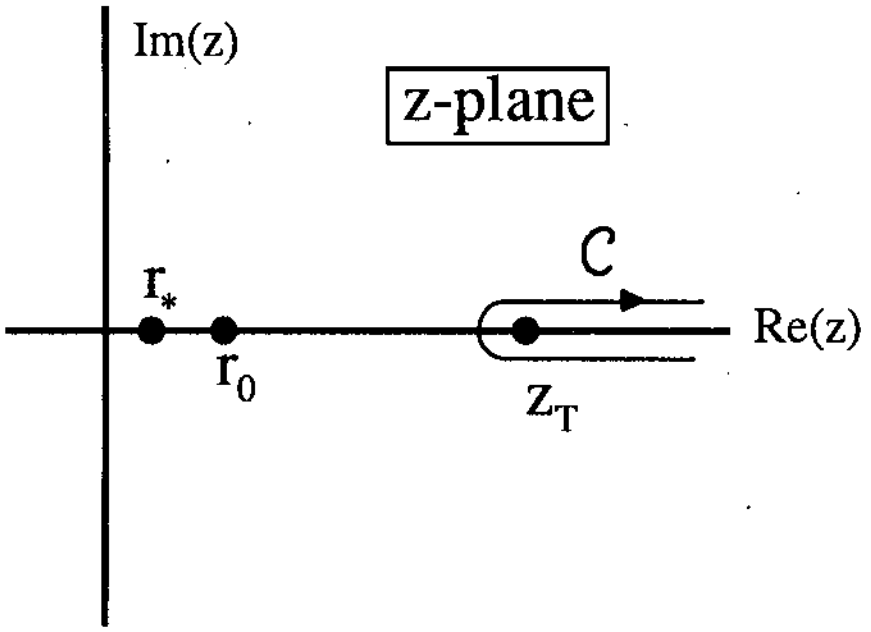
Im(z)
z-plane
C
r*
r0
zT
Re(z)

Figure 2.5: Deformation of contour in the z-plane used to find $\Delta E_{\perp}$.

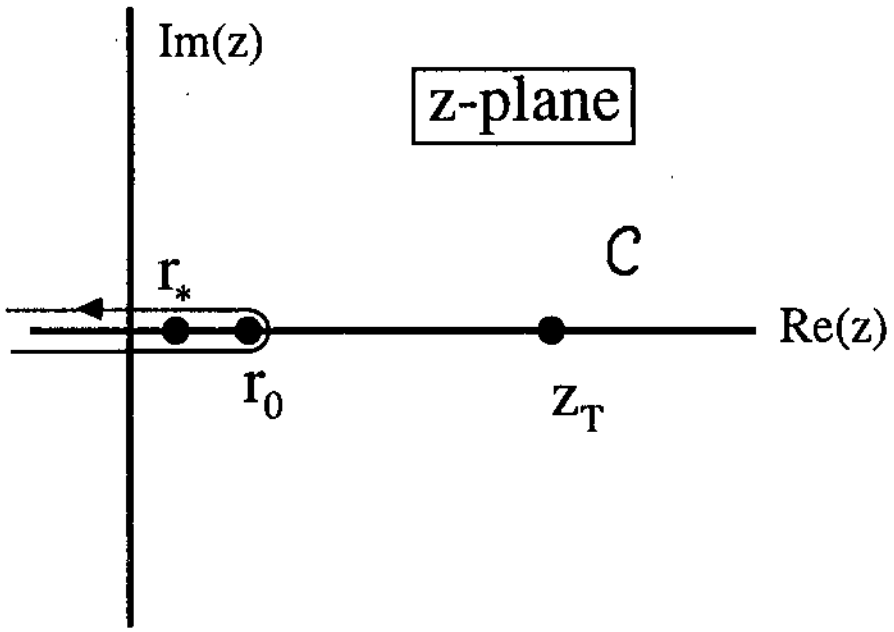
Im(z)
z-plane
C
r*
Re(z)
r0
zT

Figure 2.A1: Contour in the t-plane used to find D. The parameter t_T is of order $1/\varepsilon$ which is much greater than 1 for large values of the magnetic field.

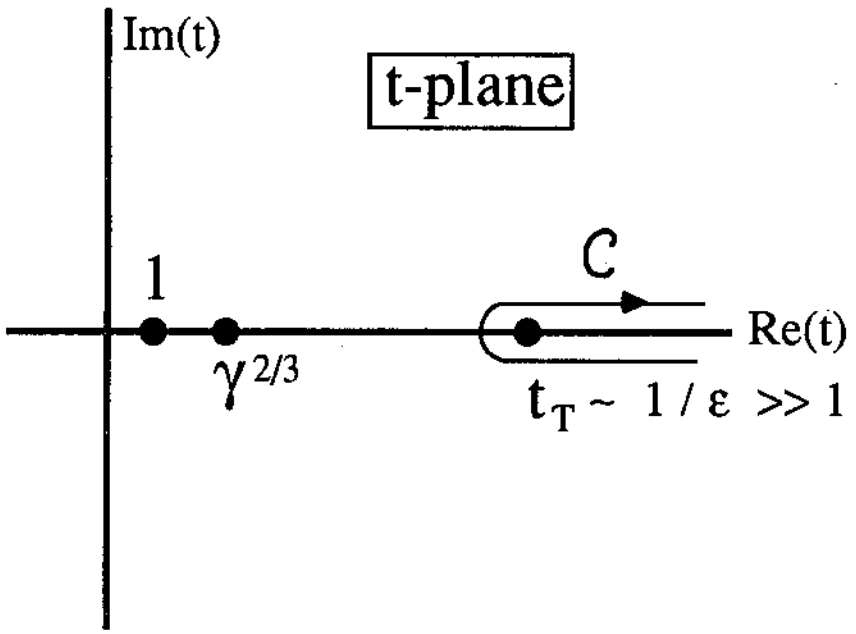
Im(t)
t-plane
C
1
Re(t)
$\gamma^{2/3}$
$t_T \sim 1/\varepsilon \gg 1$

Figure 2.A2: Contour in the t-plane used in the numerical contour integration of $B_u(\gamma)$.

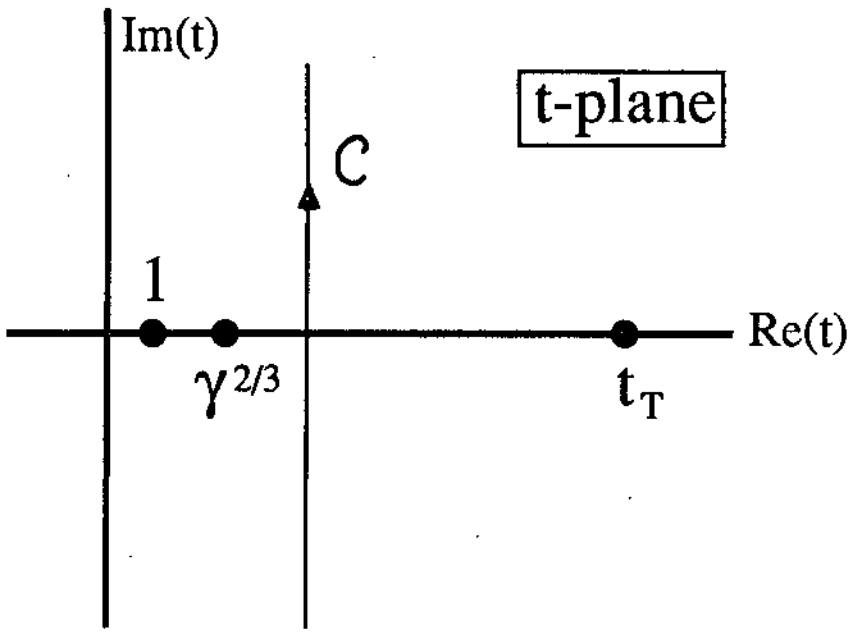
Im(t)
t-plane
C
1
Re(t)
$\gamma^{2/3}$
t_T

Figure 2.A3: The functions $A_M(\gamma)$ which show the $\gamma = (r_0 / r_*)^{3/2}$ dependence of $\Delta E_\perp$. See Eq. (2.A30) for the exact relationship between $A_M(\gamma)$ and $\Delta E_\perp$.

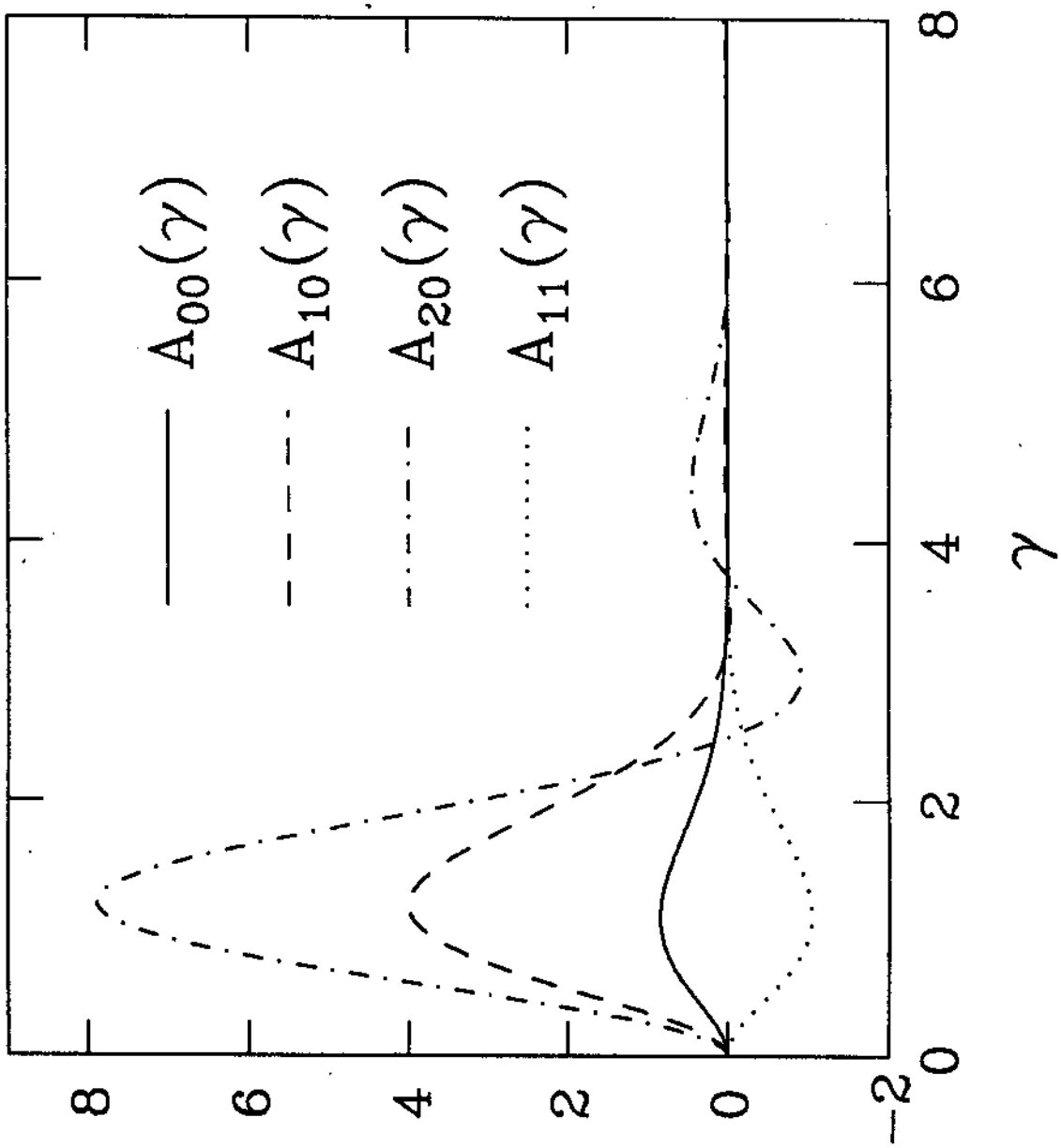
$A_{00}(\gamma)$
$A_{10}(\gamma)$
$A_{20}(\gamma)$
$A_{11}(\gamma)$
8
6
4
2
0
−2
0
2
4
6
8
γ

Chapter 3

Three-body Recombination in a Strongly Magnetized Plasma

3.1. Abstract

The three-body recombination rate is calculated for an ion introduced into a magnetically confined, weakly correlated and cryogenic pure electron plasma. The plasma is strongly magnetized in the sense that the cyclotron radius for an electron $r_{ce} = \sqrt{k_B T_e / m_e} / \Omega_{ce}$ is small compared to the classical distance of closest approach $b = e^2 / k_B T_e$, where T_e is the electron temperature and $\Omega_{ce} = eB / m_e c$ is the electron cyclotron frequency. Since the recombination rate is controlled by a kinetic bottleneck a few $k_B T_e$ below ionization, the rate may be determined by considering only the initial cascade through states of electron-ion pairs with separation of order b. These pairs may be described as guiding center atoms since the dynamics is classical and treatable with the guiding center drift approximation. In this paper, an ensemble of plasmas characterized by guiding center electrons and stationary ions is described with the BBGKY hierarchy. Under the assumption of weak electron correlation, the hierarchy is reduced to a master equation. Insight to the physics of the recombination process is obtained from the variational theory of reaction rates and from an approximate Fokker-Planck analysis. The master equation is solved numerically using a Monte Carlo simulation, and the

recombination rate is determined to be $0.070(10) n_e^2 \upsilon_e b^5$ per ion, where n_e is the electron density and $\upsilon_e = \sqrt{k_B T_e / m_e}$ is the thermal velocity. Also determined by the numerical simulation is the transient evolution of the distribution function from a depleted potential well about the ion to its steady state.

3.2. Introduction

Recent experiments have produced magnetically confined pure electron plasmas in the cryogenic temperature range [3.1]. The plasmas are strongly magnetized in the sense that $r_{ce} << b$, where $r_{ce} = \upsilon_e / \Omega_{ce}$ is the electron cyclotron radius and $b = e^2 / k_B T_e$ is the classical distance of closest approach. Here $\upsilon_e = \sqrt{k_B T_e / m_e}$ is the electron thermal speed and $\Omega_{ce} = eB / m_e c$ is the electron cyclotron frequency.

In this paper, we discuss the three- body recombination process [3.2] that occurs when an ion is introduced into one of these plasmas. Three-body recombination dominates since the rate for this process is very large at low temperature (i.e., $R_3 \sim T_e^{-9/2}$). To understand this scaling, note that the important energy scale in determining the rate is $k_B T_e$ and that this energy corresponds to an electron-ion separation of $b = e^2 / k_B T_e$. The frequency of electron-ion collisions characterized by an impact parameter in this range is $n_e b^2 \upsilon_e$, where n_e is the electron density, and the probability that another electron is close enough to carry off energy $k_B T_e$ is of order $n_e b^3$. The three-body rate is given by the product $R_3 \sim \left(n_e b^2 \upsilon_e\right)\left(n_e b^3\right)$, and this scales as $T_e^{-9/2}$. In this discussion and in the paper as a whole, we assume that the plasma density is low enough that $n_e b^3 << 1$; such a plasma is said to be weakly correlated. One can easily check that radiative recombination, where a photon carries away the binding energy, is much slower than three-body recombination in the cryogenic temperature range considered here [3.3,3.4].

The antimatter analog of the electron-ion three-body recombination process is a possible way of producing antihydrogen [3.3] for use in gravitational and spectroscopic studies [3.5]. Positron plasmas have already been produced [3.6], and antiprotons have been trapped and cooled to less than 0.1 eV [3.7]. A logical next step is to introduce antiprotons into a positron plasma (of the same character as the cryogenic strongly magnetized electron plasma) so that the antiprotons and positrons recombine. The recombination rate is a design parameter for such experiments, and that in part motivates these theoretical studies.

For the case of zero magnetic field, the three-body recombination rate has been calculated previously [3.8-3.10]. However, when a strong magnetic field is present, a constraint is imposed on the electron dynamics (the electrons cannot move freely across the field), and the rate is reduced by an order of magnitude. The previous rate obtained for $B=0$ is $R_3(B=0)=0.76(4)n_e^2 v_e b^5$ and the strong field rate obtained here is $R_3(B=\infty)=0.070(10)n_e^2 v_e b^5$.

As we shall discuss below, the rate is controlled by a kinetic bottleneck [3.10] at a binding energy of a few $k_B T_e$ below the ionization energy. The dynamics in this range is classical, since $k_B T_e$ is much smaller (four orders of magnitude smaller) than the Rydberg energy. Also, the electron dynamics may be treated by guiding center drift theory [3.11,3.12], since the cyclotron radius is much smaller than the scale length on which the interaction potential varies (i.e., $r_{ce} << b$). Equivalently, the cyclotron frequency is much larger than the next largest dynamical frequency (i.e., $\Omega_{ce} >> v_e / b$). This implies that the high-frequency cyclotron motion may be averaged out and the number of degrees of freedom correspondingly reduced; the center of the cyclotron orbit (guiding center) moves according to guiding center drift theory.

In the energy range of the bottleneck, a bound electron-ion pair form a novel atom, which we call a guiding center atom. The electron guiding center oscillates back and forth

along a field line in the Coulomb well of the ion and more slowly $\mathbf{E}\times\mathbf{B}$ drifts around the ion (see Fig. 3.1). The frequency of oscillation back and forth along a field line is of order $\omega_z \sim \sqrt{e^2/m_e b^3} \sim v_e/b$, and the frequency of the $\mathbf{E}\times\mathbf{B}$ drift motion is of order $\omega_{\mathbf{E}\times\mathbf{B}} \sim ec/Bb^3$. One can see that a consequence of the ordering $r_{ce} << b$ is the ordering $\omega_z >> \omega_{\mathbf{E}\times\mathbf{B}}$.

In this discussion and in the paper as a whole the ion is treated as stationary. This approximation makes sense when the electron motion is rapid compared to the ion motion. For example, we require that $v_e >> v_{i\parallel}$, where $v_{i\parallel}$ is the characteristic ion velocity parallel to the magnetic field. The requirements on the transverse motion are most easily stated as the frequency ordering: $\omega_{\mathbf{E}\times\mathbf{B}} >> v_{i\perp}/b, \Omega_{ci}$, where $v_{i\perp}$ is the characteristic ion velocity transverse to the field and $\Omega_{ci} = eB/m_i c$ is the ion cyclotron frequency.

With these orderings in mind, we develop a model based on guiding center electrons and stationary ions. Consider an ensemble of weakly correlated and guiding center electron plasmas with a single stationary ion located deep within the plasma at the origin of coordinates. A long way from the ion, the plasma is assumed to be in thermal equilibrium at density n_e and temperature T_e. The ion produces a Coulomb potential well, and collisional interactions allow an electron to fall into the well, that is, to become bound to the ion. Between collisions with other electrons the electron-ion pair form a guiding center atom. As the atom undergoes a sequence of collisions, the atom may be re-ionized or it may cascade in energy to very deep binding. Note that in some of these collisions the incident electron may replace the originally bound electron. At a very deep level of binding there is a sink; any electron that reaches this level is formally removed from the vicinity of the ion and returned to the background plasma. The recombination rate is then the steady state flux of electrons into the sink. We will find that the value of this rate does not depend on the exact location of the sink, provided the sink is below the kinetic bottleneck.

In Sec. 3.3, the BBGKY hierarchy for the ensemble is discussed [3.13]. The equations of the hierarchy contain two small parameters, $r_{ce}/b << 1$ and $n_e b^3 << 1$, and we analyze the equations to lowest nontrivial order in these parameters. The smallness of r_{ce}/b implies that the $\mathbf{E} \times \mathbf{B}$ drift motion that occurs during a collision is negligible; recall that $r_{ce}/b << 1$ implies that $v_e/b >> \omega_{\mathbf{E}\times\mathbf{B}}$. Because the most important collisions are close collisions (particle separation $\sim b$) and because the plasma is low density (i.e., $n_e b^3 << 1$), the hierarchy can be truncated by neglecting three-electron collisions. The first and second equations of the hierarchy then form a closed set. These two equations are formally reduced to a master equation; but the transition rates in the master equation (for steps in the recombination cascade) are not known analytically. In general, these rates depend on the complicated collision dynamics of two electrons in the force field of an ion. Consequently, a rigorous analytic solution of the master equation is not possible. However, two approximate treatments of the hierarchy equations yield important physical insights into the recombination process, so we discuss these treatments before going on to a proper numerical solution of the master equation.

The first of these treatments is discussed in Sec. 3.4, where the collisional dynamics is solved perturbatively and the hierarchy equations are reduced to a Fokker-Planck equation [3.14]. This approximation makes sense when the collisional cascade toward deeper binding takes place through many small and random steps. Each collision is assumed to produce a step in binding energy that is small compared to the energy scale on which the electron energy distribution varies. The step in energy is in fact small and the dynamics treatable perturbatively for collisions characterized by sufficiently large impact parameter. Unfortunately, it is clear from the Fokker-Planck coefficients that small impact parameter collisions make an important contribution, so the analysis in Sec. 3.4 is not the whole story. However, the analysis does provide an important insight. Consider a bound electron-ion pair and a second electron that is incident on the pair. Suppose that the

oscillation period of the bound electron is short compared to the duration of the collision. In this case, the oscillation is characterized by a good adiabatic invariant, and the collision changes the binding energy only by an exponentially small amount. We refer to the impact parameter beyond which the energy perturbation is exponentially small as the adiabatic cutoff.

In Sec. 3.5, a variational theory of the recombination rate is presented [3.15]. The underlying assumption for this treatment is the opposite of that for the Fokker-Planck treatment; the distribution function is assumed to vary on an energy scale that is small compared to a typical step size. In particular, the two-electron distribution $f_2(1,2)$ is taken to be of the thermal equilibrium form if electron 1 is bound less deeply than some energy E, and is taken to be zero if electron 1 is bound more deeply. Electron 2 is assumed to be a free electron that is incident on bound electron 1. The interaction of electron 2 with electron 1 produces a flux of electron 1 toward deeper binding: the one-way thermal equilibrium flux through the energy surface $E(1) = E$. This flux is shown to scale as the product of the Boltzmann factor $\exp(\varepsilon)$ and the phase space factor ε^{-4}, where $\varepsilon = E / k_B T_e$ and binding energy is taken to be positive toward deeper binding. The flux [$\sim \exp(\varepsilon) / \varepsilon^4$] has a strong minimum at $\varepsilon = 4$, and this minimum is the kinetic bottleneck. The variational theory takes the recombination rate to be the value of this one way flux at the bottleneck.

From the existence of the bottleneck, we may deduce the following picture. As atoms are formed and cascade to deeper binding, only a small fraction get through the bottleneck; the rest are re-ionized. If an atom makes it through the bottleneck, it continues to ever deeper binding with only a small probability of being re-ionized. Well above the bottleneck the distribution is very nearly of the thermal equilibrium form, and well below the bottleneck the distribution is depleted relative to thermal equilibrium.

This picture motivates the basic assumption of the variational theory, namely, that the distribution is of the thermal equilibrium form for $E(1) < E$ and is zero for $E(1) > E$.

Of course, the assumption is an idealization; the actual distribution does not drop off discontinuously, but rather falls off gradually over a finite range in energy. There will now be fewer atoms with $E(1) < E$ which can change to a state with $E(1) > E$ over the course of a collision. In addition, the atoms bound with $E(1) > E$ will be able to change to a state with $E(1) < E$ leading to a return flux. This is particularly a problem for large impact parameter collisions, where the step size is small. The flux associated with these collisions is diffusive in nature and is greatly overestimated by the one way flux. Another problem is the fact that the one-way flux is instantaneous. If an atom recrosses the surface $E(1) = E$ during the course of a collision, it will be counted too many times by the one-way flux. Large impact parameter collisions will again contribute most to such recrossings. To rectify these problems, the variational theory imposes a cutoff at large impact parameter. This cutoff is introduced in an *ad hoc* fashion, and the value of the cutoff is not determined within the context of the theory. Crude arguments from the Fokker-Planck analysis suggest that the cutoff should be of order b. Also, the actual one-electron distribution is not simply a function of energy, as is assumed in the variational theory, but also depends on the separation between the field line through the ion and the field line through the bound electron. One expects such a dependence in the strong magnetic field case, because the electrons are not free to move across the field.

Because neither the Fokker-Planck treatment nor the variational treatment is entirely satisfactory, the cascade dynamics is followed numerically in Sec. 3.6. Guiding center atoms are formed and then followed through a sequence of collisions, with the incident electron picked at random from a Maxwellian distribution. This procedure can be justified formally as a Monte Carlo solution of the master equation [3.16]. The solution verifies the existence of the bottleneck and determines the recombination rate. In addition, the time dependent behavior of the distribution function is obtained. The result is a quantitative

understanding of how the initially depleted potential well is filled to the steady state condition.

3.3. Basic Equations

In this section, we develop the BBGKY hierarcy [3.13] for the ensemble of guiding center plasmas described in the introduction. Anticipating that the important energy scale is $k_B T_e$, we scale the lengths by $b = e^2 / k_B T_e$, velocities by $v_e = \sqrt{k_B T_e / m_e}$, and time by b / v_e. In terms of scaled variables, Liouville's equation for the ensemble is given by [3.13,3.14]

$$\frac{\partial D_N}{\partial t} + \sum_{j=1}^{N} v_j \frac{\partial D_N}{\partial z_j} - \sum_{\substack{j=1 \\ i=0}}^{N} \frac{\partial \phi_{ji}}{\partial z_j} \frac{\partial D_N}{\partial v_j} + \left(\frac{r_{ce}}{b}\right) \sum_{\substack{j=1 \\ i=0}}^{N} \hat{z} \times \nabla_j \phi_{ji} \bullet \nabla_j D_N = 0 \quad , \tag{3.1}$$

where $D_N(\mathbf{r}_1, v_1, \cdots, \mathbf{r}_N, v_N, t)$ is the N-electron distribution normalized to unity (i.e., $\int d\mathbf{r}_1 \, dv_1 \cdots d\mathbf{r}_N \, dv_N \, D_N = 1$). We have used Cartesian coordinates with a uniform magnetic field $\mathbf{B} = B\hat{z}$ and the velocity in the $\hat{z}$ direction. Particle i=0 is the ion (i.e., $\phi_{j0} = -1/|\mathbf{r}_j|$ for $j = 1,\ldots,N$) and the remaining particles are electrons (i.e., $\phi_{ij} = -1/|\mathbf{r}_i - \mathbf{r}_j|$ for $i, j = 1,\ldots,N$).

The s-electron function is defined as [3.13]

$$f_s = \frac{V^s}{b^{3s}} \int d\mathbf{r}_{s+1} \, dv_{s+1} \cdots d\mathbf{r}_N \, dv_N \, D_N \quad , \tag{3.2}$$

where V is the plasma volume. To obtain the first equation of the hierarchy, we integrate Eq. (3.1) over the variables for the last $(N-1)$ electrons [i.e., take s=1 in Eq. (3.2)] and obtain

$$\frac{\partial f_1}{\partial t}(1)+v_1\frac{\partial f_1}{\partial z_1}-\frac{\partial \phi_{10}}{\partial z_1}\frac{\partial f_1}{\partial v_1}+\left(\frac{r_{ce}}{b}\right)\hat{z}\times\nabla_1\phi_{10}\bullet\nabla_1 f_1(1)$$
$$=n_e b^3\int d\mathbf{r}_2\,dv_2\left[\frac{\partial \phi_{12}}{\partial z_1}\frac{\partial}{\partial v_1}-\left(\frac{r_{ce}}{b}\right)\hat{z}\times\nabla_1\phi_{12}\bullet\nabla_1\right]f_2(1,2), \tag{3.3}$$

where we have set $(N-1)/V\equiv n_e$. Integrating Eq. (3.1) over the variables for the last $(N-2)$ electrons yields the second equation

$$\frac{\partial f_2}{\partial t}(1,2)+\sum_{j=1}^{2}\left[v_j\frac{\partial}{\partial z_j}-\frac{\partial \phi_{j0}}{\partial z_j}\frac{\partial}{\partial v_j}+\left(\frac{r_{ce}}{b}\right)\hat{z}\times\nabla_j\phi_{j0}\bullet\nabla_j\right]f_2(1,2)$$
$$+\left[-\frac{\partial \phi_{12}}{\partial z_1}\left(\frac{\partial}{\partial v_1}-\frac{\partial}{\partial v_2}\right)+\left(\frac{r_{ce}}{b}\right)\hat{z}\times\nabla_1\phi_{12}\bullet(\nabla_1-\nabla_2)\right]f_2(1,2)$$
$$=n_e b^3\int d\mathbf{r}_3\,dv_3\sum_{j=1}^{2}\left[\frac{\partial \phi_{j3}}{\partial z_j}\frac{\partial}{\partial v_j}-\left(\frac{r_{ce}}{b}\right)\hat{z}\times\nabla_j\phi_{j3}\bullet\nabla_j\right]f_3(1,2,3). \tag{3.4}$$

These equations involve two small parameters, $r_{ce}/b<<1$ and $n_e b^3<<1$, and we analyze the equations to lowest nontrivial order in these parameters. First, let us note that all terms of order (r_{ce}/b) may be dropped. All such terms in Eq. (3.4) and in the bracket on the right-hand side of Eq. (3.3) are compared to a term of order unity and consequently are negligible. This argument does not apply to the fourth term on the left-hand side of Eq. (3.3). We will find that the second and third term on the left combine to be of order $n_e b^3<<1$, and it is not necessarily the case that r_{ce}/b is smaller than $n_e b^3$. On the other hand, symmetry implies that the one-electron distribution is of the form $f_1(1)=f_1(z_1,\rho_1,v_1,t)$, where $\rho_1^2=x_1^2+y_1^2$, so the fourth term vanishes identically.

Physically, we are neglecting the $\mathbf{E}\times\mathbf{B}$ drift motion that occurs during a collision; recall that $r_{ce}/b<<1$ implies that $v_e/b>>\omega_{\mathbf{E}\times\mathbf{B}}$. For an electron bound to the ion, we are not neglecting the $\mathbf{E}\times\mathbf{B}$ drift motion that occurs between collisions. This motion is described by the fourth term on the left hand side of Eq. (3.3), and this term vanishes by symmetry.

On the right-hand side of Eq. (3.3), $f_2(1,2)$ is multiplied by $n_e b^3$, so a zeroth-order solution may be used for $f_2(1,2)$. Thus, the term on the right-hand side of Eq. (3.4) may be dropped, and a closed set of equations involving only $f_1(1)$ and $f_2(1,2)$ is obtained, that is, the hierarchy of equations is truncated.

This truncation procedure is different from that typically followed in plasma kinetic theory [3.17]. Focusing on the long-range nature of the Coulomb interaction, one typically rewrites $f_2(1,2)$ and $f_3(1,2.3)$ in terms of a Mayer cluster expansion and truncates the hierarchy through an expansion in the weakness of correlations, or equivalently, an expansion in the weakness of the long range interactions. Here, we are interested in close collisions (impact parameter $\sim b$) and for such collisions the interaction strength is not weak (i.e., $e^2 / b = k_B T_e$). We focus the analysis on these close collisions and neglect the effect of long range interactions; one may imagine that the functions $\phi_{ij}(\mathbf{r}_i - \mathbf{r}_j)$ are cut off for particle separation somewhat larger than b. The system is then similar to a low density neutral gas, that is, a gas for which the force range is small compared to the interparticle spacing (i.e., $n_e b^3 << 1$), and the truncation procedure used is the same as that for such a gas [3.13].

The kind of effect that is lost in this procedure is Debye shielding [3.17]. However, this is unimportant for the small particle separations of interest here; the shielded interaction is nearly identical to the bare interaction for particle separation of order b, since b is much smaller than the Debye length. Note that the inequality $n_e b^3 << 1$ implies the inequality $b << \lambda_D$. Also lost in this procedure are the relatively low frequency fluctuations (i.e., $\omega \sim \omega_p = v_e / \lambda_D$) associated with the long range interactions, but one expects these to be unimportant because of the adiabatic invariant associated with the bounce motion of a bound electron (i.e., $\omega_z >> v_e / \lambda_D$).

In rewriting Eqs. (3.3) and (3.4), it is useful to change variables from v_j to $\varepsilon_j = -\left[v_j^2 / 2 + \phi_{j0}\left(z_j, \rho_j\right)\right]$ where $j = 1,2$. The new variable, ε_j, is the binding energy of

electron j scaled by $k_B T_e$; the minus sign is introduced so that binding energy increases positively toward deeper binding. By making this change of variables, dropping the $\mathbf{E} \times \mathbf{B}$ drift terms, and dropping the three-electron interaction term, Eqs. (3.3) and (3.4) take the simple form

$$\frac{\partial f_1(1)}{\partial t} + v_1 \frac{\partial f_1(1)}{\partial z_1} = -n_e b^3 \int d\mathbf{r}_2 \, dv_2 \frac{\partial \phi_{12}}{\partial z_1} v_1 \frac{\partial f_2(1,2)}{\partial \varepsilon_1}, \tag{3.5}$$

$$\frac{\partial f_2(1,2)}{\partial t} + \left(v_1 \frac{\partial}{\partial z_1} + v_2 \frac{\partial}{\partial z_2} \right) f_2(1,2) + \frac{\partial \phi_{12}}{\partial z_1} \left(v_1 \frac{\partial}{\partial \varepsilon_1} - v_2 \frac{\partial}{\partial \varepsilon_2} \right) f_2(1,2) = 0, \tag{3.6}$$

where $\partial / \partial z_j$ is to be carried out at constant ε_j.

Since the right-hand side of Eq. (3.5) is of order $n_e b^3 << 1$, the left-hand side of the equation dominates the initial evolution of $f_1(1)$. During this evolution, $f_1(1)$ becomes nearly independent of z_1, that is, it evolves to the form

$$f_1(1) = \bar{f}_1(\rho_1, \varepsilon_1, t) + f_1'(z_1, \rho_1, \varepsilon_1, t), \tag{3.7}$$

where $f_1' / \bar{f}_1 \sim n_e b^3 << 1$. On a longer time scale (the collisional time scale), $\bar{f}_1(\rho_1, \varepsilon_1, t)$ evolves in a manner determined by the right hand side. Substituting Eq. (3.7) into Eq. (3.5) and retaining terms of order $n_e b^3$ yields the result

$$\frac{\partial \bar{f}_1}{\partial t} + v_1 \frac{\partial f_1'}{\partial z_1} = -n_e b^3 \int d\mathbf{r}_2 \, dv_2 \frac{\partial \phi_{12}}{\partial z_1} v_1 \frac{\partial f_2(1,2)}{\partial \varepsilon_1}. \tag{3.8}$$

For the energy regime $\varepsilon_1 > 0$ (the regime where electron 1 is bound to the ion), we operate on both sides of the equation with the integral $\oint_{\varepsilon_1} dz_1 / v_1(z_1, \rho_1, \varepsilon_1)$. Since the integral is carried out over a closed loop in phase space, the second term on the left is projected out and the equation reduced to the form

$$\tau_1 \frac{\partial \bar{f}_1}{\partial t}(\rho_1, \varepsilon_1) = -\frac{\partial}{\partial \varepsilon_1} n_e b^3 \oint_{\varepsilon_1} dz_1 \int d\mathbf{r}_2 \, dv_2 \frac{\partial \phi_{12}}{\partial z_1} f_2(1,2), \tag{3.9}$$

where $\tau_1 = \tau(\rho_1, \varepsilon_1)$ is the period of the oscillatory motion for electron 1.

For the energy regime $\varepsilon_1 < 0$, we don't have to solve for $\bar{f}_1$. This regime corresponds to unbound electrons that stream in from infinity and back out to infinity. By hypothesis the plasma is in equilibrium a long way from the ion, so $\bar{f}_1(\rho_1, \varepsilon_1)$ must be of the thermal equilibrium form

$$\bar{f}_1(\rho_1, \varepsilon_1) = f_{th}(\varepsilon_1) \equiv \exp(\varepsilon_1)/\sqrt{2\pi} \tag{3.10}$$

There is one aspect of this distribution that can be confusing. The spatial dependence is of the form $\exp\left[\phi_{10}(z_1, \rho_1)\right]$, which is what one expects for a bare ion. However, some of the ions have a bound electron, and the electron screens out the ion potential ϕ_{10} (this is short range screening, not long range Debye screening). The reader may ask why such screening is not manifest in Eq. (3.10). The point is that only a small fraction of the ions have a bound electron; we will verify *a posteriori* that the fraction is of order $n_e b^3 << 1$. Note in this regard that an electron that reaches the sink is declared to be recombined and is removed from the vicinity of the ion. The reason that only a small fraction of the ions have a bound electron is that the cascade time is smaller than the recombination time by a factor $n_e b^3 << 1$.

There is no small parameter in Eq. (3.6), so all of the terms are of order unity (or of order v_e / b when written in unscaled variables). In accord with Bogoliubov's ideas [3.13], one expects $f_2(1,2)$ to relax to become a functional of $f_1(1)$ on the time scale v_e / b. In the remainder of this section, we will use this functional dependence to rewrite Eq. (3.9) first as a Boltzmann-like equation and then as a master equation. This latter equation will be used as the framework for the numerical solution developed in Sec. 3.6.

After the relaxation has occurred, the term $\partial f_2(1,2)/\partial t$ in Eq. (3.6) is nonzero only because $f_1(1)$ varies in time. However, this latter variation is of order $n_e b^3$, and hence is negligible to zeroth-order in $n_e b^3$. Dropping $\partial f_2(1,2)/\partial t$ and operating on the remaining terms with $\oint_{\varepsilon_1} dz_1 / v_1 \int d\mathbf{r}_2\, d\mathbf{v}_2$ yields the result

$$\oint_{\varepsilon_1} \frac{dz_1}{v_1} \int d\mathbf{r}_2\, dv_2 \left(v_1 \frac{\partial}{\partial z_1} + v_2 \frac{\partial}{\partial z_2} \right) f_2(1,2)$$

$$= -\oint_{\varepsilon_1} \frac{dz_1}{v_1} \int d\mathbf{r}_2\, dv_2 \frac{\partial \phi_{12}}{\partial z_1} \left(v_1 \frac{\partial}{\partial \varepsilon_1} - v_2 \frac{\partial}{\partial \varepsilon_2} \right) f_2(1,2) \qquad (3.11)$$

where particle 1 is assumed to be bound (i.e., $\varepsilon_1 > 0$). The first term in the bracket on the left-hand side vanishes because the integral $\oint_{\varepsilon_1} dz_1\, \partial f_2 / \partial z_1$ is around a closed loop in phase space, and the second term in the bracket on the right-hand side vanishes because of the integration over v_2. Carrying out the integral over z_2 on the left-hand side then yields the result

$$\oint_{\varepsilon_1} \frac{dz_1}{v_1} \int d\mathbf{r}_{2\perp}\, dv_2\, v_2 \left[f_2(z_2 = +\infty) - f_2(z_2 = -\infty) \right]$$

$$= -\frac{\partial}{\partial \varepsilon_1} \oint_{\varepsilon_1} dz_1 \int d\mathbf{r}_2\, dv_2 \frac{\partial \phi_{12}}{\partial z_1} f_2(1,2) \qquad (3.12)$$

where the right-hand side is the same as the right-hand side of Eq. (3.9) (except for a factor of $n_e b^3$).

In evaluating the bracket on the left hand side, we first consider the region of phase space where $v_2 > 0$. The distribution $f_2(z_2 = -\infty)$ describes a bound electron 1 (recall that $\varepsilon_1 > 0$) and an incident electron 2 before the collision has occurred. In this region of phase space, the electrons are uncorrelated, so we may set $f_2(z_2 = -\infty) = \bar{f}_1(\rho_1, \varepsilon_1) \bar{f}_1(\rho_2, \varepsilon_2)$. The distribution $f_2(z_2 = +\infty)$ is evaluated in a region where electron 2 is coming from the collision, so electrons 1 and 2 are correlated. To evaluate the distribution in this region, we first note that Eq. (3.6) implies that $f_2(1,2) = f_2(1',2')$, where $(1',2')$ is a phase space point that evolves into (1,2). Thus, we may set $f_2(z_2 = \infty) = \bar{f}_1(\rho_1, \varepsilon_1') \bar{f}_1(\rho_2, \varepsilon_2')$, where $(\rho_1, \varepsilon_1', \rho_2, \varepsilon_2')$ evolves into $(\rho_1, \varepsilon_1, \rho_2, \varepsilon_2)$ during the collision. Again we have used the fact that the electrons are uncorrelated before the collision. Substituting these expressions into Eq. (3.12) and then substituting for the right hand side of Eq. (3.9) yields the Boltzmann-like equation [3.13]

$$\frac{\partial \bar{f}_1}{\partial t}(\rho_1,\varepsilon_1) = n_e b^3 \frac{1}{\tau_1}\oint_{\varepsilon_1}\frac{dz_1}{\upsilon_1}\int d\mathbf{r}_{2\perp}\, d\upsilon_2\,|\upsilon_2| \times\left[\bar{f}_1(\rho_1,\varepsilon_1')\bar{f}_1(\rho_2,\varepsilon_2') - \bar{f}_1(\rho_1,\varepsilon_1)\bar{f}_1(\rho_2,\varepsilon_2)\right], \tag{3.13}$$

where the absolute value sign on υ_2 is needed to make the integrand valid for $\upsilon_2 < 0$ as well as $\upsilon_2 > 0$.

To obtain a master equation, we first rewrite Eq. (3.13) in the form

$$\frac{\partial \bar{f}_1}{\partial t} = n_e b^3 \frac{1}{\tau_1}\oint_{\varepsilon_1}\frac{dz_1}{\upsilon_1}\int d\mathbf{r}_{2\perp}\, d\upsilon_2\,|\upsilon_2|\, f_{th}(\varepsilon_1)\, f_{th}(\varepsilon_2) \times\left[\frac{\bar{f}_1(\rho_1,\varepsilon_1')\bar{f}_1(\rho_2,\varepsilon_2')}{f_{th}(\varepsilon_1')\, f_{th}(\varepsilon_2')} - \frac{\bar{f}_1(\rho_1,\varepsilon_1)\bar{f}_1(\rho_2,\varepsilon_2)}{f_{th}(\varepsilon_1)\, f_{th}(\varepsilon_2)}\right], \tag{3.14}$$

where $f_{th}(\varepsilon_1)$ is the thermal distribution given in Eq. (3.10) and we have used conservation of energy ($\varepsilon_1 + \varepsilon_2 = \varepsilon_1' + \varepsilon_2'$). In the post-collision state, particle 2 is free (i.e., $\varepsilon_2 < 0$) so $\bar{f}_1(\rho_2,\varepsilon_2) = f_{th}(\varepsilon_2)$. In the pre-collision state particle 1, particle 2, or both particles 1 and 2 are free. We choose the particle with largest binding energy, and denote its variables by (ρ',ε'), that is, we define $\varepsilon' = \max(\varepsilon_1',\varepsilon_2')$ and let ρ' be the corresponding ρ_1 or ρ_2. The other particle is guaranteed to be free and to have a thermal distribution. Thus, Eq. (3.14) reduces to the form

$$\frac{\partial \bar{f}_1}{\partial t} = f_{th}(\varepsilon_1)\, n_e b^3 \frac{1}{\tau_1}\oint_{\varepsilon_1}\frac{dz_1}{\upsilon_1}\int d\mathbf{r}_{2\perp}\, d\upsilon_2\,|\upsilon_2|\, f_{th}(\varepsilon_2)\left[\frac{\bar{f}_1(\rho',\varepsilon')}{f_{th}(\varepsilon')} - \frac{\bar{f}_1(\rho_1,\varepsilon_1)}{f_{th}(\varepsilon_1)}\right]. \tag{3.15}$$

Let us define the forward transition rate

$$k_+(\rho_1,\varepsilon_1|\bar{\rho},\bar{\varepsilon}) = n_e b^3 \frac{1}{\tau_1}\oint_{\varepsilon_1}\frac{dz_1}{\upsilon_1}\int \rho_2\, d\rho_2\, d\theta_2\, d\upsilon_2\,|\upsilon_2|\, f_{th}(\varepsilon_2) \times\delta\left[\bar{\varepsilon} - \varepsilon_+(z_1,\rho_1,\varepsilon_1,\rho_2,\theta_2,\varepsilon_2)\right]\delta\left[\bar{\rho} - \rho_+(z_1,\rho_1,\varepsilon_1,\rho_2,\theta_2,\varepsilon_2)\right], \tag{3.16a}$$

where the plus indicates evolution forward in time from an initial state characterized by $(z_1,\rho_1,\varepsilon_1,\rho_2,\theta_2,\varepsilon_2)$. Here, electron 1 is initially bound (ε_1>0) and electron 2 is incident (ε_2<0), θ_2 is measured relative to θ_1 (by symmetry only θ_2-θ_1 matters), and z_1 specifies the position (or phase) of bound electron 1 when the evolution begins. The functions ε_+ and

ρ_+ are the energy and radial position of the electron with the largest energy in the post-collision state. Likewise, one can define the backward transition rate

$$k_-(\rho_1,\varepsilon_1|\overline{\rho},\overline{\varepsilon}) = n_e b^3 \frac{1}{\tau_1}\oint_{\varepsilon_1}\frac{dz_1}{v_1}\int \rho_2\, d\rho_2\, d\theta_2\, dv_2\, |v_2|\, f_{th}(\varepsilon_2)$$
$$\times\delta[\overline{\varepsilon}-\varepsilon_-(z_1,\rho_1,\varepsilon_1,\rho_2,\theta_2,\varepsilon_2)]\,\delta[\overline{\rho}-\rho_-(z_1,\rho_1,\varepsilon_1,\rho_2,\theta_2,\varepsilon_2)], \qquad (3.16b)$$

where the minus indicates evolution backward in time from an initial state characterized by $(z_1,\rho_1,\varepsilon_1,\rho_2,\theta_2,\varepsilon_2)$. The functions ε_- and ρ_- are the energy and radial position of the electron with the largest energy in the pre-collision state; these quantities may be identified with ε' and ρ' in Eq. (3.15). By time-reversal symmetry (reversal of all velocities), it follows that $k_-(\rho_1,\varepsilon_1|\overline{\rho},\overline{\varepsilon}) = k_+(\rho_1,\varepsilon_1|\overline{\rho},\overline{\varepsilon})$; so we may drop the plus and minus.

In terms of this rate, Eq. (3.15) takes the form

$$\frac{\partial\tilde{f}_1(\rho,\varepsilon)}{\partial t} = \int d\overline{\rho}\; d\overline{\varepsilon}\; f_{th}(\varepsilon)\, k(\rho,\varepsilon|\overline{\rho},\overline{\varepsilon})\left(\frac{\tilde{f}_1(\overline{\rho},\overline{\varepsilon})}{f_{th}(\overline{\varepsilon})} - \frac{\tilde{f}_1(\rho,\varepsilon)}{f_{th}(\varepsilon)}\right), \qquad (3.17a)$$

where we have dropped the subscript on ε_1 and ρ_1. To put this in the standard form for a master equation, it is useful to introduce the distribution

$$W(\rho,\varepsilon) \equiv (n_e b^3)\,[2\pi\rho\;\tau(\rho,\varepsilon)]\,\tilde{f}_1(\rho,\varepsilon),$$

where $(n_e b^3)\,[2\pi\rho\;\tau(\rho,\varepsilon)]$ is the density of states for the differential $d\rho\, d\varepsilon$. Equation (3.17a) then takes the form

$$\frac{\partial W(\rho,\varepsilon)}{\partial t} = \int d\overline{\rho}\; d\overline{\varepsilon}\; W_{th}(\rho,\varepsilon)\, k(\rho,\varepsilon|\overline{\rho},\overline{\varepsilon})\left(\frac{W(\overline{\rho},\overline{\varepsilon})}{W_{th}(\overline{\rho},\overline{\varepsilon})} - \frac{W(\rho,\varepsilon)}{W_{th}(\rho,\varepsilon)}\right), \qquad (3.17b)$$

where

$$W_{th}(\rho,\varepsilon) \equiv (n_e b^3)\,[2\pi\rho\;\tau(\rho,\varepsilon)]\,f_{th}(\varepsilon).$$

By using time-reversal symmetry plus the Liouville theorem one obtains the statement of detailed balance [3.14,3.16]

$$W_{th}(\rho,\varepsilon)\,k(\rho,\varepsilon|\overline{\rho},\overline{\varepsilon}) = W_{th}(\overline{\rho},\overline{\varepsilon})\,k(\overline{\rho},\overline{\varepsilon}|\rho,\varepsilon) \tag{3.18}$$

Also, one can verify this relation by noting that it is required for Eq. (3.17b) to conserve particle number for an arbitrary choice of $W(\rho,\varepsilon)$. Substituting this relation into Eq. (3.17b) then yields the master equation [3.16]

$$\frac{\partial W(\rho,\varepsilon)}{\partial t} = \int d\overline{\rho}\; d\overline{\varepsilon}\left[k(\overline{\rho},\overline{\varepsilon}|\rho,\varepsilon)\,W(\overline{\rho},\overline{\varepsilon}) - k(\rho,\varepsilon|\overline{\rho},\overline{\varepsilon})\,W(\rho,\varepsilon)\right] \tag{3.19}$$

3.4. Fokker-Planck Equation

In this section, we focus on collisions characterized by an impact parameter that is somewhat larger than b and reduce Eqs. (3.6) and (3.9) to a Fokker-Planck equation. Consider the case where electron 1 is bound ($\varepsilon_1>0$) at a radius $\rho_1<1$ and electron 2 is incident from infinity ($\varepsilon_2<0$) at a relatively large radius $\rho_2 \gtrsim \rho_d >> 1$. Here, the cutoff at $\rho_2 \approx \rho_d$ is introduced arbitrarily; one might imagine that an opaque disk of radius ρ_d is placed in front of each ion. For this situation, Eq. (3.6) can be solved perturbatively through an expansion in $1/\rho_2$, that is, through an expansion in the weakness of the interactions ϕ_{12} and ϕ_{20}. To simplify the analysis, we also assume that electron 1 is bound deeply enough that its oscillatory motion is simple harmonic.

It is useful to rewrite Eq. (3.6) as $(L^{(0)}+L^{(1)})f_2=0$, where

$$L^{(0)} = \frac{\partial}{\partial t} + \upsilon_1 \left.\frac{\partial}{\partial z_1}\right|_{\varepsilon_1} + \upsilon_2 \left.\frac{\partial}{\partial z_2}\right|_{\upsilon_2}, \tag{3.20a}$$

$$L^{(1)} = -\frac{\partial \phi_{12}}{\partial z_1}\,\upsilon_1 \frac{\partial}{\partial \varepsilon_1} - \left(\frac{\partial \phi_{12}}{\partial z_2} + \frac{\partial \phi_{20}}{\partial z_2}\right)\frac{\partial}{\partial \upsilon_2}, \tag{3.20b}$$

and υ_2, rather than ε_2, is treated as an independent variable. The zeroth-order orbits described by $L^{(0)}$ are such that electron 1 oscillates back and forth with a constant value of

ε_1 and electron 2 streams by with a constant value of v_2. At first glance, the operator $L^{(1)}$ appears to be of mixed order in the expansion parameter $1/\rho_2$. The quantity $\partial\phi_{12}/\partial z_1$ is of order $1/\rho_2^2$; whereas, the bracket $(\partial\phi_{12}/\partial z_2 + \partial\phi_{20}/\partial z_2)$ is of order $1/\rho_2^3$, since ϕ_{12} and ϕ_{20} cancel to lowest order leaving a dipole interaction. However, we will find that the two terms in $L^{(1)}$ contribute equally. The reason is that the derivative $\partial/\partial v_2$ will produce a factor v_2 (i.e., $\partial/\partial v_2 = v_2\,\partial/\partial\varepsilon_2$) and this factor is effectively of order ρ_2.

Let us look for a solution of the form $f_2 = f_2^{(0)} + f_2^{(1)}$, where

$$f_2^{(0)}(1,2) = \bar{f}_1(\rho_1,\varepsilon_1)\left[\exp\left(-v_2^2/2\right)/\sqrt{2\pi}\right], \tag{3.21}$$

This choice for $f_2^{(0)}$ is determined not only by the requirement that $L^{(0)}f_2^{(0)} = 0$, but also by the requirement that electrons 1 and 2 are uncorrelated in zero order, and by the fact that electron 2 is unbound and hence distributed thermally. The first-order distribution is determined by the equation

$$L^{(0)}f_2^{(1)} = -L^{(1)}f_2^{(0)}, \tag{3.22}$$

where second-order term $L^{(1)}f_2^{(1)}$ has been neglected. The operator $L^{(0)}$ is the total time derivative taken along the zeroth-order orbits; so a solution for $f_2^{(1)}$ is given by an integral over these orbits

$$f_2^{(1)} = +\int_{-\infty}^{t} dt' \left[\left(\frac{\partial\phi_{12}}{\partial z_1}v_1\right)'\frac{\partial\bar{f}_1}{\partial\varepsilon_1}(\rho_1,\varepsilon_1)\frac{e^{-v_2^2/2}}{\sqrt{2\pi}} - \left(\frac{\partial\phi_{12}}{\partial z_2}+\frac{\partial\phi_{20}}{\partial z_2}\right)'v_2\frac{e^{-v_2^2/2}}{\sqrt{2\pi}}\bar{f}_1(\rho_1,\varepsilon_1)\right]. \tag{3.23}$$

The zero order orbits are given by

$$\begin{aligned} &\varepsilon_1(t') = \varepsilon_1, \qquad v_2(t') = v_2, \qquad z_2(t') = z_2 + v_2(t'-t), \\ &z_1(t') = a_1\cos\left[\psi_1(t')\right], \qquad \psi_1(t') = \psi_1 + \omega_1(t'-t), \end{aligned} \tag{3.24}$$

where the amplitude of oscillation of particle 1 is given by $\omega_1^2 a_1^2/2 = (1/\rho_1 - \varepsilon_1)$ and the frequency by $\omega_1^2 = 1/\rho_1^3$. This follows from the deep binding approximation for the energy of particle 1, $\varepsilon_1 \equiv 1/\rho_1 - [v_1^2/2 + (1/\rho_1^3)z_1^2/2]$.

Substituting Eq. (3.23) into Eq. (3.9) yields the Fokker-Planck equation

$$\tau_1 \frac{\partial \bar{f}_1}{\partial t} = -\frac{\partial}{\partial \varepsilon_1}\left(B\, \bar{f}_1(\rho_1,\varepsilon_1) + A \frac{\partial \bar{f}_1}{\partial \varepsilon_1}(\rho_1,\varepsilon_1) \right), \tag{3.25}$$

where

$$A = +n_e b^3 \tau_1 \int_0^{2\pi} \frac{d\psi_1}{2\pi} \int dr_2 \int_{-\infty}^{+\infty} d\upsilon_2 \int_{-\infty}^{t} dt' \frac{e^{-\upsilon_2^2/2}}{\sqrt{2\pi}} \left(\upsilon_1 \frac{\partial \phi_{12}}{\partial z_1} \right) \left(\upsilon_1 \frac{\partial \phi_{12}}{\partial z_1} \right)', \tag{3.26a}$$

$$B = -n_e b^3 \tau_1 \int_0^{2\pi} \frac{d\psi_1}{2\pi} \int dr_2 \int_{-\infty}^{+\infty} d\upsilon_2 \int_{-\infty}^{t} dt' \frac{e^{-\upsilon_2^2/2}}{\sqrt{2\pi}}\, \upsilon_2 \left(\upsilon_1 \frac{\partial \phi_{12}}{\partial z_1} \right) \left(\frac{\partial \phi_{12}}{\partial z_2} + \frac{\partial \phi_{20}}{\partial z_2} \right)', \tag{3.26b}$$

and the integral $\oint dz_1 / \upsilon_1$ has been replaced by $\tau_1 \int_0^{2\pi} d\psi_1 / 2\pi$. To evaluate A, we approximate $\partial\phi_{12} / \partial z_1$ by $z_2 / \left(z_2^2 + \rho_2^2\right)^{3/2}$, use the identity

$$\frac{z}{\left(z^2+\rho^2\right)^{3/2}} = \frac{2}{\pi} \int_0^{\infty} dk\, k\, K_0(k\rho) \sin kz, \tag{3.27}$$

and substitute the orbits in Eq. (3.24). The result is the integral expression

$$\begin{aligned} A = +n_e b^3 \tau_1 \int_0^{2\pi} \frac{d\psi_1}{2\pi} \int_{-\infty}^{+\infty} dz_2 \int_{\rho_d}^{\infty} 2\pi\rho_2\, d\rho_2 \int_{-\infty}^{+\infty} d\upsilon_2 \int_{-\infty}^{t} dt' \left(\frac{2}{\pi}\right)^2 \int_0^{\infty} k\, dk \int_0^{\infty} q\, dq \\ \times \frac{e^{-\upsilon_2^2/2}}{\sqrt{2\pi}} K_0(k\rho_2)\, K_0(q\rho_2) \left(a_1\omega_1\right)^2 \sin\psi_1 \sin[\omega_1(t'-t)+\psi_1] \\ \times \sin kz_2 \sin[qz_2 + q\upsilon_2(t'-t)] \end{aligned}, \tag{3.28}$$

where a low impact parameter cutoff has been introduced at $\rho_2 = \rho_d$. Carrying out the z_2, ψ_1, q, t', and k integrals in that order then yields the result

$$A = +n_e b^3 \tau_1 \left(a_1\omega_1\right)^2 4\sqrt{2\pi} \int_0^{\infty} \frac{d\upsilon_2}{\upsilon_2}\, e^{-\upsilon_2^2/2} \int_{(\omega_1\rho_d/\upsilon_2)}^{\infty} d\xi\, \xi\, K_0^2(\xi). \tag{3.29}$$

In evaluating B, one must pay attention to the fact that ϕ_{12} and ϕ_{20} cancel to lowest order leaving a dipole interaction. Applying identity (3.27) to $\partial\phi_{12} / \partial z_2 = (z_1 - z_2) / |\mathbf{r}_1 - \mathbf{r}_2|^3$ and to $\partial\phi_{20} / \partial z_2 = z_2 / |\mathbf{r}_2|^3$ yields the approximate relation

$$\left(\frac{\partial\phi_{12}}{\partial z_2}+\frac{\partial\phi_{20}}{\partial z_2}\right)\cong\frac{2}{\pi}\int_0^\infty dq\, q\, K_0(q\rho_{12})\left(qz_1\cos qz_2-\sin qz_2\right)$$
$$+\frac{2}{\pi}\int_0^\infty dq\, q\, K_0(q\rho_2)\sin qz_2 \quad , \tag{3.30}$$

which is accurate to order $1/\rho_2^3$. Also, using identity (3.27) to evaluate $\partial\phi_{12}/\partial z_1\cong z_2/\left(z_2^2+\rho_2^2\right)^{3/2}$, substituting for the zeroth-order orbits, and evaluating the z_2, ψ_1, q, and t' integrals in that order yields the result B=A; so Eq. (3.25) reduces to

$$\tau_1\frac{\partial\bar{f}_1}{\partial t}=-\frac{\partial}{\partial\varepsilon_1}\left[A\left(\bar{f}_1+\frac{\partial\bar{f}_1}{\partial\varepsilon_1}\right)\right] \tag{3.31}$$

Of course, this result would have been anticipated since the bracket on the right must vanish for a thermal distribution [Eq. (3.10)].

What conclusions can be drawn from this simple calculation? First, we note that A is exponentially small for sufficiently large ρ_d. By using the large ξ asymptotic expansion $K_0(\xi)=\left(\pi/2\xi\right)^{1/2}\exp(-\xi)$ and evaluating the v_2 integral with the saddle point method, Eq. (3.29) reduces to the form

$$A=+n_e b^3\tau_1(a_1\omega_1)^2\frac{2\pi^2}{\sqrt{3}}\frac{\exp\left[-\frac{3}{2}(2\omega_1\rho_d)^{2/3}\right]}{(2\omega_1\rho_d)^{1/3}} \tag{3.32}$$

In terms of unscaled variables the argument of the exponential is given by $(2\omega_1\rho_d)^{2/3}\rightarrow(2\omega_1\rho_d/v_e)^{2/3}$. The exponential cutoff is simply a manifestation of an adiabatic invariant for the oscillatory motion of electron 1. This invariant is nearly conserved when the interaction field is slowly varying (i.e., $\omega_1 >> v_e/\rho_d$). Note that the existence of this invariant is not associated with the approximation that electron 1 is bound tightly enough that its oscillatory motion is simple harmonic. The result can be generalized by using action angle variables. Another conclusion follows from the observation that A is sensitive to the value of ρ_d when ρ_d is pushed down to the range $\rho_d\sim 1$ where the

expansion procedure fails. This means that small impact parameter collisions make a significant contribution and the Fokker-Planck treatment is not the whole story.

Incidentally, the analysis can be carried out when the $\mathbf{E} \times \mathbf{B}$ drift motion is retained, and a correction to A of order $\delta A \sim (r_{ce} / b)^2 A$. The smallness of the correction is simply a verification of the fact that this motion is negligible.

3.5. Variational Theory and the Kinetic Bottleneck

The variational theory of three-body recombination [3.15] can be thought of as the opposite limit from the Fokker-Planck theory; the distribution function is assumed to vary sharply compared to a step size. Anticipating the existence of a bottleneck, the variational theory presumes that the distribution $f_2(1,2)$ is zero for $\varepsilon_1 > \varepsilon$ and is of the thermal equilibrium form

$$f_2(1,2) = (1/2\pi)\, e^{\varepsilon_1 + \varepsilon_2 - \phi_{12}} \tag{3.33}$$

for $\varepsilon_1 < \varepsilon$. Here, electron 1 is bound and electron 2 is a free electron that interacts with electron 1; the value of ε_1 is ultimately chosen to be the energy location of the bottleneck. The theory requires a specification of $f_2(1,2)$ on the surface $\varepsilon_1 = \varepsilon$, and from Eq. (3.6) one can see that the term $v_1 (\partial \phi_{12} / \partial z_1)(\partial f_2 / \partial \varepsilon_1)$ convects the thermal form of f_2 to the surface for $v_1\, \partial \phi_{12} / \partial z_1 > 0$ and convects the zero value to the surface $v_1\, \partial \phi_{12} / \partial z_1 < 0$.

The first step is to calculate the flux of electrons through the surface $\varepsilon_1 = \varepsilon$. From Eq. (3.9) and from the relation

$$\frac{dN}{d\varepsilon_1} = n_e b^3 \int d\mathbf{r}_{1\perp} \oint_{\varepsilon_1} \frac{dz_1}{v_1}\, \bar{f}_1(\rho_1, \varepsilon_1) \tag{3.34}$$

one can see that the dimensionless flux toward deeper binding through the surface $\varepsilon_1 = \varepsilon$ is given by

$$R(\varepsilon) = \left(n_e b^3\right)^2 \int d\mathbf{r}_{1\perp} \oint_{\varepsilon_1=\varepsilon} \frac{dz_1}{v_1} \int d\mathbf{r}_2 \, dv_2 \; v_1 \frac{\partial \phi_{12}}{\partial z_1} f_2(1,2) \tag{3.35}$$

Here, the distribution $f_2(1,2)$ is taken to be of the thermal equilibrium form for $v_1 \, \partial\phi_{12} / \partial z_1 > 0$ and to be zero for $v_1 \, \partial\phi_{12} / \partial z_1 < 0$. In the (z_1, v_1) phase space, the loop defined by $\varepsilon_1 = \varepsilon$ is such that $v_1 > 0$ for the top half and $v_1 < 0$ for the bottom half. Consequently, $v_1 \, \partial\phi_{12} / \partial z_1 > 0$ at any point z_1 for either the top or the bottom of the loop, and Eq. (3.35) can be rewritten as

$$R(\varepsilon) = \left(n_e b^3\right)^2 \int d\mathbf{r}_{1\perp} \int dz_1 \int d\mathbf{r}_2 \, dv_2 \left| \frac{\partial \phi_{12}}{\partial z_1} \right| f_2 \tag{3.36}$$

where f_2 is of the thermal equilibrium form and is evaluated for $\varepsilon_1 = \varepsilon$. The integral over z_1 is over one half the loop in the direction of increasing z_1 (i.e., $-\sqrt{\varepsilon^{-2} - r_{1\perp}^2} < z_1 < \sqrt{\varepsilon^{-2} - r_{1\perp}^2}$.

Also, we restrict the domain of integration to the regime where $\varepsilon_1 + \varepsilon_2 - \phi_{12} < \varepsilon_1$; this insures that it is energetically possible for electron 1 to move from $\varepsilon_1 = \varepsilon$ to deeper binding and for electron 2 to escape to infinity. This restriction can be rewritten as a restriction on the domain of the v_2-integration (i.e., $v_2^2 / 2 + \phi_{12} + \phi_{20} > 0$).

One final restriction is necessary. Large impact parameter collisions produce small steps in the binding energy, some positive and some negative, and as we have seen, the evolution due to these collisions is diffusive in nature. In addition, large impact parameter collisions tend to have recrossings of the surface $\varepsilon_1 = \varepsilon$ during the course of a collision. The one-way thermal equilibrium flux being calculated here would greatly overestimate the contribution from these collisions; in fact, the contribution would diverge. For that reason, the integral in Eq. (3.36) is cut off for $|\mathbf{r}_2 - \mathbf{r}_1| \geq C / \varepsilon$, where C is a constant. To understand the scaling with ε, note that $|\mathbf{r}_1|_{max} \geq 1/\varepsilon$ and that $|\mathbf{r}_2 - \mathbf{r}_1|$ must be less than on the order of $|\mathbf{r}_1|_{max}$ for the interaction to make a substantial change in the atomic state.

It is convenient to change variables from $(\mathbf{r}_1, \mathbf{r}_2)$ to $(\bar{r}_1, \zeta, \psi, \bar{r}_{21}, \theta, \varphi)$ where

$$(\mathbf{r}_2-\mathbf{r}_1)=\bar{r}_{21}\varepsilon^{-1}\left(\sin\theta\cos\varphi\,\hat{x}+\sin\theta\sin\varphi\,\hat{y}+\cos\theta\,\hat{z}\right), \tag{3.37a}$$

$$\mathbf{r}_1=\bar{r}_1\varepsilon^{-1}\left(\sin\zeta\cos\psi\,\hat{x}'+\sin\zeta\sin\psi\,\hat{y}'+\cos\zeta\,\hat{z}'\right), \tag{3.37b}$$

and

$$\hat{z}'=\sin\theta\cos\varphi\,\hat{x}+\sin\theta\sin\varphi\,\hat{y}+\cos\theta\,\hat{z}, \tag{3.38a}$$

$$\hat{y}'=-\sin\varphi\,\hat{x}+\cos\varphi\,\hat{y}, \tag{3.38b}$$

$$\hat{x}'=\cos\theta\cos\varphi\,\hat{x}+\cos\theta\sin\varphi\,\hat{y}-\sin\theta\,\hat{z}. \tag{3.38c}$$

An important point to note is that $\hat{z}'$ is directed along the $(\mathbf{r}_2-\mathbf{r}_1)$ direction; so ζ is the angle between $(\mathbf{r}_2-\mathbf{r}_1)$ and $\mathbf{r}_1$. Rewriting Eq. (3.36) in terms of these variables, taking into account the restrictions on the domain of integration, and carrying out the υ_2-integration yields the result

$$R(\varepsilon)=\left(n_e b^3\right)^2\frac{e^{\varepsilon}}{2\pi\varepsilon^4}\int_0^C d\bar{r}_{21}\,\bar{r}_{21}^2\int_0^{\pi}d\theta\,\sin\theta\int_0^{2\pi}d\varphi\int_0^1 d\bar{r}_1\,\bar{r}_1^2$$
$$\times\int_0^{\pi}d\zeta\,\sin\zeta\int_0^{2\pi}d\psi\,\frac{|\cos\theta|}{\bar{r}_{21}^2}e^{\mu}\sqrt{2\pi}\,F(\mu), \tag{3.39}$$

where $F(\mu)=\operatorname{erfc}\left(\sqrt{\max(\mu,0)}\right)$ and

$$\mu=\varepsilon\left(\frac{1}{\sqrt{\bar{r}_1^2+\bar{r}_{21}^2-2\bar{r}_1\bar{r}_{21}\cos\zeta}}-\frac{1}{\bar{r}_{21}}\right). \tag{3.40}$$

The integrations over all angles except ζ can be carried out trivially and yield

$$R(\varepsilon)=\left(n_e b^3\right)^2\frac{e^{\varepsilon}}{\varepsilon^4}(2\pi)^{3/2}\int_0^C d\bar{r}_{21}\int_0^1 d\bar{r}_1\,\bar{r}_1^2\int_{-1}^1 dx\,e^{\mu}\,F(\mu), \tag{3.41}$$

where $x=\cos\zeta$.

The behavior of $R(\varepsilon)$ can be examined by looking at an upper bound. Using the inequality $F(\mu)e^{\mu}\le 1$ in Eq. (3.41) and carrying out the integrals yields

$$R(\varepsilon) \le \left(n_e b^3\right)^2 C \frac{e^{\varepsilon}}{\varepsilon^4} \frac{2(2\pi)^{3/2}}{3} . \tag{3.42}$$

The minimum value of the right-hand side is approximately $(2.2)\left(n_e b^3\right)^2 C$ and is attained at $\varepsilon = 4$. This strong minimum in the one-way thermal equilibrium flux is called the bottleneck; it is due to a competition between the Boltzmann factor e^{ε} and the phase space factor ε^{-4}. The variational theory takes the value of the flux at the bottleneck to be the recombination rate.

A more accurate evaluation of Eq. (3.41) can be carried out numerically. Such evaluations have been used to minimize $R(\varepsilon)$ for various values of C, and the results are shown in Figs. 3.2 and 3.3. Figure 3.2 shows the location of the minimum (or bottleneck) ε_b. As one would expect from Eq. (3.42), the location of the minimum in $R(\varepsilon)$ is insensitive to the value of C and has the approximate value $\varepsilon_b \approx 4$. Figure 3.3 displays the value of the minimum flux. The bound on the minimum flux Eq. (3.42) is always greater than the calculated value, as we would expect. In addition, the minimum flux scales as C to the first power as C goes to infinity – the same as the upper bound.

The variational theory illustrates the idea of a bottleneck and provides an order of magnitude estimate of the recombination rate but does not provide an accurate value of the rate. First, the theory has a free parameter, C, to compensate for recrossings. Although the Fokker-Planck analysis suggests that C is of order unity, its precise value is not known. Second, the bottleneck is not infinitely sharp but extends over some finite range $\Delta\varepsilon \sim O(1)$. At the low ε end of this range, the atomic states are populated according to thermal equilibrium, but the flux is not predominantly one way. At the high ε end, the flux is predominantly toward deeper binding but the atomic states are depleted relative to thermal equilibrium. There is no one surface where the states are populated according to thermal equilibrium and the flux is predominantly one way. Finally, the theory assumes that the surface defining the bottleneck depends only on ε, rather than on ε and ρ. Such an

assumption makes sense when the transitions between ρ values are more rapid than those between ε values, but this is not the case where a strong magnetic field is present.

3.6. Monte Carlo Simulation

This section presents a numerical simulation of the recombination process and a numerical determination of the rate. The simulation traces the state of an atom through a sequence of collisions with electrons from the background plasma. The distribution of atomic states is assumed to be of the thermal equilibrium form down to some energy $\varepsilon_{th} > 0$. We will choose ε_{th} to be substantially smaller than the bottleneck energy $\varepsilon_b \approx 4$ and will find from the numerical results themselves that the thermal distribution extends below ε_{th}. To initiate the simulation, an electron in an initial state chosen at random from the thermal distribution for the background plasma is allowed to collide with an atom in an initial state chosen at random from the thermal distribution of atomic states (i.e., $\varepsilon < \varepsilon_{th}$). This process is repeated until an atom is formed with binding energy greater than ε_{th}. The state of this atom is then followed through a sequence of collisions with electrons chosen at random from the thermal distribution for the background plasma. The simulation stops following the atomic state, when the state goes back into the thermal distribution ($\varepsilon < \varepsilon_{th}$) or reaches the sink ($\varepsilon > \varepsilon_s$). We will choose ε_s to be substantially larger than the bottleneck energy ($\varepsilon_s >> \varepsilon_b$) and will find from the numerical results themselves that it is very unlikely for an atom to be re-ionized once it has passed beyond the bottleneck. An atom that reaches the sink is declared to be recombined, and the steady state flux to the sink is the recombination rate.

Formally one may think of this simulation as a Monte Carlo solution of the master equation, Eq. (3.19). This equation describes a Markov process [3.16] with transition rates $k(\rho,\varepsilon|\overline{\rho},\overline{\varepsilon})$. The evolution of a guiding center atom in the state (ρ,ε) is governed by

the probability that the earliest change in state is at a time between t and $t+dt$ to a state with energy between $\bar{\varepsilon}$ and $\bar{\varepsilon}+d\bar{\varepsilon}$ and radial position between $\bar{\rho}$ and $\bar{\rho}+d\bar{\rho}$

$$P(\bar{\rho},\bar{\varepsilon},t)\,d\bar{\rho}\,d\bar{\varepsilon}\,dt = k(\rho,\varepsilon|\bar{\rho},\bar{\varepsilon})\,e^{-R(\rho,\varepsilon)t}\,d\bar{\rho}\,d\bar{\varepsilon}\,dt, \tag{3.43}$$

where the total collision rate $R(\rho,\varepsilon)$ is given by

$$R(\rho,\varepsilon) = \int k(\rho,\varepsilon|\bar{\rho},\bar{\varepsilon})\,d\bar{\rho}\,d\bar{\varepsilon} \tag{3.44}$$

Such an evolution, where the next step is dependent only on the current state rather than the past history, is what we mean by a Markov process. The Monte Carlo aspect of the simulation is the determination of the time of the transition and of the final state by a random choice weighted according to $P(\bar{\rho},\bar{\varepsilon},t)$.

The choice of $(\bar{\rho},\bar{\varepsilon})$ and t is complicated by the expression for the transition rate, Eq. (3.16a), which is not a simple function of $\bar{\rho}$ and $\bar{\varepsilon}$. It is dependent on the functions $\rho_+(z,\rho,\varepsilon,\rho_2,\theta_2,\varepsilon_2)$ and $\varepsilon_+(z,\rho,\varepsilon,\rho_2,\theta_2,\varepsilon_2)$ that must be determined by numerical integration of the equations of motion. (Here, we have replaced z_1, ρ_1, ε_1 by z, ρ, ε.) Although it is convenient to have a simple expression for the transition rate, it suffices to have a numerical method of choosing $(\bar{\rho},\bar{\varepsilon})$ in a manner consistent with the distribution $k(\rho,\varepsilon|\bar{\rho},\bar{\varepsilon})$. To this end, we choose the pre-collision variables in a manner dictated by the weighting factor in the transition rate, that is,

$$P(z,\rho_2,\theta_2,\upsilon_2)\,dz\,d\rho_2\,d\theta_2\,d\upsilon_2 = \frac{\rho_2\,d\rho_2\,d\theta_2\,|\upsilon_2|\,f_{ik}(\varepsilon_2)\,d\upsilon_2\,dz\,/\,\upsilon(z,\rho,\varepsilon)}{\int d\upsilon_2\,d\rho_2\,d\theta_2\,\rho_2\,|\upsilon_2|\,f_{ik}(\varepsilon_2)\oint_\varepsilon dz\,/\,\upsilon(z,\rho,\varepsilon)} \tag{3.45}$$

With the initial conditions chosen in this manner, the equations of motion are integrated numerically to determine $(\bar{\rho},\bar{\varepsilon})$, and it is an easy exercise to show that $(\bar{\rho},\bar{\varepsilon})$ so chosen are distributed according to $k(\rho,\varepsilon|\bar{\rho},\bar{\varepsilon})$.

A technical complication arises from the fact that the integral over ρ_2 diverges in the normalization factor above and in the total collision rate

$$R(\rho,\varepsilon) = n_e b^3 \frac{1}{\tau(\rho,\varepsilon)} \oint \frac{dz}{v(z,\rho,\varepsilon)} \int d\rho_2\, \rho_2\, d\theta_2\, dv_2\, |v_2|\, f_{th}(\varepsilon_2) \,, \tag{3.46}$$

which is obtained by substituting Eq. (3.16) into Eq. (3.44) and carrying out the integrals over the delta functions. However, we know from the Fokker-Planck analysis [see Eq. (3.32)] that the large ρ_2 collisions contribute an exponentially small amount to the diffusion coefficient. The divergence can be removed without affecting the transport by introducing a cutoff for ρ_2. We take the cutoff to be the larger of the adiabatic cutoff (i.e., the radius at which the product of the z-bounce frequency $\omega_z \sim \varepsilon^{-3/2}$ and the collision time $t_c \sim \rho / v_2$ is much greater than one) and the maximum radius at which an electron can be bound with energy ε (i.e., $\rho \sim \varepsilon^{-1}$). The second condition is necessary so that we can make the dipole approximation for the interaction potential ϕ_{12} as was done in the Fokker-Planck analysis. The cutoff can be stated simply as

$$\rho_c(\varepsilon, v_2) = C' \max\left(v_2 \varepsilon^{-3/2}, \varepsilon^{-1}\right), \tag{3.47}$$

where C' is some constant. We choose C' to be large enough that the results of the Monte Carlo simulation are insensitive to a further increase in C'.

We now wish to obtain a set of possible realizations for the temporal evolution of the state of a bound atom. To get one possible evolution we need to follow an atom through a sequence of collisions with electrons. The choice of initial state for the atom requires some explanation. Since unbound electrons stream in from infinity, where the plasma is specified to be in thermal equilibrium, we know that the distribution of states is of the thermal equilibrium form for $\varepsilon < 0$. Also, there is rapid thermalization of the weakly bound states $0 < \varepsilon << 1$ and, in steady state, thermalization down to near the bottleneck energy $\varepsilon_b \approx 4$. For the numerical work, we assume that the distribution of atomic states is thermal down to some small but positive binding energy ε_{th} ($0 < \varepsilon_{th} < \varepsilon_b$). We choose ε_{th} to be large enough that any initial state with $\varepsilon > \varepsilon_{th}$ has a reasonable probability (e.g.,

1/400 for $\varepsilon_{th} \approx 1$) of evolving through subsequent collisions to the sink. We consider transitions out of this thermal sea to deeper binding (from $\varepsilon < \varepsilon_{th}$ to $\bar{\varepsilon} > \varepsilon_{th}$). The rate of such transitions into a state $(\bar{\rho}, \bar{\varepsilon})$, where $\bar{\varepsilon} > \varepsilon_{th}$, is given by

$$k_{\downarrow}(\bar{\rho}, \bar{\varepsilon}) = \int_{\varepsilon < \varepsilon_{th}} d\rho \, d\varepsilon \, k(\rho, \varepsilon | \bar{\rho}, \bar{\varepsilon}) \, W_{th}(\rho, \varepsilon) \tag{3.48}$$

and the total rate for transitions to any state with $\bar{\varepsilon} > \varepsilon_{th}$ is given by

$$R_{\downarrow} = \int_{\bar{\varepsilon} > \varepsilon_{th}} d\bar{\rho} \, d\bar{\varepsilon} \, k_{\downarrow}(\bar{\rho}, \bar{\varepsilon}) \tag{3.49}$$

Thus, the probability that the earliest transition occurs between t^* and $t^* + dt^*$ and is to a state with energy between $\bar{\varepsilon}_0$ and $\bar{\varepsilon}_0 + d\bar{\varepsilon}_0$ and radial position between $\bar{\rho}_0$ and $\bar{\rho}_0 + d\bar{\rho}_0$ is given by

$$P(\bar{\rho}_0, \bar{\varepsilon}_0, t^*) \, d\bar{\rho}_0 \, d\bar{\varepsilon}_0 \, dt^* = k_{\downarrow}(\bar{\rho}_0, \bar{\varepsilon}_0) \, e^{-R_{\downarrow} t^*} \, d\bar{\rho}_0 \, d\bar{\varepsilon}_0 \, dt^* \tag{3.50}$$

where the subscript 0 refers to the fact that $(\bar{\rho}_0, \bar{\varepsilon}_0)$ is the initial state in the evolution.

Rather than work with $k_{\downarrow}(\bar{\rho}, \bar{\varepsilon})$ and $R_{\downarrow}$, it is useful (for numerical reasons) to introduce the inverse problem and rely on detailed balance. We will explain the reason for this after the method has been presented. If the states with $\bar{\varepsilon} > \varepsilon_{th}$ were distributed thermally, then the rate of transitions into some state (ρ, ε), where $\varepsilon < \varepsilon_{th}$, would be given by

$$k_{\uparrow}(\rho, \varepsilon) = \int_{\bar{\varepsilon} < \varepsilon_{th}} d\bar{\rho} \, d\bar{\varepsilon} \, k(\bar{\rho}, \bar{\varepsilon} | \rho, \varepsilon) \, W_{th}(\bar{\rho}, \bar{\varepsilon}) \tag{3.51}$$

Likewise, the total rate into all such states would be given by

$$R_{\uparrow} = \int_{\varepsilon < \varepsilon_{th}} d\rho \, d\varepsilon \, k_{\uparrow}(\rho, \varepsilon) = \int_{\bar{\varepsilon} > \varepsilon_{th}} d\bar{\rho} \, d\bar{\varepsilon} \, k_{\uparrow}^{-1}(\bar{\rho}, \bar{\varepsilon}) \tag{3.52}$$

where

$$k_{\uparrow}^{-1}(\bar{\rho}, \bar{\varepsilon}) \equiv \int_{\varepsilon < \varepsilon_{th}} d\rho \, d\varepsilon \, k(\bar{\rho}, \bar{\varepsilon} | \rho, \varepsilon) \, W_{th}(\bar{\rho}, \bar{\varepsilon}) \tag{3.53}$$

From detailed balance [Eq. (3.18)], it follows that $k_\downarrow(\bar{\rho},\bar{\varepsilon}) = k_\uparrow^{-1}(\bar{\rho},\bar{\varepsilon})$ and that $R_\downarrow = R_\uparrow$. Consequently, the distribution of initial states and times can be rewritten as $P(\bar{\rho}_0,\bar{\varepsilon}_0,t^*) = k_\uparrow^{-1}(\bar{\rho}_0,\bar{\varepsilon}_0)\exp(-R_\uparrow t^*)$.

We use a numerical procedure to pick $(\bar{\rho}_0,\bar{\varepsilon}_0)$ according to this distribution. First, define the quantity

$$\begin{aligned}\Phi &= \int_{\text{all }\varepsilon} d\rho\, d\varepsilon\, k_\uparrow(\rho,\varepsilon) \\ &= \left(n_e b^3\right)^2 \int_{\bar{\varepsilon}_0>\varepsilon_{th}} 2\pi\bar{\rho}_0\, d\bar{\rho}_0\, d\bar{\varepsilon}_0 \frac{d\bar{z}_0}{\upsilon(\bar{z}_0,\bar{\rho}_0,\bar{\varepsilon}_0)} f_{th}(\bar{\varepsilon}_0) \\ &\times \int \rho_2\, d\rho_2\, d\theta_2\, d\upsilon_2 \left|\upsilon_2\right| f_{th}(\varepsilon_2)\end{aligned} \tag{3.54}$$

which is the sum (or integral) of the collision frequencies for all of the atoms with $\bar{\varepsilon}_0 > \varepsilon_{th}$ (the distribution of states being assumed thermal). The procedure is to choose $(\bar{z}_0,\bar{\rho}_0,\bar{\varepsilon}_0,\rho_2,\theta_2,\varepsilon_2)$ according to their contribution to Φ and then to integrate numerically through the collision to the final $\varepsilon = \varepsilon_+(\bar{z}_0,\bar{\rho}_0,\bar{\varepsilon}_0,\rho_2,\theta_2,\varepsilon_2)$ and $\rho = \rho_+(\bar{z}_0,\bar{\rho}_0,\bar{\varepsilon}_0,\rho_2,\theta_2,\varepsilon_2)$. Reject this try if $\varepsilon > \varepsilon_{th}$, but retain it if $\varepsilon < \varepsilon_{th}$. One can show that $(\bar{\rho}_0,\bar{\varepsilon}_0)$ so determined are distributed according to $k_\uparrow^{-1}(\bar{\rho}_0,\bar{\varepsilon}_0)$. Also if N_T is the total number of trys and $N_\uparrow$ is the number retained, then as N_T becomes large $R_\uparrow \cong \left(N_\uparrow / N_T\right)\Phi$.

Technical complications arise again from the fact that the integrals over ρ_2 and $\bar{\varepsilon}_0$ diverge in the expression for Φ [Eq. (3.54)]. The divergence in ρ_2 can be removed by introducing a cutoff for ρ_2 as we did in Eq. (3.47). The divergence in $\bar{\varepsilon}_0$ we remove by introducing a lower bound ε_c such that $\varepsilon_c > \varepsilon_{th}$ (see Fig. 3.4). This cutoff is chosen large enough so that the average change in ε during a collision (i.e. $\langle\Delta\varepsilon\rangle$) is much less than $\varepsilon_c - \varepsilon_{th}$. We check that the results are insensitive to to a further increase in ε_c.

One may now ask why did we have to consider the inverse problem when an analogous algorithm could have been defined for the original problem. The answer is efficiency. Most $(\bar{\rho}_0,\bar{\varepsilon}_0)$ chosen in the inverse algorithm are close to ε_{th}, that is, within $\langle\Delta\varepsilon\rangle$. In addition, the transitions normally lead to a smaller value for ε compared to $\bar{\varepsilon}_0$.

This implies that most transitions have $\varepsilon < \varepsilon_{th}$, leading to few rejections. The opposite would be true of a forward algorithm. Most initial (ρ,ε) would not be within $(\Delta\varepsilon)$ of ε_{th} and transitions would normally lead to a smaller value for $\bar{\varepsilon}_0$ when compared to ε. Hence most transitions would have $\bar{\varepsilon}_0 < \varepsilon_{th}$, leading to many rejections. It is therefore preferable to use the inverse algorithm.

Once we have the initial state $(\bar{\rho}_0,\bar{\varepsilon}_0)$ we continue to follow the evolution through a sequence of collisions until the bound electron is re-ionized or enters the sink. The procedure is then repeated many times with the initial time (t^*) of each evolution measured relative to the initial time of the previous evolution. This ensures that the flux through $\varepsilon = \varepsilon_{th}$ is given by $R_\downarrow$. We refer to a sequence of $N_\uparrow$ such evolutions as a time history for one member of the ensemble of plasmas. Figure 3.5 shows a graphical representation of a sample time history.

There are three well-separated time scales in a time history. The smallest of these is the duration of a collision: $(v_e / b)^{-1}$ in unscaled variables and unity in scaled variables. (Figure 3.5 is drawn as though a collision were instantaneous.) The second is the time between collisions: $(n_e b^2 v_e)^{-1}$ in unscaled variables and $(n_e b^3)^{-1}$ in scaled variables. This is the time scale for the duration of an evolution. The third is the time for an electron to make a transition out of the thermal sea to a state with $\varepsilon > \varepsilon_{th}$: $(n_e^2 b^5 v_e)^{-1}$ in unscaled variables and $(n_e b^3)^{-2}$ in scaled variables. This is the time between evolutions. Since the plasma is weakly correlated (i.e., $n_e b^3 << 1$), the three time scales are ordered as $(v_e / b)^{-1} << (n_e v_e b^2)^{-1} << (n_e^2 v_e b^5)^{-1}$. In other words, a collision is complete before another begins and an evolution is complete before another begins.

Each member of the ensemble of plasmas has an associated time history, and the distribution function $W(\rho,\varepsilon,t)$ that appears in the master equation [i.e., Eq. (3.19)] can be constructed as an ensemble average over the time histories.

The boundary conditions on the integrodifferential master equation are $W(\rho,\varepsilon,t)=W_{th}(\rho,\varepsilon)$ for $\varepsilon<\varepsilon_{th}$ and $W(\rho,\varepsilon,t)=0$ for $\varepsilon>\varepsilon_s$. These are enforced by the method by which initial states $(\overline{\rho}_0,\overline{\varepsilon}_0)$ are chosen and the removal of atoms which reach the sink. The initial condition on $W(\rho,\varepsilon,t)$ between ε_{th} and ε_s is $W(\rho,\varepsilon,t=0)=0$. This initial condition is built into the time history since no evolution can start before $t=0$.

By invoking the equality of the temporal average and the ensemble average, we can obtain steady state quantities from a single time history. For example, the steady state flux to the sink (the recombination rate) is given by $R_3=R_s=\Phi N_s/N_T$, where N_s is the number of the initial tries which reach the sink in the course of their subsequent evolution. Likewise, the steady state distribution is given by

$$W_{ss}(\rho,\varepsilon)\approx\frac{R_\uparrow}{N_\uparrow}\frac{1}{\Delta\varepsilon\,\Delta\rho}\sum_{ij}t_{ij}\,\Delta\theta(\varepsilon_{ij};\varepsilon,\Delta\varepsilon)\,\Delta\theta(\rho_{ij};\rho,\Delta\rho)\,, \tag{3.55}$$

where $N_\uparrow/R_\uparrow$ is the total elapsed time in the time history,

$$\Delta\theta(x;x_0,\Delta x)=\begin{cases}1, & \text{if } x_0\le x\le x_0+\Delta x,\\ 0, & \text{otherwise,}\end{cases}$$

and t_{ij} is the time spent in the j th state in the i th evolution.

Not only can steady state flow rates and distribution functions be obtained; one can estimate the time-dependent distribution function $W(\rho,\varepsilon,t)$. This needs to be examined in order to see how the steady state is established. The straightforward way to do this is to generate many time histories, that is, many realizations of the ensemble of plasmas. One would then count how many of these histories are in a state (ρ,ε) at time t as an estimate of the distribution function. The problem is that very few realizations would be in any given state at any given time; more specifically only $n_e b^3$ of the histories generated. To compound the problem, each time history is very expensive to generate since one must numerically integrate through many collisions. What we choose to do instead is to use one time history and manipulate it to generate a large subensemble of the ensemble of plasmas.

An easy way to see how this is done is to first understand that each evolution in a time history is independent of the other evolutions. The time at which an evolution starts is not dependent on the details of that evolution or any other. This will allow us to place the $N_\uparrow$ evolutions in the time history at any time between 0 and $N_\uparrow / R_\uparrow$ with equal probability and to thereby generate an infinite number of realizations of the ensemble. These realizations are a large subensemble that gives us a good estimate of $W(\rho,\varepsilon,t)$. When the average over this subensemble is done one finds that

$$W(\rho,\varepsilon,t) \approx \frac{R_\uparrow}{N_\uparrow}\frac{1}{\Delta\varepsilon\,\Delta\rho}\sum_{ij} t_{ij}\;\Delta\theta(\varepsilon_{ij};\varepsilon,\Delta\varepsilon)\,\Delta\theta(\rho_{ij};\rho,\Delta\rho)\;\theta\left(\sum_{l=1}^{j} t_{il}\,;t\right) \tag{3.56}$$

where

$$\theta(x;x_0)=\begin{cases}1, & \text{if } x\le x_0,\\ 0, & \text{otherwise.}\end{cases}$$

The earlier statement that a temporal average is equal to an ensemble average in steady state can now be justified. Consider a time such that $t_\infty >> \left(n_e b^2 \upsilon_e\right)^{-1}$. For such a time $\theta\left(\sum_{l=1}^{j} t_{il}\,;t_\infty\right)=1$ for all i and j, so that Eq. (3.56) reduces to Eq. (3.55) [i.e., $W(\rho,\varepsilon,t_\infty)=W_{th}(\rho,\varepsilon)$].

Since we now have an estimate of the time-dependent distribution function, all physically meaningful average quantities can be estimated along with their time dependence. We now present the results of a Monte Carlo simulation. The recombination process is simulated by generating 20,000 evolutions. The value of ε_{th} used is 1, and the value of ε_c used is 4. The ρ_2 cutoff C' is 4. The following results are found to be insensitive to a further increase in ε_c or C'. The value for which an atom is considered recombined ε_s is 20, well below the expected bottleneck at $\varepsilon_b \sim 4$. Only 1/400 of the evolutions reach ε_s. This corresponds to a numerically calculated recombination rate $R_3 \approx 0.070(10) n_e^2 b^5 \upsilon_e$.

The existence of the bottleneck is illustrated in Fig. 3.6. This is a plot (as a function of ε) of the fraction of the evolutions $N_\varepsilon / N_\uparrow$ that make it to the energy ε. Note that almost all, 399 out of 400, of the evolutions lead to re-ionization, but all of the evolutions that make it past $\varepsilon = 10$ eventually reach the sink at ε_s. This allows the unambigious definition of a recombined atom as one which reaches the sink. It also confirms that there is some energy ε_b between $\varepsilon_{th} = 1$ and $\varepsilon = 10$ such that if an atom is bound with less energy ($\varepsilon < \varepsilon_b$) it is more likely to be ionized and if it is bound with more energy ($\varepsilon > \varepsilon_b$) it is more likely to be recombined. The bottleneck energy ε_b can be determined from Fig. 3.6 by finding the energy for which the fraction $N_\varepsilon / N_\uparrow$ is twice its constant value for deep binding. This value is found to be $\varepsilon_b \approx 4.9(10)$, which agrees with the expected bottleneck of $\varepsilon_b \approx 4.0 \rightarrow 4.5$ shown in Fig. 3.2. In addition, the finite width of the bottleneck is evidenced by the smooth approach of $N_\varepsilon / N_\uparrow$ to its constant value at deep binding. If the bottleneck was infinitely sharp we would see a discontinuous jump of $N_\varepsilon / N_\uparrow$ at ε_b to its value at deep binding.

The time dependent distribution function, divided by its thermal equilibrium value $W(\rho, \varepsilon, t) / W_{th}(\rho, \varepsilon)$ is shown in Fig. 3.7. For convenience we plot this function in $(\varepsilon\rho, \varepsilon)$ space rather than (ρ, ε) space. The maximum value of $\varepsilon\rho$ is unity, so the boundary of the space is rectangular. We display the distribution function for four different times ($t n_e b^2 v_e = 0, 0.1, 1$ and 10) as well as the time asymptotic result ($t = \infty$). The value of the distribution function is indicated by the shade of gray displayed on the $(\varepsilon\rho, \varepsilon)$ plane. Black corresponds to thermal equilibrium and white to total depletion. We first concentrate on the steady state function Fig. 3.7(e) which remains at its thermal equilibrium value until $\varepsilon \approx 4$ then precipitously drops off from that value. This again confirms the existence of the bottleneck and justifies the initial formation process with $\varepsilon_{th} = 1$. To more dramatically show the bottleneck, the ρ-integrated time dependent distribution function

$$W(\varepsilon,t) \equiv \int_0^{1/\varepsilon} d\rho\, W(\rho,\varepsilon,t) \tag{3.57}$$

divided by its thermal value is shown in Fig. 3.8. We display the ρ-integrated distribution function at three different times ($t n_e b^2 v_e = 0.1, 1$ and 10) as well as the time asymptotic result ($t = \infty$). We again focus your attention to the steady state values shown as diamonds. The ρ-integration takes the average of the full distribution function shown in Fig. 3.7 along a horizontal line of constant ε. This allows us to display in a more quantitative way how quickly the distribution function is depleted by many orders of magnitude as one moves beyond the bottleneck.

Another interesting feature of Fig. 3.7(e) is illustrated by the average $\varepsilon\rho$ value

$$\langle \varepsilon\rho \rangle \equiv \frac{1}{W_{ss}(\varepsilon)} \int_0^{1/\varepsilon} d\rho\, (\varepsilon\rho)\, W_{ss}(\rho,\varepsilon) \tag{3.58}$$

which is plotted in Fig. 3.9. This graph shows that the value of the moment $\langle \varepsilon\rho \rangle$ is larger than the value for a thermal equilibrium distribution. This has a rather simple explanation. First, remember that collisions that do not involve an electron exchange do not change ρ values. In $(\varepsilon\rho, \varepsilon)$ space this corresponds to remaining on the same line through the origin, $\varepsilon = (1/\rho)\,\varepsilon\rho$. To change the value of ρ [i.e., jump off the line, $\varepsilon = (1/\rho)\,\varepsilon\rho$] a collision involving an electron exchange must occur; but only a small fraction of the collisions, ($\approx 1/100$) involve electron exchange. What happens is that below the bottleneck an atom hops along a line of constant ρ until an electron exchange collision occurs. Initially, the atom will usually be formed at a large ρ value. It will then have to wait for the rare exchange collision to be able to jump to the lines with smaller ρ. This causes a traffic jam of atoms at large ρ since the routes to smaller ρ are partially blocked. The final result is that the distribution function is skewed toward larger ρ values, and this increases the moment $\langle \varepsilon\rho \rangle$ relative to the thermal equilibrium value.

We now turn our attention to the time dependence of the distribution function; that is, to the question of how fast the steady state is established. The evolution of the distribution function $W(\rho,\varepsilon,t)$ from its initial condition to its steady state is illustrated in Figs. 3.7 and 3.8. One can see a front of occupation that moves to deeper binding as time progresses.

The location of the front as a function of time [i.e., $\varepsilon = \varepsilon(t)$] is shown in Fig. 3.10. It is obtained by plotting the time for which the ρ-integrated distribution function reaches one-half of its steady state value. This time is also characteristic of how long it takes a typical atom to cascade to a given energy ε. At large time, the location of the front scales as $\sqrt{t}$. This scaling can be explained by a simple argument. Assume that the rate of a collision of an electron with an atom R_a is proportional to the area within the cutoff radius $R_a \sim \rho_c^2$, where ρ_c is defined in Eq. (3.47). Note that for large ε, ρ_c scales as ε^{-1}. From an independent numerical calculation, the average step in energy $\langle\Delta\varepsilon\rangle$ is found to be proportional to ε for both electron exchange and nonexchange collisions, that is $\langle\Delta\varepsilon\rangle \sim \varepsilon$. For energies below the bottleneck we make the further assumption that the atom must step in energy toward deeper binding during the course of each collision until it reaches the sink. To populate a certain energy level we must wait long enough for the average atom to reach that level, so the rate at which the front moves is determined by

$$\frac{d\varepsilon}{dt} = R_a \langle\Delta\varepsilon\rangle \sim \varepsilon^{-1} \qquad (3.59)$$

which has the solution $\varepsilon(t) \sim \sqrt{t}$. The prediction of this simple argument is that the location of the front should scale as $\sqrt{t}$ for large binding energies – a prediction the data supports.

To show the relationship between the Monte Carlo simulation and the analytic work, a set of runs are done using different values of ε_{th}. Only the one-way rate of ε_{th} crossing $R_\uparrow(\varepsilon_{th})$ is measured. The results are shown in Fig. 3.11. Also plotted is the

numerical evaluation of the flux integral Eq. (3.41) for three values of the free parameter C, the adiabatic cutoff. The rate $R_\uparrow(\varepsilon_{th})$ can be compared to the one-way flux expressed analytically in Eq. (3.41). Recall that the analytic calculation of the one-way flux may count a collision multiple times because of recrossings of the surface $\varepsilon = \varepsilon_{th}$ during the course of one collision. We introduced the adiabatic cutoff C to compensate for this effect. The Monte Carlo rate $R_\uparrow(\varepsilon_{th})$ does not have this problem since it only considers the state before and after a collision, that is, $R_\uparrow(\varepsilon_{th})$ is the one-way flux corrected for recrossings. A comparison of the two results determines the value C which would compensate for recrossings. From Fig. 3.11 one can see that the minimum $R_\uparrow(\varepsilon_{th})$ at $\varepsilon_{th} \approx 5$ corresponds to an adiabatic cutoff of $C = 1.2$. Also shown in Fig. 3.11 is the recombination rate determined by the Monte Carlo simulation R_3 which is a factor of 6 less than the minimum value of $R_\uparrow(\varepsilon_{th})$. This difference is caused by the finite width of the bottleneck and the skewing of the distribution function towards larger ρ values.

3.7. Conclusions and Discussion

By using a Monte Carlo simulation, we have calculated the three-body recombination time R_3^{-1} for ions that are introduced into a cryogenic and strongly magnetized pure electron plasma. The rate given by $R_3 = 0.070(10)\, n_e^2 v_e b^5$ is an order of magnitude smaller than the rate obtained previously for an unmagnetized plasma. Also determined by the simulation is the characteristic time for an electron-ion pair to cascade to a given level of binding. For deep binding, this time is given by Fig. 3.10 to be of order an evolution time $\left(n_e v_e b^2\right)^{-1}$ multiplied by ε^2.

It is instructive to discuss these two quantities in terms of a simple physical example. Consider a cryogenic pure electron plasma that is confined in a Penning trap; the plasma has the shape of a long column (say, of length L) with the radial confinement

provided by an axial magnetic field and the axial confinement by electrostatic fields applied at each end. Suppose that an ion transits the full length of the plasma, drifting with a small velocity $v_{i\parallel}$ along the magnetic field. If the transit time is long compared to the recombination time (i.e., $(R_3 L / v_{i\parallel}) >> 1$), the ion recombines with nearly 100% probability, and the electron-ion pair is deeply bound when it exits the plasma. If the transit time is long compared to the evolution time but small compared to the recombination time, the probability of recombination during transit is given by $R_3 L / v_{i\parallel}$. For a typical recombined pair, the depth of binding is given by the plot of $\varepsilon(t)$ in Fig. 3.10, where the time is to be interpreted as $t = (L / v_{i\parallel})$. It is important that the binding be deep enough to avoid ionization by the electrostatic confinement field at the end of the trap. (The external field should be small compared to the binding field.) If the transit time is short compared to the evolution time, the calculated recombination rate (steady state flux to the sink) is not applicable. For this case, it is very unlikely that a recombined pair would survive the electric field at the end of the plasma.

Next, let us re-examine the approximations used in the theory. The guiding center approximation breaks down at sufficiently deep binding [i.e., $\varepsilon \gtrsim (b / r_{ce})^{2/3}$] and all three degrees of freedom begin to interact on an equal footing. The motion becomes chaotic, and the perpendicular kinetic energy (that had been tied up in the cyclotron adiabatic invariant) is shared with the other degrees of freedom. One might worry that this would lead to ionization, but it cannot since the perpendicular kinetic energy is of order $k_B T_e$ and the binding energy is much larger than $k_B T_e$. Of course this assumes that the guiding center approximation does not break down until the binding energy is well below the bottleneck. Also, the one-way flux to deeper binding below the bottleneck is not changed qualitatively by the breakdown of the guiding center approximation. The nature of the bottleneck and of the flux is determined by a competition between the Boltzmann factor and a phase space

factor, and this competition is modified only slightly (by one power of ε in the phase space factor) when all degrees of freedom are involved.

At sufficiently deep binding, classical mechanics no longer provides an adequate description of the dynamics, and one might worry that quantum effects (e.g., metastable states) would modify the evolution rate. In this paper, quantum effects have not been considered at all; we assume that the classical description is valid down to binding energies such that the bound pair can survive the electrostatic confinement field at the end of the trap.

Finally, the analysis treats the ions as stationary. The ion motion parallel to the magnetic field is negligible compared to the electron motion provided that $v_{i\parallel} << v_e$. The condition that the perpendicular motion be negligible is more restrictive. For an electron-ion pair that is separated by the distance $r = |\mathbf{r}_e - \mathbf{r}_i|$, the frequency of the $\mathbf{E} \times \mathbf{B}$ drift motion of the electron around the ion is $\omega_{\mathbf{E}\times\mathbf{B}} = ec / Br^3$. The transverse ion motion is characterized by two frequencies Ω_{ci} and $v_{i\perp} / r$; so the condition that the ion motion be slow compared to the electron motion is $v_{i\perp} / r , \Omega_{ci} << ec / Br^3$. In these inequalities, the electron-ion separation may be replaced by b, since we follow the dynamics only for binding energies $\varepsilon > \varepsilon_{th} \equiv 1$. The rest of phase space (i.e., $\varepsilon < \varepsilon_{th}$, which corresponds to $r > b$) is characterized by a thermal equilibrium electron distribution and we do not care if the ion motion is negligible or not. By using $r \approx b = e^2 / mv_e^2$ the inequalities can be rewritten as $v_{i\perp} << (r_{ce} / b) v_e$ and $1 << (m_i / m_e)(r_{ce} / b)^2$.

When the latter of these two inequalities is reversed, the ion cyclotron frequency is larger than the $\mathbf{E} \times \mathbf{B}$ drift frequency. In this case, the electron and ion $\mathbf{E} \times \mathbf{B}$ drift together across the magnetic field with the velocity $v_{\mathbf{E}\times\mathbf{B}} \equiv ec / Bb^2 = v_e(r_{ce} / b)$. The results of our calculation should still apply since the drifting pair maintain a constant separation. It does not matter to the cascade process whether the electron is $\mathbf{E} \times \mathbf{B}$ drifting around a fixed ion at constant separation or the electron and ion are drifting together at constant separation.

When the first of the two inequalities is reversed, the ion can run away from the electron before the electron completes an $\mathbf{E}\times\mathbf{B}$ drift circuit around the ion. In this case, one expects a substantial reduction in the recombination rate. A simple dimensional argument suggests a rate of order $R_3 \sim n_e^2 \upsilon_e r_0^5$, which is a reduction by the factor $(r_0 / b)^5$, where r_0 is the electron-ion separation for which the $\mathbf{E}\times\mathbf{B}$ drift velocity equals the perpendicular ion velocity (i.e., $\upsilon_{i\perp} = ec / Br_0^2$). A detailed analysis of the recombination rate for the case where ion motion is included will be presented in a future paper.

3.7. References

[3.1] J.H. Malmberg, T.M. O'Neil, A.W. Hyatt and C.F. Driscoll, "The Cryogenic Pure Electron Plasma," in *Proceedings of 1984 Sendai Symposium on Plasma Nonlinear Phenomena* (Tohoku U. P., Sendai, Japan, 1984), pp. 31-37.

[3.2] D.R. Bates, Adv. At. Mol. Phys. **20**, 1 (1985).

[3.3] G. Gabrielse, S.L. Rolston, L. Haarsma and W. Kells, Phys. Lett. A **129**, 38 (1988).

[3.4] D.R. Bates and A. Dalgarno, *Atomic and Molecular Processes* (Academic, New York, 1962), p. 245.

[3.5] G. Gabrielse, Hyperfine Interactions **44**, 349 (1988).

[3.6] C.M. Surko, M. Leventhal and A. Passner, Phys. Rev. Lett. **62**, 901 (1989).

[3.7] G. Gabrielse, X. Fei, K. Helmerson, S.L. Rolston, R.T. Tjoelker, T.A. Trainor, H. Kalinowsky, J. Hass and W. Kells, Phys. Rev. Lett. **57**, 2504 (1986); G. Gabrielse, X. Fei, L.A. Orozco, R.L. Tjoelker, J. Haas, H. Kalinowsky, T.A. Trainor and W. Kells, Phys. Rev. Lett. **63**, 1360 (1989).

[3.8] P. Mansbach and J.C. Keck, Phys. Rev. **181**, 275 (1969).

[3.9] D.R. Bates, A.E. Kingston and R.W.P. McWhirter, Proc. R. Soc. London **A267**, 297 (1962); S. Byron, R.C. Stabler and P.I. Bortz, Phys. Rev. Lett. **9**, 376 (1962); A.V. Gurevich and L.P. Pitaevskii, Sov. Phys. JETP **19**, 870 (1964).

[3.10] B. Makin and J.C. Keck, Phys. Rev. Lett. **11**, 281 (1963).

[3.11] R.G. Littlejohn, Phys. Fluids **24**, 1730 (1981).

[3.12] T.G. Northrop, *The Adiabatic Motion of Charged Particles* (Interscience, New York, 1963).

[3.13] G.E. Uhlenbeck and G.W. Ford, *Lectures in Statistical Mechanics* (American Mathematical Society, Providence, R.I., 1963).

[3.14] E.M. Lifshitz and L.P. Pitaevskii, *Physical Kinetics* (Pergamon, Oxford, 1981).

[3.15] J.C. Keck, Adv. Chem. Phys. **13**, 85 (1967).

[3.16] N.G. Van Kampen, *Stochastic Processes in Physics and Chemistry* (North-Holland, New York, 1981).

[3.17] N.A. Krall and A.W. Trivelpiece, *Principles of Plasma Physics* (San Francisco Press, San Francisco, 1986).

This chapter has appeared, with only minor changes, as an article in Physics of Fluids B [1.1].

Figure 3.1: Drawing of guiding center atom. In order of descending frequency, the electron executes cyclotron motion, oscillates back and forth along a field line in the Coulomb well of the ion, and $\mathbf{E} \times \mathbf{B}$ drifts around the ion.

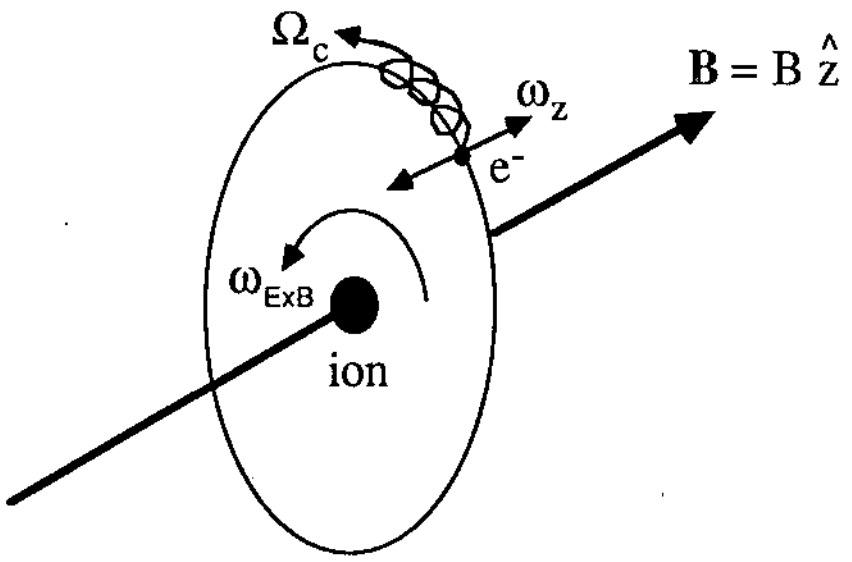
Ω_c
ω_z
e^-
$\mathbf{B} = B\,\hat{z}$
ω_{ExB}
ion

Figure 3.2: Energy that gives the minimum flux (i.e., the location of the bottleneck) as a function of the adiabatic cutoff used in the integration. The dashed line shows the estimate of $\varepsilon_b = 4$ predicted by Eq. (3.42). The quantity C is the adiabatic cutoff defined in Sec. 3.5.

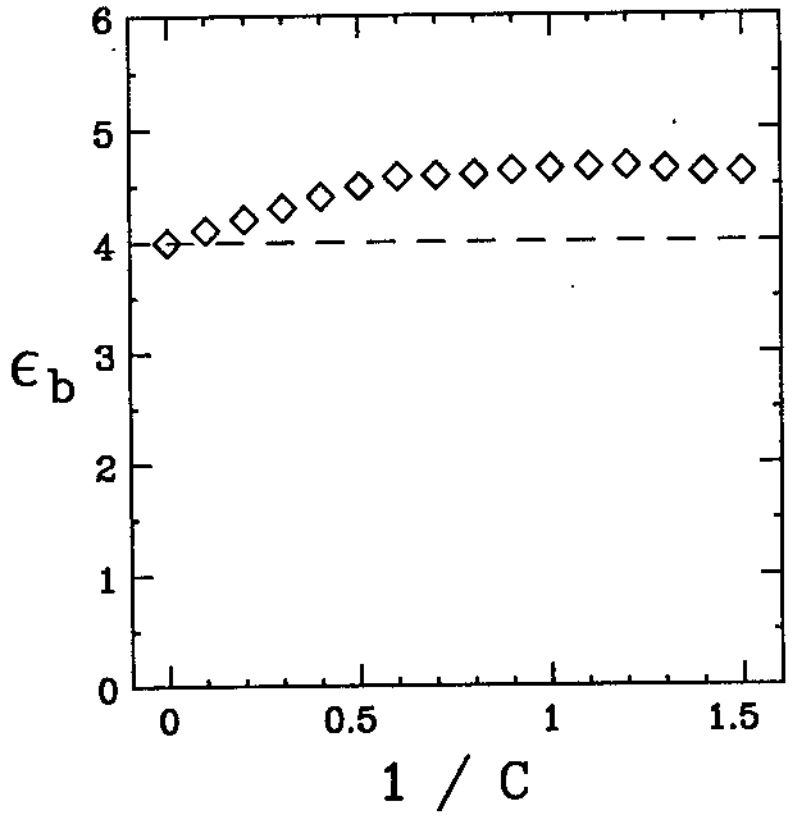
6
5
4
3
2
1
0
ϵ_b
0
0.5
1
1.5
1 / C

Figure 3.3: The minimum value of the one-way thermal equilibrium flux as a function of adiabatic cutoff used. The dashed line is the upper bound given by Eq. (3.42). Note that for large values of the adiabatic cutoff C, the one-way thermal equilibrium flux approaches the upper bound.

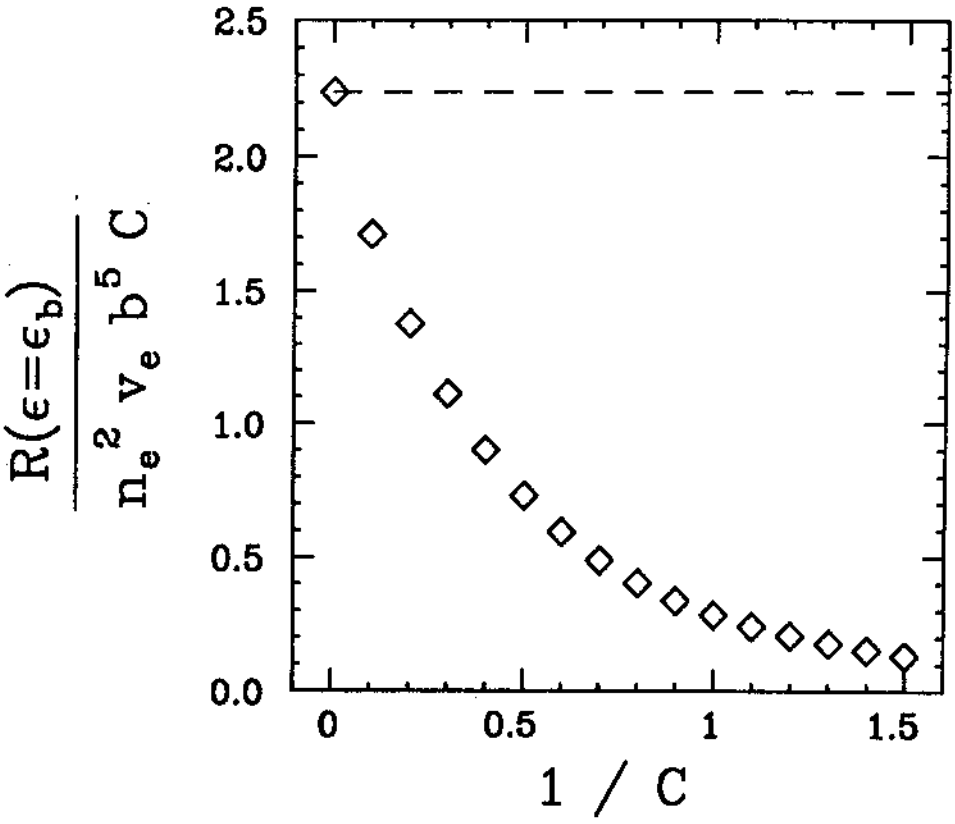
$\frac{R(\epsilon=\epsilon_b)}{n_e^2 v_e b^5 C}$
2.5
2.0
1.5
1.0
0.5
0.0
0
0.5
1
1.5
1 / C

Figure 3.4: Relative location of the energies ε_{th}, ε_c, ε_b, and ε_s; and a typical step size $\Delta\varepsilon$.

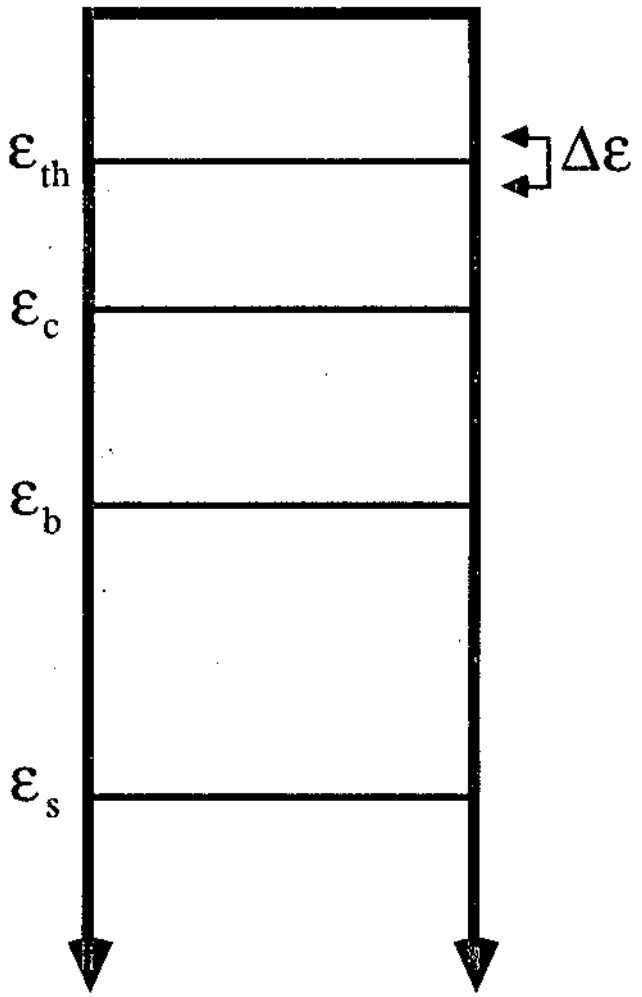
ε_{th}
$\Delta\varepsilon$
ε_c
ε_b
ε_s

Figure 3.5: An example of a time history showing the order of the time scales. The state of the atom (ρ, ε) is plotted as a function of time. The square corners show the duration collision [i.e., $t \sim (v_e / b)^{-1}$] as being effectively instantaneous on the time scale of an evolution. Three evolutions are shown. The duration of an evolution is of order $(v_e n_e b^2)^{-1}$, and the time between evolutions is of order $(v_e n_e^2 b^5)^{-1}$.

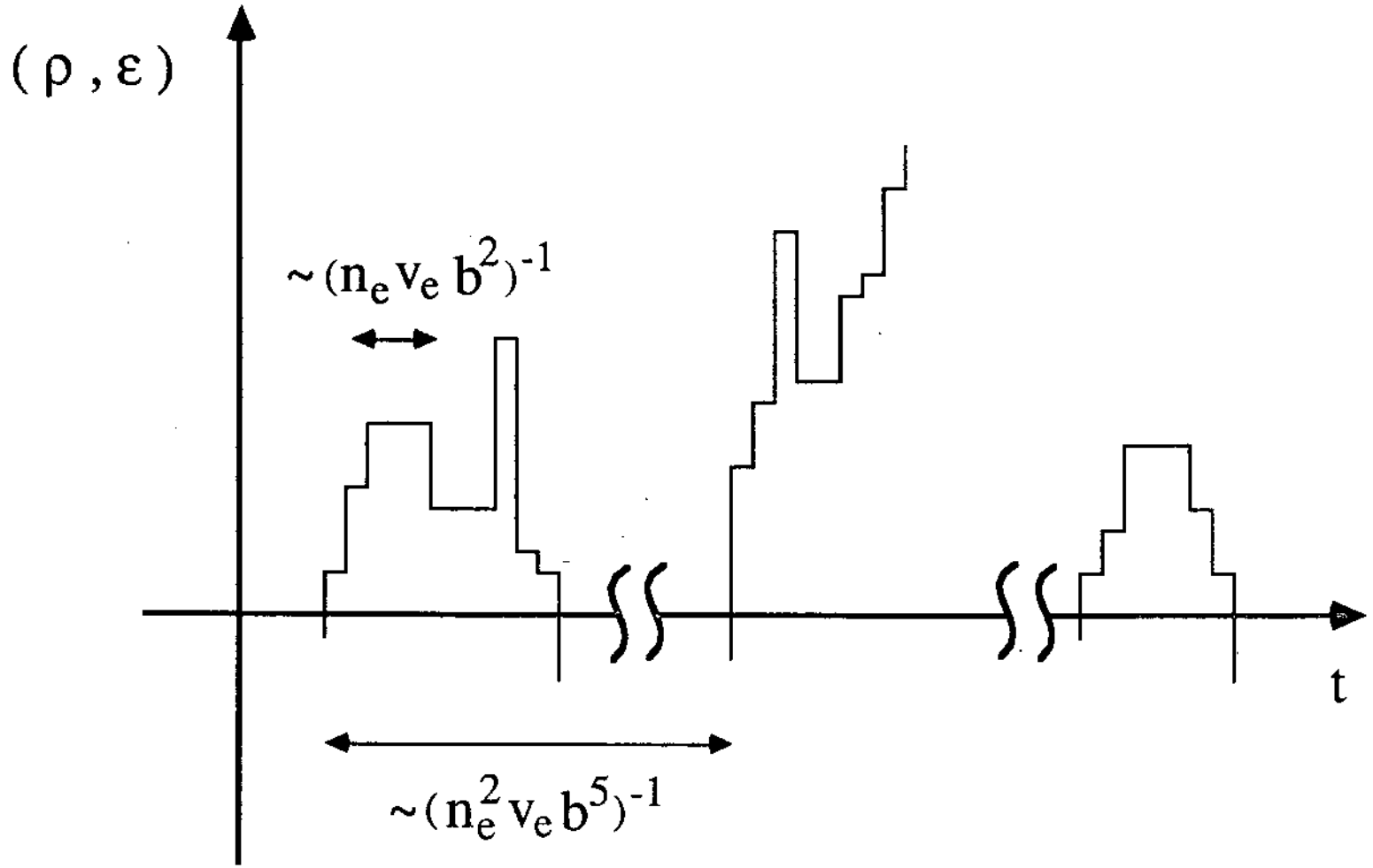
(ρ , ε)
~ (n_e v_e b^2)^-1
t
~ (n_e^2 v_e b^5)^-1

Figure 3.6: Number of evolutions which reach ε (i.e., N_ε), divided by the total number of evolutions $N_\uparrow$. This figure shows that one can unambigiously define a recombined atom as an atom which reaches the sink and that a bottleneck of finite width exists near $\varepsilon \approx 4$.

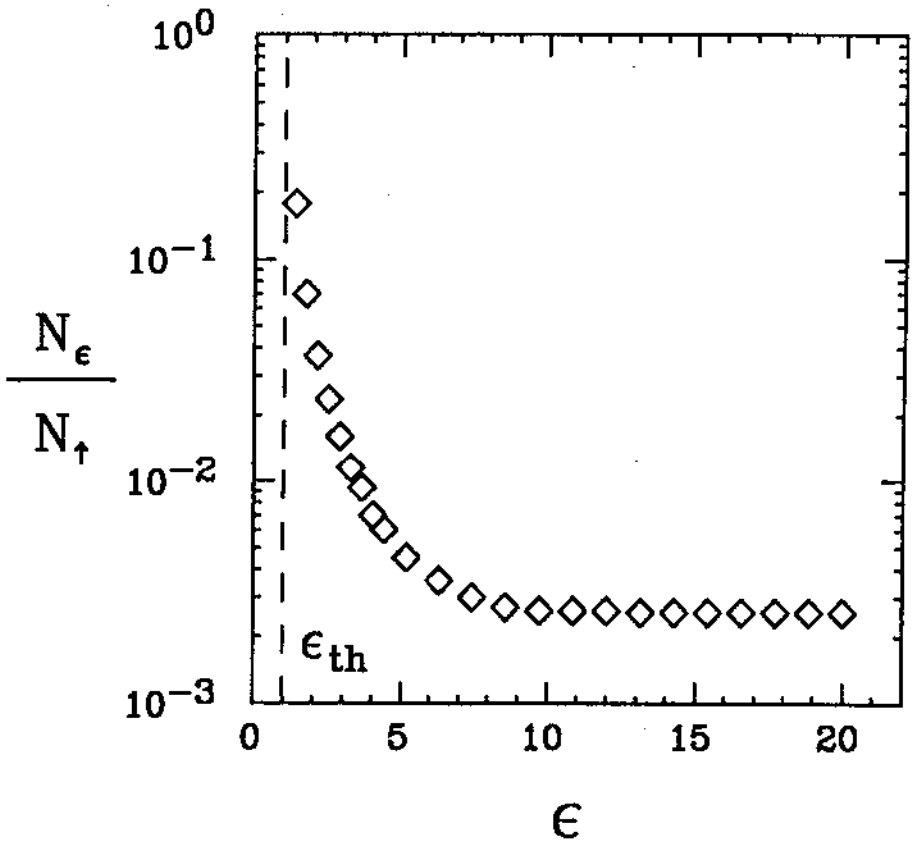
10^0
10^{-1}
10^{-2}
10^{-3}
$\frac{N_\epsilon}{N_\uparrow}$
ϵ_{th}
0
5
10
15
20
ϵ

Figure 3.7: Time dependent distribution function divided by its thermal value. Shown are its value at four different times (a) $t = 0$ (initial condition), (b) $t = (1/10)\left(n_e \upsilon_e b^2\right)^{-1}$, (c) $t = \left(n_e \upsilon_e b^2\right)^{-1}$, (d) $t = 10\left(n_e \upsilon_e b^2\right)^{-1}$ and its steady state value (e). All scales are linear.

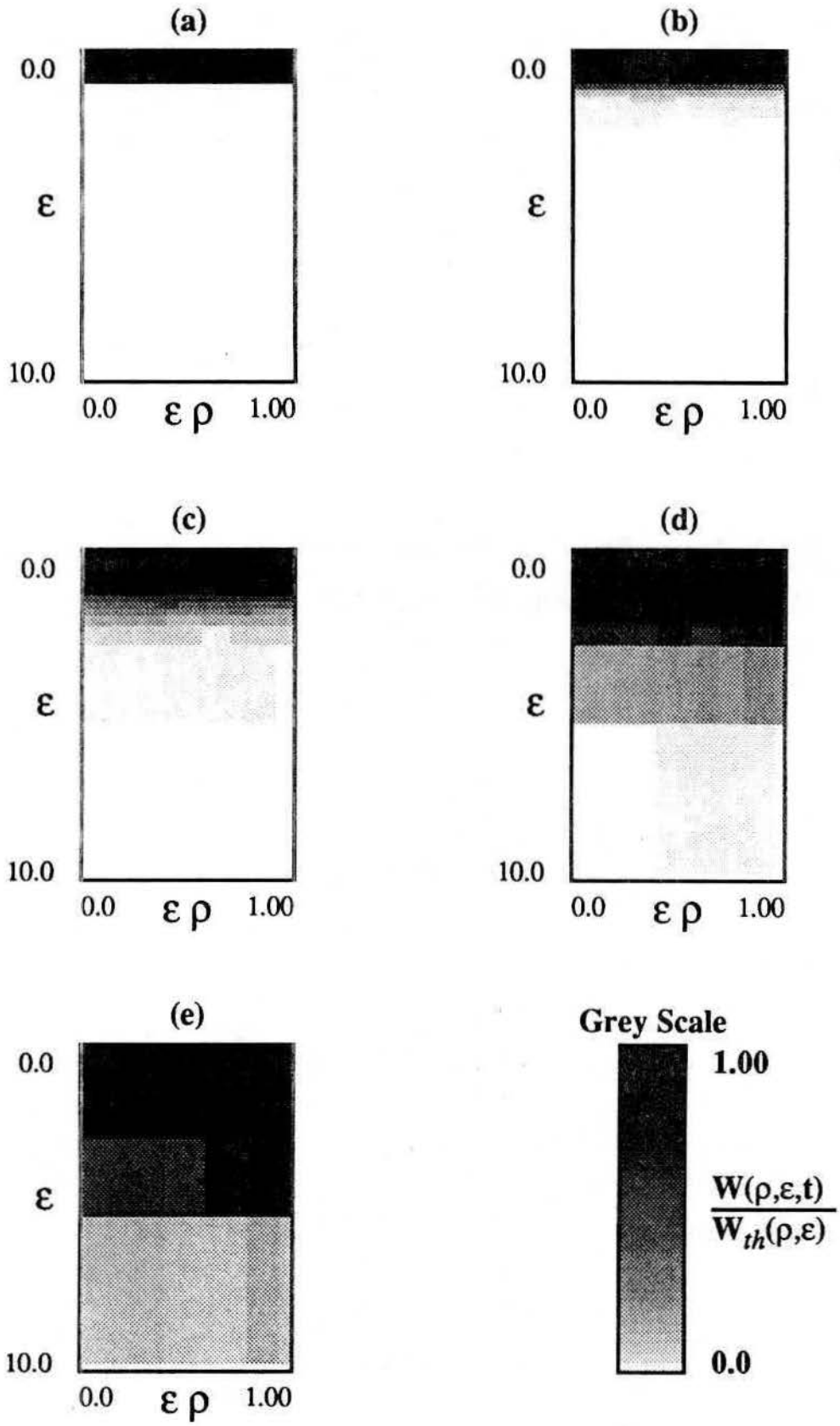
(a)
0.0
ε
10.0
0.0
ε ρ
1.00
(b)
0.0
ε
10.0
0.0
ε ρ
1.00
(c)
0.0
ε
10.0
0.0
ε ρ
1.00
(d)
0.0
ε
10.0
0.0
ε ρ
1.00
(e)
0.0
ε
10.0
0.0
ε ρ
1.00
Grey Scale
1.00
W(ρ,ε,t)
W_th(ρ,ε)
0.0

Figure 3.8: The ρ-integrated distribution function at various times. The time marked ∞ corresponds to steady state. The dashed line is thermal equilibrium.

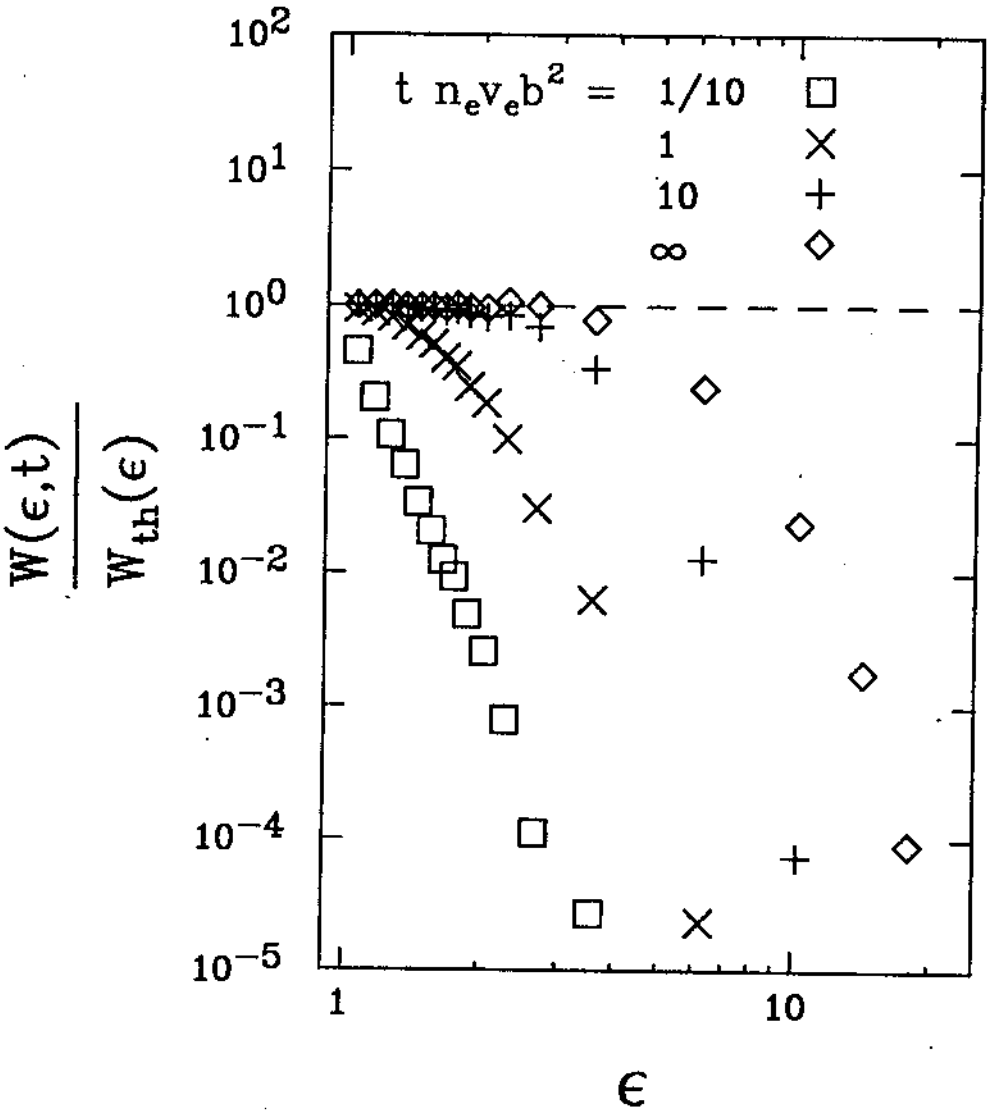
10^2
10^1
10^0
10^{-1}
10^{-2}
10^{-3}
10^{-4}
10^{-5}
1
10
ϵ
$\frac{W(\epsilon,t)}{W_{th}(\epsilon)}$
t $n_e v_e b^2$ = 1/10
1
10
∞

Figure 3.9: The ρ-integrated moment $\langle \varepsilon\rho \rangle$ in steady state for different values of ϵ. The dashed line shows the value expected if the distribution is thermal.

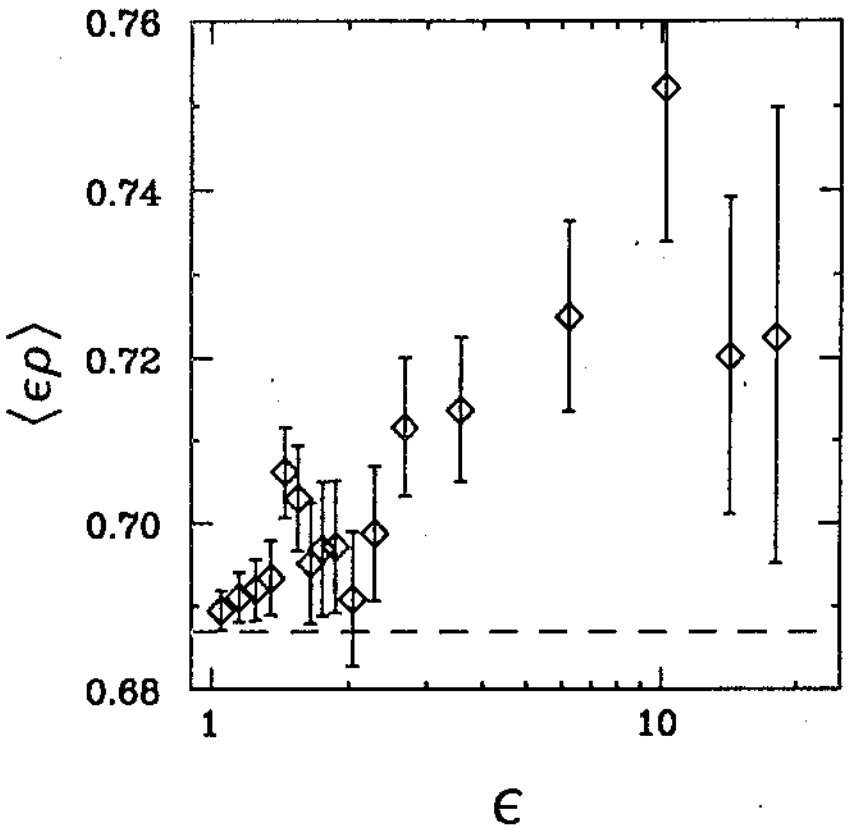
0.76
0.74
0.72
0.70
0.68
1
10
⟨εp⟩
ε

Figure 3.10: Location of the front of occupation as a function of time. The time is when the ρ-integrated distribution function reaches 1/2 of its steady state value.

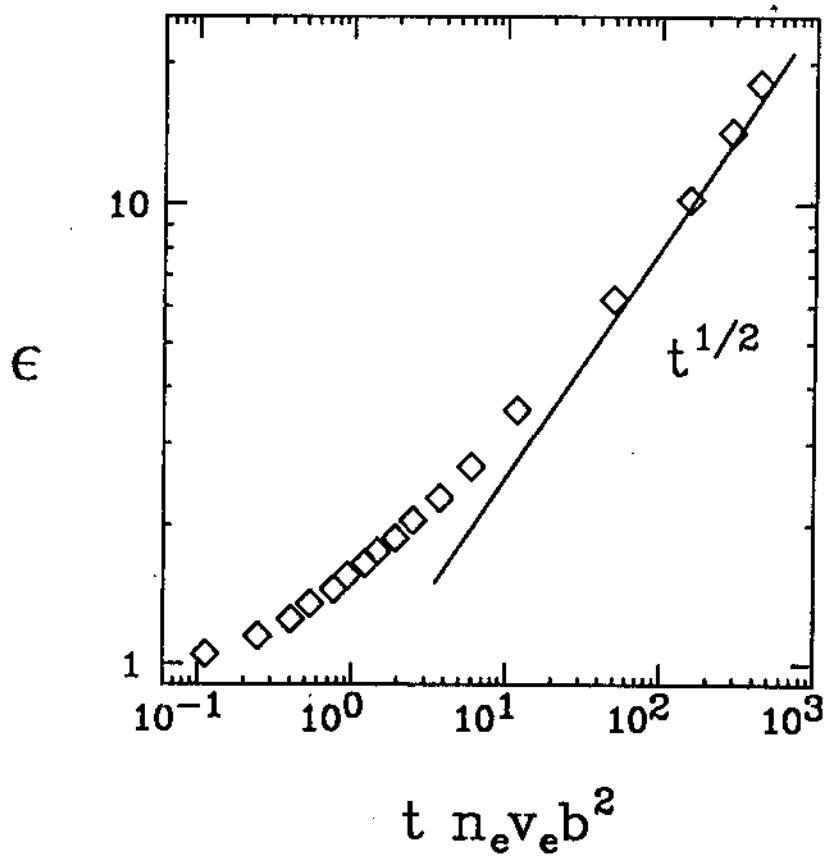
10
1
ϵ
$t^{1/2}$
10^{-1}
10^{0}
10^{1}
10^{2}
10^{3}
$t\ n_e v_e b^2$

Figure 3.11: One-way rate of crossing a surface of constant energy if the system is in thermal equilibrium. Shown is the Monte Carlo calculation of this rate ($\Diamond$) and the analytic estimate Eq. (3.41) of this rate for three values of the adiabatic cutoff C. Also shown is the Monte Carlo estimate of the recombination rate R_3.

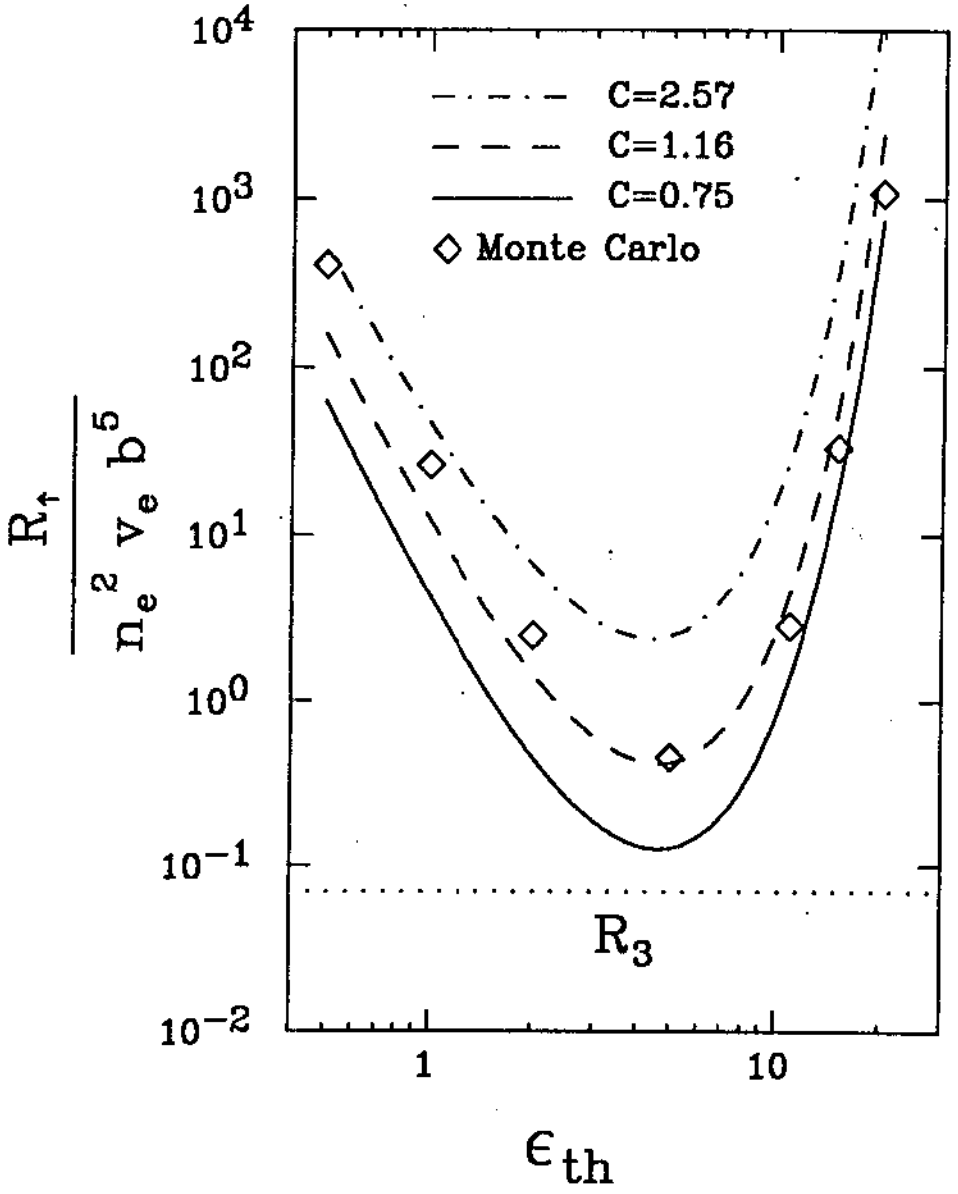
C=2.57
C=1.16
C=0.75
Monte Carlo
R_3
10^4
10^3
10^2
10^1
10^0
10^{-1}
10^{-2}
1
10
ϵ_{th}
$\frac{R_\uparrow}{n_e^2 v_e b^5}$